



GRAVITY AND MAGNETIC SIGNATURES OF METEORITE IMPACT STRUCTURES

JÜRI PLADO

TARTU 2000

**GRAVITY AND MAGNETIC SIGNATURES
OF METEORITE IMPACT STRUCTURES**

JÜRI PLADO



TARTU ÜLIKOOLI
KIRJASTUS

Department of Biology and Geography, University of Tartu, Tartu, Estonia

Dissertation is accepted for the commencement of the degree of Doctor of Philosophy (in Geology) on June 1st, 2000 by the Council of the Department of Biology and Geography, University of Tartu

Opponent: Dr. Boris Ivanov, Institute for Dynamics of Geospheres, Russian Academy of Sciences, Russia

The thesis will be defended at the University of Tartu, Estonia, on September 22nd, 2000 at 14.15

The publication of this dissertation is granted by the University of Tartu

© Jüri Plado, 2000

Tartu Ülikooli Kirjastuse trükikoda
Tiigi 78, Tartu 50410
Tellimus nr. 409

CONTENTS

LIST OF ORIGINAL PUBLICATIONS	6
ABSTRACT	7
INTRODUCTION	9
GEOPHYSICAL ANOMALIES OF IMPACT STRUCTURES	13
Gravity	13
Magnetics	14
Electrical methods	15
Seismic	16
Radiometric	17
PROCESSES CAUSING GRAVITY AND MAGNETIC ANOMALIES OF IMPACT STRUCTURES	18
Gravity	19
Magnetics	23
GRAVITY AND MAGNETIC MODELLING OF IMPACT STRUCTURES: CASE STUDIES	29
CONCLUSIONS	33
ACKNOWLEDGEMENTS	35
REFERENCES	36
SUMMARY IN ESTONIAN: Meteoriiitsete plahvatusstruktuuride gravi- ja magnetomeetria	42
PUBLICATIONS	45

LIST OF ORIGINAL PUBLICATIONS

- I **Plado J.**, Pesonen L. J., Koeberl C. and Elo S., 2000. The Bosumtwi meteorite impact structure, Ghana: A magnetic model. *Meteoritics & Planetary Science* 35, 723–732.
- II **Plado J.**, Pesonen L. J., Elo S., Puura V. and Suuroja K., 1996. Geophysical research on the Kärđla impact structure, Hiiumaa Island, Estonia. *Meteoritics & Planetary Science* 31, 289–298.
- III **Plado J.**, Pesonen L. J. and Puura V., 1999. The effect of erosion on gravity and magnetic signatures of complex impact structures: geophysical modelings and applications. In: (eds. B. O. Dressler and V. L. Sharpton) Large Meteorite Impacts and Planetary Evolution II, Boulder, Colorado. *Geological Society of America Special Paper* 339, 229–239.

ABSTRACT

The present thesis summarises geophysical signatures of meteorite impact structures with special focus on Kärddla (Estonia) and Bosumtwi (Ghana) craters. The various geological and physical processes causing the observed gravity and magnetic anomalies of impact structures are described in the synopsis. Two important aspects in geophysical modelling of impact structures are discussed. *First*, the role of petrophysical properties of impactites and target rocks in constraining the geophysical model is emphasised with two examples (Papers I and II). *Second*, the effect of progressive erosion on gravity and magnetic anomalies of impact craters is analysed using a novel simulation technique (Paper III).

Most impact structures produce discernible gravity and magnetic anomalies. Most of the processes causing these anomalies occur during the excavation and modification stages of impact cratering, and are completed during the post-impact development of a structure. However, impact related gravity and magnetic anomalies may be modified or even obliterated by post-impact geological processes. The most common geophysical signature of a simple impact structure is a negative gravity anomaly produced by the formation of breccias and possible post-impact sediments. The negative anomaly may be surrounded by a positive gravity ring due to denser uplifted rocks along the crater rim. In complex structures, the negative gravity may consist a central positive peak due to central uplift of denser target material. The magnetic anomalies of impact structures show more variety due to the vector nature of magnetisation and its dependence on site latitude. Moreover, the impact and post-impact processes may produce new magnetisations or destroy the pre-existing ones. Nevertheless, an overall weak magnetic relief is often associated with simple impact structures. The complex structures usually show more complicated magnetic features.

The gravity and/or magnetic modelling methods used to obtain a view of the subsurface features of impact structures are demonstrated with two examples: the 1.07 Ma old Bosumtwi (Paper I) and ~455 Ma old Kärddla structures (Paper II). In both cases, the petrophysical determinations of rock properties were vital to achieve a satisfactory model of the structure. In the case of the 4-km-wide Kärddla structure, a 2.5-dimensional model was constructed to describe simultaneously the gravity and magnetic effects of the structure. The model is based on ground gravity and magnetic data, supplemented with determination of physical properties of samples and with the geological concept of the crater's internal structure based on drill cores. The model suggests that the positive ring anomalies around the central gravity and magnetic minimum are due to uplifted crystalline rim wall rocks. The negative gravity and magnetic anomalies generally result from impact breccias and post-impact sediments, which display low densities and weak magnetisations.

For the Bosumtwi structure (rim-to-rim diameter = 11.5 km), a high-resolution aeromagnetic map was analysed to investigate the distribution of buried magnetic material within the structure. The model is supported by petro-physical and palaeomagnetic measurements of samples collected around the structure. The model suggests that anomalously magnetic material inside the structure has been formed during the impact processes and preserved since, particularly in the northern part of the structure. The magnetic data also outline the possible location of a central uplift not previously documented.

A hypothetical model of a complex impact structure in Precambrian target rocks, with a diameter of 30 km, was created to investigate changes in the gravity and magnetic anomalies of impact structures as a function of erosion. The effect of erosion was simulated by removing sequentially 1-km-thick layers from the structure, and calculating the gravity and magnetic anomalies of the remaining model. The major effect of erosion is a pronounced decrease in the amplitude of the negative gravity anomaly with only a minor change in diameter. The amplitude of the central positive gravity anomaly due to the structural uplift also decreases with erosion but not as rapidly as the main anomaly. The magnetic anomaly, on the other hand, decreases significantly after the erosion of the highly magnetic impact melt layer.

INTRODUCTION

Approximately 170 hypervelocity meteorite impact structures had been identified on earth by 1999 (Pesonen *et al.*). Given 3–5 new discoveries per year, the number of structures will soon reach 200. Compared to other terrestrial planets or natural satellites, this still relatively small number on earth is due to the thick atmosphere and active geological processes that continuously reshape the earth's surface. Most of the discovered structures are concentrated in cratonic areas of northern Europe, Australia and North America, where intensive research programs have been initiated to identify and study them. Due to difficulties in identification, relatively young age of oceanic crust, and disintegration of small projectiles in the water column, no impact craters on the oceanic crust have been found so far. However, there is evidence for an impact-related Ir anomaly and disturbance of large volumes of sediments in the Bellinghausen Sea (Eltatin impact, Gersonde *et al.*, 1997). Five impact structures have been discovered on shelf areas (Fohn, Montagnais, Mjølnir, Ust-Kara, Chicxulub; Gorter and Glikson (2000), Grieve and Shoemaker (1994) and references therein). Convergent plate tectonic processes of subduction and crustal collision have been obliterated a great number of impact structures. Therefore, only a few strongly deformed structures are known, *e.g.* Sudbury, Canada (Milkereit *et al.*, 1992; Deutsch and Grieve, 1994); Vredefort, South Africa (Reimold and Gibson, 1996), and Gardnos, Norway (French *et al.*, 1997).

The diameters of the impact structures range from few tens of meters to ~300 km (Vredefort). The morphological types of terrestrial impact structures depend on impact size and are similar to those on other terrestrial planets and moons. These range from simple bowl-shaped structures to complex craters (with central uplift) and to peak ring structures. Structure age varies from recent to ~2.006 Ga (Grieve and Pesonen, 1996).

The role of geophysical techniques in impact cratering research has increased recently due to three factors. *First*, because most directly observable impact craters have already been discovered, innovative and indirect methods are needed. *Second*, geophysical data and their analyses provide an internal view of impact structures. *Third*, impact structures may contain valuable economic deposits such as ores, diamonds, oil, gas, or water (see *e.g.* Masaitis, 1992). Geophysical data, coupled with drilling, have helped to discover these deposits in many structures.

The most commonly used geophysical methods in the investigation of impact structures involve potential fields like gravity, magnetic and electric (Pilkington and Grieve, 1992), but electromagnetic, seismic and radiometric methods have also been successfully used (see Henkel, 1992; Grant *et al.*, 1997; Jansa *et al.*, 1989; Pesonen *et al.*, 1999). The modelling of gravity and magnetic fields over impact structures, together with petrophysical and palaeomagnetic

data, allows estimation of the structure's morphometric parameters, volumes and approximate distribution of rocks with anomalous physical properties within the structure. Finally, modelling may specify the geologic and impact history of a specific structure.

The present thesis describes geophysical signatures and processes responsible for gravity and magnetic anomalies of impact structures. It is based on three original publications and includes a discussion of gravity and magnetic models used to describe the Bosumtwi impact structure in Ghana (Paper I), Kärđla crater in Estonia (Paper II), and the erosion history of a hypothetical impact structure in the Baltic Shield (Paper III). The major contents of these papers are summarised below.

Paper I:

Plado J., Pesonen L. J., Koeberl C. and Elo S., 2000. The Bosumtwi meteorite impact structure, Ghana: A magnetic model. *Meteoritics & Planetary Science* **35**, 723–732.

The paper presents a new magnetic model of the Bosumtwi meteorite impact structure (centre co-ordinates 06°30'N; 01°25'W) in Ghana, West Africa, based on a high-resolution airborne geophysical survey (Pesonen *et al.*, 1998; Ojamo *et al.*, 1997). This 10.5 km wide and 1.07 Ma old structure, containing Lake Bosumtwi, truncates the regional north-east trending magnetic patterns of ~2.1 Ga old Birimian-Tarkwaian rocks. The residual magnetic anomaly map of the structure shows a magnetic “halo” — a circular zone of low gradients — reflecting the rim of the structure beyond the present shoreline. The map also shows a group of differently shaped negative anomalies that are bordered by two positive anomalies to the north and south. This type of anomaly is typical for anomalously magnetic body located near equatorial latitudes with magnetisation subparallel to the present magnetic field. The negative anomalies with an amplitude of 10–30 nT and diameters of ~1 km surround a central positive one, pointing to a possible location of a central uplift. The authors interpret the negative anomaly patches to reflect bodies of impact melt or melt-rich suevites below the lake sediments.

The model is constrained by physical property determinations of ejected impactites and target rocks. These data differentiate the physical properties of pre-impact early Proterozoic metasediments (target rocks) and melt-rich suevites. Suevites have low densities (~2040 kgm⁻³), high porosities (~25%), and high magnetisations (susceptibility ~330 × 10⁻⁶ SI; intensity of the natural remanent magnetisation (NRM) ~40 mA m⁻¹) compared to the target rock values (density ~2510 kgm⁻³; porosity ~8%; susceptibility ~150 × 10⁻⁶ SI, and NRM ~0.6 mA m⁻¹). As found in many other impact structures, the NRM of suevites prevails over induced magnetisation (Koeningsberger ratio > 3). Palaeo-

magnetic studies of suevites show stable NRMs with predominantly normal polarity during alternating field and thermal treatments. The main magnetic carrier is magnetite, but hematite is also present. The normal polarity NRM component, believed to have been acquired during the onset of the Jaramillo normal polarity epoch, is primary and dates the impact event. The occasionally isolated reversed component is presumably secondary and may have been acquired during weathering at the subsequent reversed polarity epoch. The modelling shows that highly magnetic normally-polarized material is associated mainly with the north-central part of the lake. At the north-eastern part of the structure, a biotite-rich granitic intrusion is exposed. It is possible that shock decomposed biotite into ferrimagnetic iron oxides.

Paper II

Plado J., Pesonen L. J., Elo S., Puura V. and Suuroja K., 1996. Geophysical research on the Kärđla impact structure, Hiiumaa Island, Estonia. *Meteoritics & Planetary Science* **31**, 289–298.

This paper presents geophysical anomalies of the buried 4-km-wide and 500-m-deep Kärđla impact crater (centre co-ordinates 58°59'N, 22°40'E). The anomalies depict a nearly circular, ~ -3 mGal gravity and ~ -100 nT magnetic anomalies 4 km in diameter. Petrophysical measurements and modelling show that the negative gravity anomaly is due to (i) low density ($\sim 2460 \text{ kgm}^{-3}$) of the autochthonous breccia produced by fracturing and crushing of the target rocks, (ii) very low density ($\sim 2390 \text{ kgm}^{-3}$) of the allochthonous breccia which partly fills the structure, and (iii) low density ($\sim 2560 \text{ kgm}^{-3}$) of the post-impact sediments compared to the unshocked crystalline target ($\sim 2630 \text{ kgm}^{-3}$). Because of extensive marine sedimentation into the bowl-shaped topographical feature, the post-impact sediments (~ 300 m of Ordovician lime-, silt- and sandstones) are approximately three times thicker than those in the surroundings beyond the structure proper. The negative gravity anomaly is surrounded by a circular positive anomaly, which corresponds to the rim wall of the structure and is caused by denser uplifted Proterozoic crystalline rocks.

The negative magnetic anomaly is due to weak magnetisations of the impact breccias. The thick post-impact sedimentary infill with very weak magnetisation also contributes to the negative magnetic anomaly. The fractured subsurface crystalline rim wall rocks, however, give rise to positive magnetic anomalies that encircle the central negative anomaly.

In addition to the model of the structure, petrophysical data of Kärđla rocks provide valuable hints of the impact origin of the structure. The paper provides a summary of physical properties (density, porosity, P-wave velocity, magnetic susceptibility, intensity of NRM, and electric resistivity) of impactites, unshocked target rocks and post-impact sediments. The physical properties of

the impact-produced rocks differ significantly from those of unshocked Precambrian bedrock in the surroundings. In subautochthonous granitic rocks, porosity and electrical conductivity decrease, but density and P-wave velocity increase downwards from the impact point. These gradual changes in physical properties are due to decrease of shock-originated fractures in the target rocks because of the vanishing shock and rarefaction waves, and are consistent with an impact origin for Kärddla.

Paper III

Plado J., Pesonen L. J. and Puura V., 1999. The effect of erosion on gravity and magnetic signatures of complex impact structures: geophysical modelings and applications. In: (eds. B. O. Dressler and V. L. Sharpton) Large Meteorite Impacts and Planetary Evolution II, Boulder, Colorado. *Geological Society of America Special Paper* **339**, 229–239.

This article investigates the changes in the gravity and magnetic anomalies of impact structures as a function of progressive erosion. To the authors knowledge, this is the first time that the erosional effect on geophysical signatures has been investigated quantitatively (see also Pilkington and Grieve, 1992). Gravity and magnetic models of an idealised medium-sized (30 km in diameter, 1 km deep) complex impact structure were created. We analysed the effect of erosion on gravity and magnetic anomalies by modelling the structure after sequentially eroding 1 km intervals from the upper surface down to six kilometers (six erosional levels).

The major effect of erosion is a pronounced decrease in the amplitude of the negative gravity anomaly with a minor change in its diameter, thus progressively flattening the anomaly. The amplitude of the central positive anomaly due to the structural uplift also decreases with erosion, although not as rapidly as the main anomaly. Therefore, erosion may amplify the gravity response of the central uplift with respect to the total anomaly. The erosional model was tested with data of 13 structures for which both gravity data and erosion level estimates are available.

The magnetic model (being located at middle northern latitudes) consists of a remanently magnetised impact melt body and a concentric target region with lower magnetisation. The structure creates a circular positive anomaly, surrounded by a negative anomaly, which is produced mainly by the melt layer. In the central part, the positive anomaly is distorted by a negative anomaly, which corresponds to the central uplift. This type of anomaly pattern is typical for a structure with a magnetic melt body at middle northern latitudes. The removal of impact melt by erosion significantly decreases the amplitudes of the anomalies.

GEOPHYSICAL ANOMALIES OF IMPACT STRUCTURES

Several geological, geochemical and geophysical methods have been used to identify and prove the impact origin for some geological structures. The most definite proofs in confirming for impact origin are: (i) a historic record of a meteorite impact, *e.g.* Kaali, Estonia (Meri, 1984); (ii) the discovery of meteorite fragments, either in or nearby the structure, *e.g.* Meteor Crater, USA (Mittlefehldt *et al.*, 1992), Macha, Russia (Gurov, 1996); or (iii) enrichment of impact-derived rocks, either impact breccias and melt rocks or distal ejecta with siderophile, especially platinum group elements, *e.g.* Gardnos (French *et al.*, 1997), Bosumtwi, Ghana (Koeberl and Shirey, 1993) and Fohn structure (Gortler and Glikson, 2000). Shock metamorphic features, such as shatter cones, planar features or planar deformation features (PDF's), quartz polymorphs: stishovite or coesite, melted particles or melt bodies, has proved to be an indicator of impact (French and Short, 1968; Stöffler, 1974; Koeberl and Anderson, 1996). Geophysical methods alone are generally inadequate to prove impact origins but are often applied to impact structure studies because they provide certain diagnostic features. The most traditional methods are gravity and magnetics, but also electric, electromagnetic, seismic and radioactive techniques have been used.

Gravity

The gravity anomaly over an impact crater depends on (i) the size and morphology of the structure, (ii) the density contrast between impact-related rocks and surroundings, and (iii) structure depth. Most impact structures yield a negative gravity anomaly, *e.g.* Siljan, Sweden (Dyrelius, 1988), Ries, Germany (Pohl *et al.*, 1977), Roter Kamm, Namibia (Brandt *et al.*, 1998), Kärddla (Paper II). If filled with relatively denser post-impact material, tektonised and/or deeply eroded, for example, Sudbury (McGrath and Broome, 1994), the structure may reveal positive gravity effects. Complex impact structures (the transition diameter between single and complex craters is 2 km in sedimentary and 4 km in crystalline terrain; Grieve and Pesonen, 1992) often yield a gravity high in the centre of the gravity low. This local gravity positive is caused by central uplift which has elevated denser target rocks (*e.g.* Manicouagan, Canada; Sweeney, 1978). Deeply eroded complex impact structures may only show the positive gravity signature due to central uplift, for example, Marquez Dome, USA (Wong *et al.*, 1993).

Pilkington and Grieve (1992), who analysed the maximum amplitude (Δg) of the gravity low of 53 terrestrial impact craters, show that the amplitude increases with the crater diameter (D). For smaller craters ($D < 20$ km), Basilevsky *et al.* (1983) proposed a linear relationship ($\Delta g = -D$), where D = kilometres and Δg = milligals. This relationship is defined by a simple hemispherical fracture volume model. In reality, a significant scatter around this trend occurs due to lithological variability and processes such as erosion, post-impact infill and burial. For larger structures ($D > 30$ km), the maximum negative gravity anomaly reaches a limit of ~ -30 mGal, beyond which the anomaly no longer depends on the diameter. This is due to lithostatic pressure, which eliminates the effect of impact-induced fracturing in the deep roots of large structures. The amplitude of a gravity anomaly also decreases with increased erosion (Paper III; Pilkington and Grieve, 1992), as well as due to burial (Plado and Puura, 1995).

In a plan view, especially over the smaller and younger structures, the gravity anomalies are distinctly circular and bowl-shaped, *e.g.* Wolf Creek, Australia (Fudali, 1979), Kärđla (Paper II), and Lappajärvi, Finland (Elo *et al.*, 1992). However, in most cases, the lateral density variations in bedrock and impacted rocks partially distort and can even mask impact-related anomalies.

Magnetics

The magnetic anomaly of an impact structure depends on (i) the size and shape of the structure, (ii) the intensity and direction of magnetisation of the impactites, with respect to the magnetisation of unshocked target rocks, (iii) the local geomagnetic field, and (iv) the altitude (distance from measurement level to the source). Magnetic anomalies related to impact structures are usually more complicated than gravity anomalies, due to the large variations of magnetisations in impact-related and target rocks. The anomalies are further complicated, because magnetisation of rocks is a vector sum of the induced and remanent magnetisations, which depend on the direction of the present and ancient earth's magnetic fields, respectively. Therefore, magnetic anomalies of impact structures also depend on site latitude. The principal magnetic characteristics of impact structures is a magnetic low (Pilkington and Grieve, 1992), *e.g.* Meteor Crater (Regan and Hinze, 1975) and Kärđla (Paper II). However, complex impact structures, especially larger ones, may show high amplitude — short wavelength anomalies within the weak magnetic relief, near and above the central uplift, for example, Manicouagan (Coles and Clark, 1978) and Acraman, Australia (Williams, 1994). If an impact melt with high remanent magnetisation is present within the structure, the magnetic low may be broken locally by high amplitude anomalies (Henkel, 1992). Several impact structures show only

positive magnetic features, and some show no impact-related magnetic signatures (Pilkington *et al.*, 1995).

The amplitudes of magnetic anomalies of impact structures have a large variation from zero to several thousand nT. Unlike gravity anomalies, crater diameter and amplitude of the magnetic anomaly is uncorrelated. Generally, it is impossible to outline the impact structure with only magnetic features. Erosion of allochthonous breccias and impact melt layers reduces the amplitude of impact-related magnetic anomalies (Paper III). Post-impact burial also decreases considerably the amplitude of impact anomalies, because the amplitude of a magnetic anomaly decreases rapidly with altitude (Kearey and Brooks, 1994).

Palaeomagnetic studies are sometimes used to date an impact event and specify the nature of magnetisation, *e.g.* Lappajärvi (Pesonen *et al.*, 1992), Iso-Naakkima, Finland (Pesonen *et al.*, 1996), Siljan (Elming and Bylund, 1991), Acraman (Williams, 1994). Typically, oriented samples for palaeomagnetic studies are collected from available outcrops. However, this technique has its limitations. First, the internal structure of an impact crater may remain unsampled if it is buried. Second, the outcropping rocks may include secondary remanent magnetisations resulting from weathering or lightning. To improve the use of palaeomagnetic dating of impact sites, fully-oriented drill cores provide optimal results.

Electrical methods

Various electrical methods have been used to study impact structures, because impact causes differences in resistivities between impacted and target lithologies. These are principally due to an impact-induced increase in porosity and fluid content in impactites. The effect of impact to resistivities could be illustrated with an example of Kärddla rocks (Paper II), where water-saturated drill core samples reveal low resistivity of impact breccias ($\sim 5500 \Omega\text{m}$) and fractured basement granites ($\sim 2500 \Omega\text{m}$) relative to target granites ($\sim 100 \text{k}\Omega\text{m}$). Resistivity of fractured granites from the upper part of the central uplift ($21 \text{k}\Omega\text{m}$) and rim wall ($15 \text{k}\Omega\text{m}$) lie between these two extremes. The electrical methods include utilising artificially generated direct (*e.g.* Brandt *et al.*, 1994) and alternating (*e.g.* Henkel, 1992) currents. However, alternating field measurements are more common due to their lower cost and higher effectiveness.

Electromagnetic soundings have been made in Siljan (Henkel, 1992), Lappajärvi (Elo *et al.*, 1992), Karikkoselkä, Finland (Lehtinen *et al.*, 1996). These investigations show clear anomalies related to impact structures, and assigned to low resistivities of impact breccias compared to surrounding rocks. Henkel (1992) has shown a radial distribution of low resistivities, which extends beyond the crater edge, in Siljan and Dellen, Sweden. This reflects the

extension of fracturing outside of the impact crater. Higher resistivities in the central part of the structure were measured, and attributed to less fractured uplifted target rocks.

Magnetotelluric surveys have been carried out at structures in Siljan (Zhang *et al.*, 1988), Charlevoix, Canada (Marechal and Chouteau, 1990) and Araguainha, Brazil (Masero *et al.*, 1994). In Siljan, no shallow subsurface conductive zone was found. The deeper (5–20 km) low-resistivity zone, was attributed to fluid migration through impact-induced fractures. A subhorizontal conductive zone at the depth of ~1.5 km, interpreted as an impact related fault, was found in Charlevoix. In Araguainha, a low resistivity subsurface zone extends to the depth of 1 km at 9 to 20 km from the centre, whereas it thickens away from the centre.

Ground Penetrating Radar (GPR) has been used in shallow subsurface investigations of a few small impact structures. GPR measures the dielectric contrasts of the subsurface strata, which may correspond to changes in stratigraphy or lithology. In Meteor Crater (Pilon *et al.*, 1991), GPR was used to map the crater wall and the base of the ejecta blanket beyond the structure. In the geophysical survey across the Roter Kamm structure (Grant *et al.*, 1997), GPR was used to delineate deposits beneath the regional post-impact eolian sand sheet. The GPR record from the Pretoria Saltpan crater, South Africa (Brandt *et al.*, 1994) shows dipping reflections representing the outer section of the raised rim. The bedrock surface and an anomalous till layer under the elevated part of the rim were detected in a possible impact structure, Tor, Sweden (Henkel *et al.*, 1996). In radargrams of Ilumetsa structure, Estonia (Plado *et al.*, 2000), numerous small dislocations can be observed in the whole volume under the elevated rim and under the crater floor. The reflector that corresponds to the surface of the Devonian sandstones is interrupted under the elevated part of the rim.

Seismic

Seismic refraction and reflection surveys provide detailed images of the subsurface structure of impact craters (Pilkington and Grive, 1992). Refraction methods have been used to describe the vertical and horizontal extent of shock-induced fracturing in autochthonous breccias (Ackerman *et al.*, 1975), to determine the thickness of the allochthonous breccia lens (Millman *et al.*, 1961; Sander *et al.*, 1964), and to characterise the central uplift (Green and Chetty, 1990). Reflection studies, on the other hand, provide the most detailed geophysical information on the subsurface structure of impact structures, especially of marine structures. The most recent studies have been made in the Montagnais structure, located on the outer continental shelf of Nova Scotia, Canada (Jansa *et al.*, 1989), the Mjølnir structure in the central Barents Sea (Tsikalas *et al.*, 1998), and the Fohn structure in the Timor Sea, northwest of Australia (Gorter

and Glikson, 2000). The seismic reflection surveys have yielded information on the height and diameter of the central uplift, the thickness of allochthonous breccia lenses and the extent of brecciation in these marine impact craters. In Mjølner, the gravity model is based on the seismic data.

Radiometric

Airborne gamma-ray spectrometry has been applied to study the 10.5 km-wide Bosumtwi impact structure (Ojamo *et al.*, 1997; Pesonen *et al.*, 1998). Gamma radiation data were recorded with a NaI crystal (volume 33.5 l) measuring U^{238} , Th^{232} and K^{40} . Radiometric data, especially potassium content clearly reveal high concentrations at the inner rim wall of the structure. A map of equivalent K concentration also shows fragmentary evidence of the outer ring around the crater with the diameter of 17–20 km. The Jänisjärvi structure in western Karelia (Russia) also has a distinct K ring anomaly associated with its rim. The cause of these anomalies has not been studied thoroughly.

PROCESSES CAUSING GRAVITY AND MAGNETIC ANOMALIES OF IMPACT STRUCTURES

Impact cratering process begins when the projectile first contacts the planetary surface and ends with the final movements and adjustments of the crater structure and fall back of the debris in and around the crater. Unlike geological processes, hypervelocity impact affects large volumes of earth's crust (as deep as the Mohorovičić discontinuity) in a very short time interval (minutes). The cratering process is divided into three stages: (i) contact and compression, (ii) excavation, and (iii) modification (Melosh, 1989). The first stage is very short, 10^{-3} to 10^{-1} seconds, and depends on the size, composition and velocity of the projectile. Supersonic shock waves originate at the point of initial contact. These waves propagate into both the projectile and the target. The compression of rocks beyond their Hugoniot Elastic Limit (HEL — the stress that differentiates elastic from plastic behaviour of the solid medium through which the compressive wave travels) produces irreversible structural and physical changes in the minerals and rocks. The HEL is about 5–10 GPa for most minerals and rocks (Koeberl and Anderson, 1996). Rarefaction waves, unloading from high pressure, immediately follow the shock waves. Most of the kinetic energy of the projectile transfers to the target during this stage. Due to very high pressures, which reach hundreds of GPa, the projectile and part of the target may either vaporise or melt upon uploading.

During the excavation stage, the crater, which exceeds the projectile size, opens. The excavation stage lasts for seconds or even a few minutes, depending on the size of the impact. A shock wave propagates radially into the target, distributing the kinetic energy from the projectile over a steadily increasing mass of target material. The average energy density in the shocked material and the shock and particle velocity decrease as the shock front expands in the target (Gault *et al.*, 1968). The shock wave and the following rarefaction initiate an excavation flow that opens the structure. While part of the target ejects outwards and forms an ejecta blanket around the structure, part of it injects into the target and forms pseudotachylitic or fragmental dikes. The excavation stage ends with the formation of a transient cavity — the roughly parabolic cavity generated directly by the cratering flow field prior to any modification by slumping and dynamic rebound (Croft, 1985).

During modification, gravity causes broken rock particles, shocked debris and part of the rim to slide onto the floor of the transient cavity. In the centre of simple structures, a lens of allochthonous breccias forms, causing the structure to decrease in depth. At the same time, the rim walls collapse, and the structure widens. Complex structures develop from a bowl-shaped transient crater by gravitational collapse. The formation of the central uplift starts before the debris slides back into the transient cavity. Modelling and observations show that

allochthonous breccias fill mostly the circular moat between the central uplift and the rim (Melosh, 1989). The rims of complex craters collapse by landslides associated with block faulting that transports large amounts of material from the unstable crater rim to the interior of the structure. In very large structures, the central uplift may exceed its stability and collapse after an initial rise. Consequently, a ring of peaks forms in the central part of the structure.

Most of the processes that produce gravity and magnetic anomalies over impact structures occur in the second (excavation) and third (modification) stage of cratering. The post-impact processes, *e.g.*, cooling of the structure with associated hydrothermal processes, possible erosion or sedimentary infilling and regional tectonics, also influence gravity and magnetic signatures of impact structures. In the following, the processes responsible for geophysical anomalies are described separately for gravity and magnetics. The effects of various processes on gravity and magnetic data are summarised in Tables 1 and 2.

Gravity

During excavation, a supersonic shock wave propagates radially into the target rocks from the impact point. The shock front, representing an abrupt rise in pressure, the particle velocity, the enhanced density and the internal energy, travels and weakens away from the impact centre. The shock crushes the pores, vaporises any water in the pores and transfers heat to the target material. Strong shocks deposit sufficient heat to melt or vaporise rock. The high pressure in a shock wave is relieved by the propagation of tensile rarefaction waves that start from free surfaces into the already shocked material. A rarefaction wave is equal in strength to the shock wave but has the opposite sign. The sum of the pressure in the two waves is zero on the free surface, but at some distance below the surface, rarefaction waves arrive later, developing strong compression and tensile phases (Melosh, 1989). Rocks beneath the crater floor and in the nearest surroundings (autochthonous breccias) are fractured mainly by tensile rarefaction waves. However, in the central part of the excavating structure, where shock exceeds HEL, the fracturing is also produced directly by the shock wave.

The presence of fractures increases porosity, which reduces the density of the material and thus gives rise to a negative residual gravity anomaly above the structure. Fractures develop within rocks between different minerals as well as within grains. Shock-metamorphic features (Koeberl, 1997), the formation of shatter cones (at shock pressures of 2–30 GPa), planar fractures and planar deformation features (PDF's; 5–45 GPa), and diaplectic glasses (30–40 GPa) cause a decrease in density. For example, the density of quartz drops with increasing shock from 2650 to 2190 kgm⁻³ if glass is formed. According to Stöfler (1974), the density changes are abrupt and take place at ~15 GPa (formation

Table 1. A list of processes producing and modifying gravity anomalies of impact structures

Process	Effect	Impact gravity signature
Stage: Impact excavation		
Propagation of shock and rarefaction waves	• Fracturing of target rocks and minerals	Negative
	• Formation of high-pressure polymorphs occurring mainly in allochthonous breccias	Positive
	• Mineralogic diaplectic changes in breccias	Negative
	• Melting	Negative
	• Uplift of the crater rim wall	Surrounding positive
Elastic rebound (begins).	• Rise of the central uplift (complex structures only)	Central positive
Stage: Impact modification		
Elastic rebound (completes)	• Rise of the central uplift	Central positive
Debris falling and sliding into the transient cavity	• Formation of allochthonous breccias	Central negative
	• Formation of melt sheets	Negative
Stage: Post-impact development		
Hydrothermal processes	• Formation of new minerals in pores and fractures of impact breccias	Reduced central negative or positive anomaly
Sedimentation	• Infill of topographic depression	Negative
	• Coverage of the whole structure	Screened
	• Compaction	Reduced
	• Metamorphism	Reduced or removed
Erosion	• Removal of impact stratigraphies	Reduced or removed

of intensive PDF's), at ~30 GPa (conversion of quartz to a diaplectic glass), and 42.5 GPa (the beginning of melting). On the other hand, the density of high-pressure polymorphs is higher than their parent-minerals. The most common polymorphs of quartz are coesite (which develops at pressures >12 to 15 GPa) and stishovite (>30 GPa) with densities of 2896 and 4290 kgm⁻³, respectively. Koeberl (1997) has also listed jadeite (3240 kgm⁻³), which forms from plagioclase (2360–2760 kgm⁻³), majorite (3670 kgm⁻³) from pyroxene (3200–3520 kgm⁻³), and ringwoodite (3900 kgm⁻³) from olivine (3220–4340 kgm⁻³). However, these polymorphs are usually rare and, therefore, contribute little to observable gravity anomalies, because their effect is overwhelmed by fracturing.

Shock and rarefaction waves, weakening with time and distance, produce fewer fractures away from impact centre. Subsurface fracturing extends out of the crater beyond the crater rim (Zenchenko and Tsvetkov, 1999), but generally, has relatively little effect on the gravity anomaly (Gurov and Gurova, 1982).

The phenomena of increasing density and decreasing porosity with depth have been documented in measurements from drillings in Ries (Ernstson and Pohl, 1974), Siljan (Dyreljus, 1988), Iso-Naakkima (Pesonen *et al.*, 1996), Puchezh-Katunki, Russia (Masaitis, 1999) and Kärddla (Paper II). In the 55 km wide Siljan structure, low densities persist to depths of 5 km. The K1 drillcore at the centre of the Kärddla crater reveals an impact-generated trend of gradual changes in all petrophysical properties of autochthonous granites. For example, relatively high porosity (~10 %) at 567 m depth decreases to ≤5 % at 815 m depth — still higher than that of unshocked granites (0.9 %). In this interval the wet density increases from 2350 to 2520 kgm⁻³ and the grain density increases from 2500 to 2600 kgm⁻³, which is lower than the grain density of the unshocked target (~2650 kgm⁻³), and could be caused by increased amount of closed pores and planar features.

The crater rim is composed of uplifted pre-impact rocks and ejected debris. The rim forms during the excavation stage when strong horizontal compressive forces push outward from the crater's centre. Structural rim uplift is fractured and injected by subhorizontal breccia dikes (Melosh, 1989). The crater rim usually gives rise to a positive gravity anomaly due to uplift of deeper and denser lithologies. In uneroded structures, the positive gravity effect is masked by porous ejected debris overlying the uplift. In Kärddla crater (Paper II), formed in a shallow sea, the ejecta cover was mostly removed by tsunami waves and marine erosion. The uplifted subsurface crystalline rim of Kärddla crater produces circular and positive (up to 2 mGal) gravity features surrounding the central low (–3 mGal).

The central uplift (or the central peak ring) of complex craters forms by elastic rebound. The uplift starts during the excavation of the rim wall before infill. Therefore, the central uplift is composed of deformed and fractured rocks that originally underlay the transient crater and is uplifted by distances comparable to the depth of the transient cavity. It is very likely that denser crustal ma-

terial is uplifted, especially in large impacts. Therefore, uplift usually produces a positive gravity anomaly in the central part of the structure. Pilkington and Grieve (1992) have listed 17 terrestrial structures with a distinct central gravity high. There are at least four new additions to this list (Marquez Dome, Wong *et al.*, 1993; Mount-Toodina, Australia, Plescia *et al.*, 1994; Chicxulub, Mexico, Espindola *et al.*, 1995; and Mjøltnir, Tsikalas *et al.*, 1998). Grieve (1988) has noted that during rebound, particle velocities in the central portion are directed upward and inward, leading to a state of compression in the central uplift. This process reduces initial impact induced porosity and further increases the density relative to the surrounding autochthonous breccias. It has also been observed in Kärddla data, where the fractured granites at the top of the central uplift are denser than those at the unshocked crater basement (Paper II). However, the central uplift in Kärddla produces no observable gravity anomaly probably due to its great depth and small size.

After the excavation flow has opened the transient crater, shocked debris, broken pieces of rock, impact melt and a portion of the rim moves back into the cavity simultaneously with its collapse. A lens (simple structures) or ring-shaped body (complex structures) of allochthonous breccias, which contain a porous mixture of differently shocked target material with a possible addition of melt, forms. Allochthonous breccias cause most of the negative gravity anomaly due to their high porosity and low density, with respect to target rocks, and due to subsurface nature. High density contrast between allochthonous breccias and crystalline target rocks has been observed in several terrestrial impact structures of $\sim 400 \text{ kgm}^{-3}$ in Lappajärvi and Mien, Sweden, structures (Elo *et al.*, 1992; Henkel, 1992), 330 kgm^{-3} in Jänisjärvi, Russia (Dabizha and Feldman, 1982), and 240 kgm^{-3} in Kärddla (Paper II).

At shock pressures $>45 \text{ GPa}$ minerals start to melt by fusion. At higher pressures ($>60 \text{ GPa}$) whole rock melting takes place (Koeberl and Anderson, 1996). At these pressures breccias with melt clasts (*e.g.*, suevitic breccias), impact melt breccias and/or separate impact melt bodies within the allochthonous breccias will form. The density contrast between impact melts and surrounding rocks is usually not as great as between allochthonous breccias and the target. For example, the impact melt in Lappajärvi is only slightly less dense ($2520\text{--}2600 \text{ kgm}^{-3}$) than the crystalline target rocks ($\sim 2700 \text{ kgm}^{-3}$; Elo *et al.*, 1992). In Jänisjärvi, the density difference between impact melt and surrounding gneisses is $\sim 240 \text{ kgm}^{-3}$ (Dabizha and Feldman, 1982). Therefore, impact melt gives rise to the negative gravity anomaly, but it is less than that produced by the same volume of meltless allochthonous breccias. In Paper I of this work, the authors theorize that the negative gravity of the Bosumtwi structure is weaker in the northern part of the structure due to possible high content of impact melt breccias. Future shipborne gravity surveys will show if this theory is correct.

In the presence of water, local post-impact hydrothermal processes may be active due to the impact-related thermal effect. Resulting, hydrothermal ore deposits occur at Siljan (Pb, Zn, and Ag sulfides; Johansson, 1984) structure.

Kinnunen and Lindqvist (1998) have reported post-impact, low temperature hydrothermal agate nodules, chlorite, mordenite, smectite and kaolinite as vesicle fillings in melt rocks of the Sääksjärvi meteorite impact structure in Finland. The influence of hydrothermal activity on the porosity, density, and gravity field depends on the size of the structure, presence of water, chemical composition of the target and projectile. Hydrothermal activity most likely slightly decreases the negative amplitude of previously formed structures if partial or full closure of impact-produced fractures and pores by secondary minerals takes part.

Once the impact structure has been formed in the sedimentary basin, the topographic depression starts to fill with low-density, post-impact sediments, adding to the central negative gravity anomaly. The post-impact sediments may bury the entire structure (*e.g.*, Kärdla; Puura and Suuroja, 1992). If so, the gravity features will become screened by the increasing overlying sediments. Moreover, continuous sedimentation (or burial under ice sheets during glaciation) increases lithostatic pressure, which compacts underlying rocks (including impactites) and reduces the amount of pores and fractures, which, in turn, reduces the amplitude of the gravity anomaly. The depth at which fractures are essentially closed by lithostatic pressure is 8 km (Perrier and Quiblier, 1974). Metamorphic processes or tectonism may further modify or even obliterate impact features in rocks, as well as the gravity anomalies of impact structures, *e.g.* Sudbury (McGrath and Broome, 1994), and Vredefort (Henkel and Reimold, 1998).

Little research has been attempted to estimate changes in the gravity anomaly of impact structures as a function of erosion (*e.g.* Pesonen *et al.*, 1993). Pilkington and Grieve (1992) were the first to point out a decreasing trend in the amplitudes of the negative gravity anomalies caused by progressive erosion. In Paper III, the effect of erosion on the gravity anomaly of a 30 km wide hypothetical complex structure in Precambrian target rocks was investigated. The major effect of erosion is a pronounced decrease in the amplitude of the negative anomaly with only a minor change in anomaly diameter. The amplitude of the central positive anomaly due to central uplift also decreases with erosion, although not as significantly as the main anomaly. The diameter of the central positive gravity anomaly is mainly unaffected by erosion.

Magnetics

Several impact-related processes are able to create new and to modify or even destroy pre-existing magnetisations. However, the study of the magnetic effects of impacts entails many variables, such as induced magnetisation, which depends on the magnetic susceptibility of the rock and on the direction and

Table 2. A list of processes producing and modifying magnetisations in impact structures

Process	Effect
Stage: Impact excavation	
Propagation of shock waves	<ul style="list-style-type: none"> • Shock demagnetisation • Shock magnetisation (SRM) • Mineralogical changes, production of new magnetic minerals, or destruction of magnetic minerals • Uplift of the crater rim wall may move deeper magnetic rocks upwards, especially in complex targets
Elastic rebound (begins)	<ul style="list-style-type: none"> • Rise of the central uplift may move deeper magnetic rocks upwards (complex structures only)
Stage: impact modification	
Elastic rebound (completes)	<ul style="list-style-type: none"> • Rise of the central uplift may move deeper magnetic rocks upwards (complex structures only)
Debris falling and sliding into the transient cavity	<ul style="list-style-type: none"> • Pre-impact and impact-caused magnetisations obtain random orientation and thus cancel each other in the allochthonous breccias
Cooling below Curie point (begins)	<ul style="list-style-type: none"> • Impact breccias and melts acquire thermoremanent magnetisation (TRM) which may wipe out all previous remanences
Stage: Post-impact development	
Cooling below Curie point (completes)	<ul style="list-style-type: none"> • Impact breccias and melts acquire thermoremanent magnetisation (TRM)
Oxidation	<ul style="list-style-type: none"> • Nature of primary ferromagnetic minerals changes
Hydrothermal alteration	<ul style="list-style-type: none"> • Produces an overprint by chemical remanent magnetisation (CRM) • Destroys pre-existing magnetic phases
Sedimentation	<ul style="list-style-type: none"> • Fills the topographic depression with sediments that are usually non-magnetic • Coverage of the whole structure screens the impact magnetic signatures
Erosion	<ul style="list-style-type: none"> • Removal of impact stratigraphies reduces magnetic anomalies

intensity of the present geomagnetic field, and the natural remanent magnetisation (NRM). The latter marks the geomagnetic field at the time of, or subsequent to, impact, and plays a great role in producing magnetic anomalies, especially if dominates the induced magnetisation. A few minerals, notable magnetite, hematite and pyrrhotite, are able to carry significant magnetisations (for details, see *e.g.* Butler, 1992). Although very small FeNi particles, magnetic constituents of the projectile, are common in impactites (*e.g.* Lappajärvi, Fregerslev and Carstens, 1976), their contribution to magnetic anomalies is negligible due to their very small volumetric amount.

Laboratory and nuclear site experiments (*e.g.* Hargraves and Perkins, 1969; Nagata, 1971; Pohl *et al.*, 1975; Cisowski and Fuller, 1978; Pesonen *et al.*, 1997) have shown that shock waves can cause appreciable changes in the magnetic properties of rocks. Depending on the magnitude of the ambient field, shock intensity and magnetic hardness of the magnetic minerals, rocks may either acquire a shock remanent magnetisation (SRM) or lose some of their magnetisation (shock demagnetisation).

Hargraves and Perkins (1969) tested tuff from around of an underground nuclear explosion at the Nevada Test Site, USA. The orientation of NRM of most of the samples was close to that of the local earth's magnetic field, suggesting remagnetisation due to the shock. Pohl *et al.* (1975) carried out magnetising and demagnetising experiments, where relatively low stresses (up to 1 GPa) were applied to basalt with and without the ambient magnetic field. In the magnetising experiments, SRM was produced proportional to the intensity of the applied magnetic field and increased with the applied peak stress. SRM was always parallel to the applied magnetic field. The longitudinal SRM (achieved when the applied stress was parallel to the ambient magnetic field) was slightly higher than the transverse SRM (stress and magnetic field were perpendicular). The produced SRM was unstable with respect to the alternating field demagnetisation, but increased when higher stress was applied. This observation concurs with later investigations by Cisowski *et al.* (1976) and Pesonen *et al.* (1997), who demonstrated the increase of the coercive force and coercivity of remanence with increasing shock at higher stresses (up to 35 GPa). The mechanism of the magnetic shock hardening is ascribed to changes in domain size or movements of domain walls in multidomain ferromagnetic minerals, production of lattice defects and/or changes in crystallographic anisotropy of the magnetic grains.

The presence of SRM in natural conditions has been reported only in the Slate Island impact structure, Canada (Halls, 1979). In this case, the SRM is shown to have been acquired during impact and is restricted to low-coercivity grains of magnetite. On the other hand, remanent magnetisation may also be destroyed by shock (shock demagnetisation). As noticed by Cisowski and Fuller (1994), the role of demagnetisation is more important for the relatively weak magnetic field intensity, as on earth. Hargraves and Perkins (1969) tested samples from Meteor Crater, and the Nevada atomic test site. They found that shock

pressure may have a substantial demagnetising effect on the NRM of rocks with magnetite or titaniferous magnetite as the dominant ferrimagnetic constituent.

Scott *et al.* (1997) reported magnetic models of four Canadian impact structures: West Hawk, Deep Bay, Clearwater East and Clearwater West, and interpreted the observed negative magnetic anomalies to be partly produced by basement rocks below the impact structures. They attribute the zone of reduced magnetisation to the partial demagnetisation of magnetite by the impact-induced stress. However, the reversed magnetisation of impactites may be the reason in some of these structures. Jelenska (1975), Cisowski and Fuller (1978) and Pesonen *et al.* (1997) have reported a shock-produced decrease in the magnetic susceptibility in natural rocks.

Shock waves may produce mineralogical changes responsible for the nature of magnetisation of impact and target rocks. For example, biotite, which is paramagnetic, may decompose to pyroxene, alkali feldspar, silicate glass and ferromagnetic iron oxides (Feldman, 1995), and give rise to the magnetisation of the rock. Granovsky *et al.* (1979) have shown that the degree of oxidation and, therefore, decomposition of biotite increases with increased shock. Iron oxides, which acquire magnetisation in the direction of the magnetic field at the time of decomposition (chemical remanent magnetisation, CRM) and during cooling below the blocking temperatures (thermochemical remanent magnetisation, TCRM), may occur in impact breccias. This may be the case in the Bosumtwi impact structure (Paper I), where the northwestern part of the target is iron- and biotite-rich (Koeberl *et al.*, 1998). It is possible that the melt-suevites acquired their NRM directions by post-shock thermochemical processes and that the carrier of this TCRM is newly-formed magnetite subsequent to biotite decomposition. Chao (1968) found amphibole from the Ries structure that has also been oxidised into magnetite and to poorly crystalline or amorphous material. Decomposition of clinopyroxene into an aggregate of amphibole, plagioclase, clinopyroxene, and magnetite is reported from Puchezh-Katunsky structure (Feldman, 1995).

The formation of the central peak or peak ring brings the compressed and hot target material near the earth's surface. The uplift decreases the distance from the measurement to the source, and, therefore, amplifies the magnetic response of the uplift. This is particularly true when an impact crater is formed at the complex target composed of less magnetic sedimentary rocks and more magnetic crystalline basement. For example, the central magnetic anomaly of the Haughton structure, Canada, is produced by high remanent magnetisations (Q up to 50) in strongly shocked and uplifted gneissic rocks. Pohl *et al.* (1988) suggest that high NRM of the central uplift at Haughton is due to thermoremanent magnetisation (TRM, see below). The uplifted rim wall may also give rise to a magnetic anomaly. For example, an uplifted crystalline rim inside weakly magnetic sediments gives rise to circular positive magnetic features around the Kärddla crater (Paper II).

During the modification stage, debris sliding down from rim walls, falling from the sky or brought into the structure by the tsunami wave (in marine structures only), are all free to rotate until deposited to form an allochthonous breccia unit. This, theoretically, should produce a random orientation of pre-impact and/or impact-induced magnetisation vectors in these breccia deposits (Beals *et al.*, 1963). This randomising process should therefore yield a weak magnetic signature. The situation applies only to relatively small structures, where the temperature does not rise above the Curie-points of the magnetic carriers (*i.e.*, when TRM is absent). This hypothesis is testable because it resembles the conglomerate test in palaeomagnetism (Butler, 1992).

Impact melt rocks or heated impact breccias may acquire TRM in the direction of the magnetic field when cooled below the Curie temperatures of the magnetic minerals, *e.g.*, Manicouagan (Larochelle and Currie, 1967), Lappajärvi (Pesonen *et al.*, 1992). The near-surface melt layers cool relatively quickly, but the cooling time of the buried melt pockets may be sufficient to acquire magnetisation in a direction different from the magnetic field at the time of impact due to secular variation of the earth's magnetic field. The cooling time for melt layers inside the allochthonous breccia lens of 15 km-wide craters is about 100,000 years (Melosh, 1989). The composition and magnetic properties of target rocks largely control the content and magnetic contrasts of impactites, and, therefore, the magnetic anomaly. High magnetisation is observable when ferrimagnetic phases existed in the target rocks or were created by oxidation (see above), as in impactites of the Mien and Dellen structures (Henkel, 1992). The observed magnetic anomalies of impact structure are often due to remanent magnetisation. For example, high Koeningsberger ratios of breccias and impact melts are observed at Mien ($Q \sim 10$; Stanfors, 1973) and Haughton ($Q > 10$; Pohl *et al.*, 1988). In the Vredefort structure, impact-derived temperatures were sufficient to completely remagnetise the entire basement of the structure. Very high Koeningsberg values (> 30 ; Hart *et al.*, 1995) are attributed to the ultrafine ($< 5 \mu\text{m}$) magnetite particles formed along shock-induced PDF's (Hart and Cloete, 1999).

Impact-induced magnetic signatures can be modified and obliterated by a whole range of geological processes. Alteration may produce a chemical remanence magnetisation (CRM) or destruct pre-existing magnetic phases. Post-impact oxidation caused by circulating water in cracks and fractures may lead to conversion of magnetite to hematite with lower remanent magnetisation intensity, *e.g.* Siljan (Elming and Bylund, 1991). If new magnetic carriers are produced and the magnetic field is present, the impactites may acquire magnetisations sufficient to influence the local magnetic field over the structure. In the Lake St. Martin impact structure, Canada (Coles and Clark, 1982) a strong and stable remanence magnetisation gives rise to the intensive magnetic anomaly. This magnetisation is proposed to be chemical due to extensive post-impact alteration of mafic silicates. Steiner and Shoemaker (1994) have reported two-polarity magnetisation of the Manson impact breccias. They measured samples

that carry a secondary reversed polarity magnetisation (by hematite) that is roughly antipodal to the characteristic normal polarity magnetisation (by magnetite). The presence of the reversed CRM suggests impact near a polarity reversal such that the impact-induced hydrothermal activity occurred in the succeeding reversed polarity interval.

Burial of an impact structure by weakly magnetic sediments also contributes to a reduced magnetic signature. Analogous to gravity, all magnetic features are weakened by an increasing thickness of overlying sediments. Erosion and tectonism also have destructive effects on impact-induced magnetic anomalies. Paper III demonstrates that the impact-derived magnetic signature decreases markedly after the removal of allochthonous breccias and melted rocks.

GRAVITY AND MAGNETIC MODELLING OF IMPACT STRUCTURES: CASE STUDIES

Gravity and magnetic modelling are used to simulate the internal structure of impact craters. It has been successfully used, *e.g.* to describe the central uplift in the Manicouagan structure (Sweeney, 1978), to investigate density and magnetic distribution in Vredefort (Henkel and Reimold, 1998), to determine the shape of the causative body for the magnetic anomalies in Manicouagan and Lake St. Martin structures (Coles and Clark, 1978; 1982), and to investigate the extent of autigenic brecciation affected by oxidation in Tvären, Sweden (Ormö and Blomqvist, 1996).

To construct a realistic geophysical model of an impact structure, knowledge of the processes that are able to change structures and properties during and after the impact, is necessary. In addition, geophysical field data and sufficient petrophysical data of impactites, as well as pre- and post-impact rocks are needed. To speed up the modelling process, proper computer software is recommended.

Nowadays, large sets of gravity and magnetic field data are possessed by progressive national geological surveys. However, these data sets are very different in their scale and precision. Modelling, especially for smaller structures, sometimes requires new linear or areal (in the case of complicated regional field) measurements.

Gravity analysis presumes density measurements of impact-influenced, target and post-impact rocks. These measurements may be taken from surface outcrops and/or drillcores. To simulate natural conditions, wet densities (density of a water-saturated rock) are typically used in gravity modelling. In larger structures, seismic methods and litho-stratigraphic information may be required to estimate density and subsurface geometry of deeper lithologies. Magnetic modelling requires data of both induced and remanent magnetisations of different rock types within and outside the crater. In modelling software, induced magnetisation is expressed by magnetic susceptibility (χ), intensity (H), and direction (D and I) of the magnetic field at a particular site. The contribution of remanent magnetisation is incorporated by the direction and intensity of NRM measured from oriented rock samples.

Present-day computer software allow rapid calculation of the gravity and magnetic responses of the model bodies along profiles measured in nature or obtained from geophysical maps. In forward modelling the gravity and/or magnetic response curves of the model with specified physical properties are calculated. Changing the model parameters (geometry and physical properties) the response curves that match with the measured curves are found. This is generally done by trial and error or using optimisation techniques. However, there are an infinite number of theoretical solutions, for an observed gravity or

magnetic anomaly. To decrease the ambiguity and to find the most reasonable model, reliable petrophysical and geological data are needed.

Most of the software programmes allow 2.5-dimensional modelling of gravity and magnetic sources together or separately. The author used GravMag (Pedley, 1991) in Paper II, GMM (GeoVista AB, 1994), and ModelVision (Encom Technology Pty Ltd, 1998) in Papers I and III. GravMag allows modelling of several polygons in the vertical plane. For each polygon, the third dimension is given by entering the half strike length, and the edges in the strike direction are vertical. The profile is always perpendicular to the strike direction and cuts the polygonal body exactly in its centre. GMM has two advantages over GravMag. First, each body may be at an arbitrary angle to the profile, with any strike and lateral offset. Second, the offset prisms may be created in relation to the profile. These features allow inclusion of the influence of anomalous bodies beyond the impact structure. The disadvantage of both software is that the bodies have to be quadrangular in the horizontal plane. For circular structures, this feature produces slight underestimations in the modelled sizes of polygons.

In the case of Kärddla (Paper II), the NE-SW gravity and magnetic profiles were interpolated from local gravity and magnetic data. The geophysical model, consisting of 10 prisms with polygonal cross section, describes simultaneously gravity and magnetic effects of the structure. First, a gravity model based on the density measurements, drillings and cross-section by Puura and Suuroja (1992) was created. Second, the model was modified to include magnetic effects in order to find a fit between the observed and calculated magnetic curves. For two bodies (post-impact sediments and allochthonous impact breccias) observed magnetic susceptibilities were used. The other bodies, such as autochthonous breccias and the rim wall, were divided into polygons with variable susceptibilities. Because the remanent vectors of unoriented drill-core samples could not be reoriented with viscous remanent magnetisation technique (*e.g.* Järvelä *et al.*, 1995) and due to the lack of of the NRM directions, only the induced magnetisation was used to describe the magnetic properties of different polygons. This technique produces errors in the shapes of polygons, especially those that have high magnetisations and are closer to the surface. Due to relatively low NRM of sediments and randomised NRM vectors in allochthonous breccias, the effect of remanence is significant only in the rim wall area of the Kärddla model. The model illustrating approximately the shapes of different impacted and post-impact bodies, producing the circular negative gravity and magnetic anomalies surrounded by positive anomalies.

ModelVision is a geophysical modelling package for the display, analysis and simulation of magnetic and gravity data. It allows the display of field measurements and the creation of models in the horizontal plane or along user-defined profiles. It allows to calculate a response curve or field for a polygon, prism, tabular body, sphere, ellipsoid, or horizontal cylinder with user-defined properties, geometry and location.

To investigate the distribution of buried magnetic material inside the Bosumtwi impact structure (Paper I), several 50 m thick prismatic bodies with horizontal upper and lower surfaces, and with vertical sides, were used. In the model, the uppermost prism was located at the depth of 200 m, based on the scaling by Grieve and Pesonen (1992), and Grieve and Robertson (1979). The Koeningsberger ratio and remanence directions of ejected impact breccias were assigned to the bodies. However, assuming that impactites inside the structure contain either more magnetic material or were originally more magnetic than ejecta rocks, ten times higher magnetisations were used. It is possible that ejected breccias have lost some of their magnetisation due to weathering on the surface. Identical magnetic properties were assigned to all prisms. Therefore, the prisms form a homogeneous structure with a complicated shape in plan view, and maximum thickness of 400 m at the northern part of the structure. In cross-sections, the model can be described as a half-lens. It is bounding the possible location of the central uplift on the north, but also existing on the western and eastern side of the uplift. The modelled structure was defined as a melt-rich suevite lens. The relative freshness of the crater, the lack of post-impact deformation and significant erosion suggest that the impact-produced allochthonous rocks were deposited symmetrically around the central uplift. Thus, breccias should also fill the southern part of the crater, but without high magnetisation. The biotite-rich granite intrusions, exposed north-west of the lake (Koeberl *et al.*, 1998), may have acquired high magnetisations due to magnetite produced from biotite during impact excavation (Table 2). It is also possible that the southern part of the structure is filled by great landslides of relatively less-magnetic metasediments that were part of a mountain range at the southern side of the lake.

ModelVision package was also used to model density and magnetisation contrasts of a hypothetical impact structure 30 km in diameter, and to investigate the changes in the gravity and magnetic anomalies as a function of erosion (Paper III). The first model consists of several symmetrical vertical prism bodies with horizontal upper and lower surfaces, vertical sides, and 16 corner points on a plan view. The diameter of prisms decreased stepwise downward until vanishing at the depth of 7 km. The thickness of each prism was 500 m, except the two prisms describing the allochthonous impact breccia with thicknesses of 500 and 300 m, and the prism of the impact melt, which had a thickness of 200 m. The morphometric parameters of the model followed calculations by Croft (1985) and Melosh (1989). Physical properties of different layers were assigned according to literature values of typical Precambrian background rocks and impactites in Fennoscandia. Density variations included the fracturing effect of target rocks, allogenic brecciation, impact melting, and rise of the central uplift and post-impact sedimentation. In the magnetic model, NRM was set in the direction of the time of the impact (assumed to be 1.93 Ga) in Fennoscandia. The same time was assigned to the direction of TRM of impact melts and allochthonous breccias, whereas the autochthonous breccias were assumed to

acquire a SRM in the same ambient direction as TRM, and detrital remanence magnetisation of post-impact sediments. The magnetic model also included a rise of more magnetic basement rocks due to the central uplift.

The same model was used for gravity and magnetic exercises. However, because the processes affecting magnetics are different from gravity, the magnetic properties of each structure should be studied individually and separately from the gravity model. To confirm density and magnetic prisms, we assumed the following conditions: (i) the TRM was active only in the impact melt sheet, which cooled immediately after the impact, and (ii) post-impact physical-chemical processes did not substantially affect physical properties of the rocks.

We then calculated the gravity and magnetic anomalies of the model to simulate the initial pre-erosional situation. Gravity and magnetic anomalies were then calculated stepwise for models, where the topmost 1 km thick layer was successively removed and the remaining prisms represent subsequent erosion levels from 1 km to 7 km depth. The model showed that the amplitude and diameter of the negative gravity anomaly significantly decreases due to erosion. Because the decrease is much stronger in amplitude, the erosion progressively flattens the gravity signature of an impact structure. Moreover, we observed that erosion enlarges the gravity response of the central uplift with respect to the total anomaly. The removal of a strongly remanent magnetised impact melt body by erosion significantly decreases the amplitude of the magnetic anomalies. The erosion modelling was tested with real data of impact structures where the erosion has been estimated on geological grounds.

CONCLUSIONS

Various geophysical methods, used in impact cratering research, can supply an internal view of a buried impact structure. These methods have often provided the first clue of an impact origin of a structure. Moreover, palaeomagnetic techniques may provide an age estimate of an impact event. Geophysical data are, however, often unambiguous and do not prove the impact origin.

Gravity anomalies over impact craters depend on the (i) size and morphology of the structure, (ii) the density contrast between impacted and surrounding target rocks, and (iii) the depth of the structure. Most impact structures show a negative gravity anomaly. If filled with relatively denser post-impact material, tectonised and/or deeply eroded, the structure may show positive gravity effects. Complex impact structures may also reveal gravity highs due to central uplift. Gravity anomalies over impact structures are produced by different processes during cratering. These include:

- fracturing and brecciation of target rocks and minerals (major negative effect),
- formation of high-pressure polymorphs (minor positive effect),
- mineralogic diaplectic changes (minor negative effect),
- uplift of the crater rim wall (positive effect surrounding the central negative anomaly),
- formation of allochthonous breccias and melt sheets (major negative effect).

Magnetic anomalies of impact structures depend on (i) the size and shape of the structure, (ii) the intensity and orientation of magnetisation of the impactites with respect to the surrounding target rocks, (iii) the ancient and present geomagnetic field, and (iv) the altitude (distance from measurement level to the source). Due to considerable variations in magnetisations of both impact-related and target rocks and due to the vector nature of magnetisations, magnetic anomalies over the impact structures are usually much more complicated than gravity anomalies. The principal characteristic of impact structures is weak magnetic relief, although high-amplitude, short-wavelength anomalies inside the overall magnetic low, near and above the central uplift may occur. If impact melt bodies with high remanent magnetisation are present inside the structure, the magnetic low may be locally broken by high amplitude anomalies. However, several proven impact structures show only positive magnetic features or show no observable impact-related magnetic signatures at all. Impact cratering may

- demagnetise pre-existing magnetisations (shock demagnetisation),
- produce shock magnetisation,
- cause mineralogical changes producing (or destroying) magnetic minerals,
- uplift the crater rim wall, as well as the central uplift and redistribute the target magnetisations,

- produce a random orientation of pre-impact and impact-caused magnetisations in the allochthonous breccias,
- give a rise to thermoremanent or thermochemical magnetisation.

A wide range of post-impact processes, such as hydrothermal alteration, sedimentation, erosion, metamorphism, tectonics, *etc.*, are able to overprint, mask, destroy or remove the specific impact-generated physical properties, and therefore change the geophysical anomalies.

Despite the relatively complicated nature of gravity and magnetic signatures, modelling is a very useful tool to investigate the internal structure of impact craters, especially buried craters. Modern computer software provides relatively rapid ways to estimate distribution of densities and magnetisations within a structure. However, to obtain a realistic model, sufficient amounts of petro-physical data of oriented samples from impactites, fractured target rocks and unaffected target rocks are needed.

ACKNOWLEDGEMENTS

I am thankful to my supervisors, Dr. Väino Puura and Dr. Lauri J. Pesonen, for their co-operation and support during my studies and for their critical review of the present thesis. Special thanks to the co-authors of my papers, Dipl. Eng. Seppo Elo, Dr. Christian Koeberl, and MSc. Kalle Suuroja, and to the reviewers. I also thank all my colleagues from the University of Tartu and Geological Survey of Finland for their generous scientific support. Geological Survey of Estonia and Geological Survey of Finland provided geophysical data at Kärddla and Bosumtwi structures, respectively. I thank my family and friends for the intellectual support during my studies.

Financial support for my studies and research has been supplied by Estonian Science Foundation, European Science Foundation, NorFa and Centre for International Mobility (CIMO).

REFERENCES

- Ackermann H.D., Godson R.H. and Watkins J.S., 1975. A seismic refraction technique used for subsurface investigations at Meteor Crater, Arizona. *Journal of Geophysical Research* 80, 765–775.
- Basilevsky A.T., Ivanov B.A., Florensky K.P., Yakovlev O.I., Feldman V.I., Granovsky L.V. and Sandovsky M.A., 1983. *Impact Craters on the Moon and Planets*. Nauka, Moscow, 200 pp.
- Beals C.S., Innes M.J.S. and Rottenberg J.A., 1963. Fossil meteorite craters. In: (eds. B.M. Middlehurst and G.P. Kuiper) *The Moon, Meteorites and Comets*. University of Chicago Press, Chicago, 235–284.
- Brandt D., Reimold W.U. and Durrheim R.J., 1994. Geophysical signature of the Pretoria Saltpan impact structure and a possible satellite crater. *Meteoritics* 29, 379–384.
- Brandt D., Reimold W.U., Franzen A.J., Koberl C. and Wendorff L., 1998. Geophysical profile of the Roter Kamm impact crater, Namibia. *Meteoritics & Planetary Science* 33, 447–453.
- Butler R.F., 1992. *Magnetic Domains to Geologic Terranes*. Blackwell Scientific Publications, Boston, 319 pp.
- Chao E.C.T., 1968. Pressure and temperature histories of impact metamorphosed rocks – based on petrographic observations. In: (eds. B.M. French and N.M. Short) *Shock Metamorphism of Natural Materials*. Mono Book Corp., Baltimore, 135–158.
- Cisowski S. and Fuller M., 1978. The effect of shock on the magnetism of terrestrial rocks. *Journal of Geophysical Research* 83, 3441–3458.
- Cisowski S. and Fuller M., 1994. Paleomagnetic record of impacts. *EOS, Transactions, American Geophysical Union* 75, 121.
- Cisowski S.M., Dunn J.R., Fuller M., YeeMing Wu, Rose M.F. and Wasilewski P.J., 1976. Magnetic effects of shock and their implications for lunar magnetism (II). *Proceedings of the Lunar Science Conference 7th*, 3299–3320.
- Coles R.L. and Clark J.F., 1978. The central magnetic anomaly, Manicouagan structure, Quebec. *Journal of Geophysical Research* 83, 2805–2808.
- Coles R.L. and Clark J.F., 1982. Lake St. Martin impact structure, Manitoba, Canada: Magnetic anomalies and magnetizations. *Journal of Geophysical Research* 87, 7087–7095.
- Croft S.K., 1985. The scaling of complex craters. *Journal of Geophysical Research* 90 (suppl.), C828–C842.
- Dabizha A.I. and Feldman V.I., 1982. The geophysical properties of some astroblemes in the USSR. *Meteoritika* 40, 91–101 (in Russian).
- Deutsch A. and Grieve R.A.F., 1994. The Sudbury structure: constraints of its genesis from Lithoprobe results. *Geophysical Research Letters* 21, 963–966.
- Dyrelius D., 1988. The gravity field of the Siljan ring structure. In: (eds. B.M. French and N.M. Short) *Deep Drilling in Crystalline Bedrock*, vol. 1: The Deep Gas Drilling in the Siljan Impact Structure, 85–94.
- Elming S.Å. and Bylund G., 1991. Paleomagnetism and the Siljan impact structure, central Sweden. *Geophysical Journal International* 105, 757–770.
- Elo S., Jokinen T. and Soininen H., 1992. Geophysical investigations of the Lake Lapajärvi impact structure, western Finland. *Tectonophysics* 216, 99–109.

- Encom Technology Pty Ltd., 1995. *ModelVision, Geophysical data display, analysis and modeling, Version 1.20*. Milson's Point, Australia, 212 pp.
- Ernstson K. and Pohl J., 1974. Some comments on the geophysical logging measurements in the Nördlingen 1973 research borehole. *Geologica Bavarica* 72, 81–90.
- Espindola J.M., Mena M., Delafuente M. and Camposenriquez J.O., 1995. A model of the Chicxulub impact structure (Yukatan, Mexico) based on its gravity and magnetic signatures. *Physics of the Earth and Planetary Interiors* 92, 271–278.
- Feldman V.I., 1995. The conditions of shock metamorphism. *Geological Society of America Special Paper* 293, 121–132.
- Fregerslev S. and Carstens H., 1976. Fe-Ni metal in impact melt rocks of Lake Lappajärvi, Finland. *Contributions to Mineralogy and Petrology* 55, 255–263.
- French B.M. and Short N.M., eds., 1968. *Shock metamorphism of natural materials*. Mono Book Corporation, Baltimore, 644 p.
- French B., Koeberl C., Gilmour I., Shirey S.B., Dons J.A. and Naterstad J., 1997. The Gardnos impact structure, Norway: Petrology and geochemistry of target rocks and impactites. *Geochimica et Cosmochimica Acta* 61, 873–904.
- Fudali R.F., 1979. Gravity investigation of Wolf Creek crater, western Australia. *Journal of Geology* 87, 55–67.
- Gault D.E., Quaide W.L. and Oberbeck V.R., 1968. Impact cratering mechanics and structures. In: (B.M. French and Short N.M., eds.) *Shock metamorphism of natural materials*. Mono Book Corporation, Baltimore, 87–99.
- GeoVista, 1994. *GMM gravity and magnetic modelling, Users manual*. Geovista AB, Luleå, 41 pp.
- Gersonde R. and Deutsch A., 2000. New field of impact research looks to the oceans. *EOS, Transactions, American Geophysical Union* 81, 223–228.
- Gersonde R., Kyte F.T., Bleil U., Diekmann B., Flores J.A., Gohl K., Grahl G., Hagen R., Kuhn G., Sierro F.J., Völker D., Abelman A. and Bostwick J.A., 1997. Geological record and reconstruction of the late Pliocene impact of the Eltanin asteroid in the Southern Ocean. *Nature* 390, 357–363.
- Gorter J.D. and Glikson A.Y., 2000. Origin of a late Eocene to pre-Miocene buried crater and breccia lens at Fohn-1, North Bonaparte Basin, Timor Sea: A probable extraterrestrial connection. *Meteoritics & Planetary Science* 35, 381–392.
- Granovsky L.B., Nikishina N.N., Sazonova L.V., Feldman V.I., Malysheva T.V. and Polyakova N.P., 1979. A study of biotites from allogene breccia of impact crater Jänisjärvi. *Proceedings of the Lunar and Planetary Science Conference, 10th*, 458–460.
- Grant J.A., Koeberl C., Reimold W.U. and Schultz H., 1997. Gradation of the Roter Kamm impact crater, Namibia. *Journal of Geophysical Research* 102, 16327–16338.
- Green R.W. and Chetty P., 1990. Seismic refraction studies in the basement of the Vredefort Structure. *Tectonophysics* 171, 105–113.
- Grieve R.A.F., 1988. The formations of large impact structures and constraints on the nature of Siljan. In: (eds. A. Bodnen and K.G. Eriksson) *Deep Drilling in Crystalline Bedrock, vol. 1, The Deep Gas Drilling in the Siljan Impact Structure, Sweden and Astroblemes*. Springer-Verlag, New York, 328–348.
- Grieve R.A.F. and Pesonen L.J., 1992. The terrestrial impact cratering record. *Tectonophysics* 171, 357–376.

- Grieve R.A.F. and Pesonen L.J., 1996. Terrestrial impact craters: their spatial and temporal distribution and impacting bodies. *Earth, Moon and Planets* 72, 553–591.
- Grieve R.A.F. and Robertson P.B., 1979. The terrestrial cratering record, 1, Current status of observations. *Icarus* 28, 212–229.
- Grieve R.A.F. and Shoemaker E.M., 1994. The record of past impacts on Earth. In: (ed. T. Gehrels) *Hazards due to comets and asteroids*. University of Arizona Press, Tuscon, 417–462.
- Grieve R.A.F., Garvin J.B., Coderre J.M. and Rupert J., 1989. Test of a geometric model for the modification stage of simple impact crater development. *Meteoritics* 24, 83–88.
- Gurov E.P., 1996. The group of Macha craters in Western Yakutia. *Lunar and Planetary Science XXVII*, 473–474.
- Gurov E.P. and Gurova E.P., 1982. Some regularities of the area spreading of fractures around El'gygytgyn crater. *Lunar and Planetary Science XIII*, 291–292.
- Halls H.C., 1979. The Slate Islands meteorite impact site: A study of shock remanent magnetization. *Geophysical Journal of the Royal Astronomical Society* 59, 553–591.
- Hargraves R.B. and Perkins W.E., 1969. Investigations of the effect of shock on natural remanent magnetism. *Journal of Geophysical Research* 74, 2576–2589.
- Hart R.J. and Cloete M., 1999. Impact-related magnetic rocks from the Vredefort impact structure. *Meteoritics & Planetary Science* 34, A50–A51.
- Hart R.J., Hargraves R.B., Andreoli M.A.G., Tredoux M. and Doucouré C.M., 1995. Magnetic anomaly near the center of the Vredefort structure: Implications for impact-related magnetic signatures. *Geology* 23, 277–280.
- Henkel H., 1992. Geophysical aspects of meteorite impact craters in eroded shield environment, with special emphasis on electric resistivity. *Tectonophysics* 216, 63–89.
- Henkel H. and Reimold E.U., 1998. Integrated geophysical modelling of a giant, complex impact structure: anatomy of the Vredefort Structure, South Africa. *Tectonophysics* 287, 1–20.
- Henkel H., Tiirmaa R., Fleetwood Å. and Blomquist G., 1996. Tor — en meteoritnedslagskrater i Härjedalen, bildad efter istiden. Kungliga Tekniska Högskolan, Institutionen för Geodesi och Fotogrammetri, Stockholm, 59 pp (in Swedish with English Summary).
- Jansa L.F., Pe-Piper G., Robertson P.B. and Friedenreich O., 1989. Montagnais: A submarine impact structure on the Scotian Shelf, eastern Canada. *Geological Society of America Bulletin* 101, 450–463.
- Järvelä J., Pesonen L.J. and Pietarinen H., 1995. On palaeomagnetism and petrophysics of the Iso-Naakkima impact structure, southeastern Finland. Open File Report Q19/29.1/3232/95/1, Laboratory for Palaeomagnetism, Dept. of Geophysics, Geological Survey of Finland, Espoo, 43 pp.
- Jelenska M., 1975. Stress dependence of magnetization and magnetic properties of igneous rocks. *Pure and Applied Geophysics* 113, 635–649.
- Johansson A., 1984. Geochemical studies of the Boda Pb-Zn deposit in the Siljan astrobleme, central Sweden. *Geologiska Föreningens I Stockholm Förhandlingar* 106, 15–25.
- Kearey P. and Brooks M., 1994. *An Introduction to Geophysical Exploration*. Blackwell Scientific Publications, Oxford, 254 pp.
- Kinnunen K.A. and Lindqvist K., 1998. Agate as an indicator of impact structures: An example from Sääksjärvi, Finland. *Meteoritics & Planetary Science* 33, 13–30

- Koeberl C., 1997. Impact cratering: The mineralogical and geochemical evidence. *Oklahoma Geological Survey Circular* 100, 30–54.
- Koeberl C. and Anderson R.R., 1996. Manson and company: Impact structures in the United States. *Geological Society of America Special Paper* 302, 1–29.
- Koeberl C. and Shirey S.B., 1993. Detection of a meteoritic component in Ivory Coast tektites with rhenium-osmium isotopes. *Science* 261, 595–598.
- Koeberl C., Reimold W.U., Blum J.D. and Chamberlain C.P., 1998. Petrology and geochemistry of target rocks from the Bosumtwi impact structure, Ghana, and comparison with Ivory Coast tektites. *Geochimica et Cosmochimica Acta* 62, 2179–2196.
- Laroche A. and Currie K.L., 1967. Paleomagnetic study of igneous rocks from the Manicouagan structure, Quebec. *Journal of Geophysical Research* 72, 4163–4169.
- Lehtinen M., Pesonen L.J., Puranen R. and Deutsch A., 1996. Karikkoselkä — a new impact structure in Finland. *Lunar and Planetary Science* XXVII, 739–740.
- Marechal M. and Chouteau M., 1990. A magnetotelluric investigation of the structural geology beneath Charlevoix Crater, Quebec. *Physics of Earth and Planetary Interiors* 60, 120–131.
- Masaitis V.L., 1992. Impact craters: Are they useful? *Meteoritics* 27, 21–27.
- Masaitis V.L., 1999. Impact structures of northeastern Eurasia: The territories of Russia and adjacent countries. *Meteoritics & Planetary Science* 34, 691–711.
- Masero W., Schnegg P.A. and Fontes S.L., 1994. A magnetotelluric investigation of the Araguainha impact structure in Mato Grosso-Goiás, central Brasil. *Geophysical Journal International* 116, 366–376.
- McGrath P.H. and Broome H.J., 1994. A gravity model for the Sudbury structure along the Lithoprobe seismic line. *Geophysical Research Letters* 21, 955–958.
- Melosh H.J., 1989. *Impact Cratering. A Geologic Process*. New York, Oxford University Press, 245 pp.
- Meri L., 1984. *Hõbevalgem*. Tallinn, Eesti Raamat, 216 pp (in Estonian).
- Milkereit B., Green A. and the Sudbury Working Group, 1992. Deep geometry of the Sudbury structure from seismic reflection profiling. *Geology* 20, 807–811.
- Millman P.M., Liberty B.A., Clark J.F., Willmore P. and Innes M.J.S., 1961. The Brent crater. *Publications of the Dominion Observatory, Ottawa* 24, 1–43.
- Mittlefehldt D.W., See T.H. and Hörz F., 1992. Projectile dissemination in impact melts from Meteor crater, Arizona. *Lunar and Planetary Science* XXIII, 919–920.
- Nagata T., 1971. Introductory notes on shock remanent magnetization and shock demagnetization of igneous rocks. *Pageoph* 89, 159–177.
- Ojamo H., Pesonen L.J., Elo S., Hautaniemi H., Koeberl C., Reimold W.U. and Plado J., 1997. The Bosumtwi impact structure, Ghana: International geophysical co-operation at the best. In: (eds. P. Kaikkonen, K. Komminaho and H. Salmirinne) *Sovelletun geofysiikan XI neuvottelupäivät*. Oulun yliopisto, Oulu, 10–11.
- Ormö J. and Blomqvist G., 1996. Magnetic modelling as a tool in the evaluation of impact structures, with special reference to the Tvären Bay impact crater, SE Sweden. *Tectonophysics* 262, 291–300.
- Pedley R.C., 1991. GRAVMAG — User Manual. Interactive 2.5 D Gravity and magnetic modelling Program. British Geological Survey, Keyworth, Nottingham (unpubl.).
- Perrier R. and Quiblier J., 1974. Thickness changes in sedimentary layers during compaction history: Methods for quantitative evaluation. *American Association of Petroleum Geologists Bulletin* 58, 507–528.

- Pesonen L.J., Marcos N. and Pipping F., 1992. Palaeomagnetism of the Lappajärvi impact structure, western Finland. *Tectonophysics* 216, 123–142.
- Pesonen L.J., Masaitis V. and Lindström M., 1993. Report on topic 4: Terrestrial craters, geophysics, economics and formations. In: (eds. A. Montanari and J. Smit) Post-Nördlingen Newsletter, Scientific Network of the ESF, 8–11.
- Pesonen L.J., Järvelä J., Sarapää O. and Pietarinen H., 1996. The Iso-Naakkima meteorite impact structure: Physical properties and paleomagnetism of a drill core. *Meteoritics & Planetary Science* 31, A105–A106.
- Pesonen L.J., Deutsch A., Hornemann U. and Langenhorst F., 1997. Magnetic properties of diabase samples shocked experimentally in the 4.5 to 35 GPa range. *Lunar and Planetary Science* XXVIII, 1087–1088.
- Pesonen L.J., Koeberl C., Ojamo H., Hautaniemi H., Elo S. and Plado J., 1998. Aero-geophysical studies of the Bosumtwi impact structure, Ghana. *Geological Society of America, Abstracts with Programs* 30, A–190.
- Pesonen L.J., Lahti M. and Kinnunen K.A., 1999. Meteorite impact structures — their economic importance and the role of geophysics. In: *Extended Abstract Book, EAGE 61st Conference and Technical Exhibition, Helsinki, Finland*. Paper 5–32, 4pp.
- Pilkington M. and Grieve R.A.F., 1992. The geophysical signature of terrestrial impact craters. *Reviews of Geophysics* 30, 161–181.
- Pilkington M., Jansa L.F. and Grieve R.A.F., 1995. Geophysical studies of the Montagnais impact crater, Canada. *Meteoritics* 30, 446–450.
- Pilon J.A., Grieve R.A.F. and Sharpton V.L., 1991. The subsurface character Of Meteor Crater, Arizona, as determined by ground probing radar. *Journal of Geophysical Research* 96, 15,563–15,567.
- Plado J. and Puura V., 1995. Gravity and magnetic signatures of differently eroded buried impact craters, calculated from Kärdla crater. *Annales Geophysicae* 13 (suppl. III), C741.
- Plado J., Henkel H. and Olofsson B., 2000. Geophysical studies at the Ilumetsa impact site. In: (eds. J. Plado and L.J. Pesonen) *Meteorite Impacts in Precambrian Shields. Programme and Abstracts, the 4th Workshop of the European Science Foundation Impact Programme, Lappajärvi-Karikkoselkä-Sääksjärvi, Finland, May 24–28, 2000*. Geological Survey of Finland and University of Helsinki, 86.
- Plescia J.B., Shoemaker E.M. and Shoemaker C.S., 1994. Gravity survey of the Mount Toodyna impact structure, South Australia. *Journal of Geophysical Research* 99, 13167–13179.
- Pohl J., Bleil U. and Hornemann U., 1975. Shock magnetization and demagnetization of basalt by transient stress up to 10 kbar. *Journal of Geophysics* 41, 23–41.
- Pohl J., Stoffler D., Gall H. and Ernst K., 1977. The Ries impact crater. In: (eds. D.J. Roddy *et al.*) *Impact and Explosion Cratering, Pergamon, New York*, 343–404.
- Pohl J., Eckstaller A. and Robertson P.B., 1988. Gravity and magnetic investigations in the Haughton impact structure, Devon Island, Canada. *Meteoritics* 23, 235–238.
- Puura V. and Suuroja K., 1992. Ordovician impact crater at Kärdla, Hiiumaa Island, Estonia. *Tectonophysics* 216, 143–156.
- Regan R.D. and Hinze W.J., 1975. Gravity and magnetic investigations of Meteor Crater, Arizona. *Journal of Geophysical Research* 80, 776–788.
- Reimold W.U. and Gibson R.L., 1996. Geology and evolution of the Vredefort Impact Structure, South Africa. *Journal of African Earth Sciences* 23, 125–162.

- Sander G.W., Overton A. and Bataille R.D., 1964. Seismic and magnetic investigation of the Deep Bay crater. *Journal of the Royal Astronomical Society of Canada* 58, 16–30.
- Scott R.G., Pilkington M. and Tanczyk E.I., 1997. Magnetic investigations of the West Hawk, Deep Bay and Clearwater impact structures, Canada. *Meteoritics & Planetary Science* 32, 293–308.
- Stanfors R., 1973. The Mien structure — A cryptoexplosion formation in the Fennoscandian basement. PhD. Thesis, Lund University, Sweden, 144 pp.
- Steiner M. and Shoemaker E., 1994. Two-polarity magnetization of the Manson impact breccias. *Geological Society of America, Abstracts with Programs* 30, A–190.
- Stöffler D., 1974. Deformation and transformation of rock-forming minerals by natural and experimental processes: 2. Physical properties of shocked minerals. *Fortschritte der Mineralogie* 51, 256–289.
- Sweeney J.F., 1978. Gravity study of great impact. *Journal of Geophysical Research* 83, 2809–2815.
- Tsikalas F., Gudlaugsson S.T., Eldholm O. and Faleide J.I., 1998. Integrated geophysical analysis supporting the impact origin of the Mjølner structure, Barents Sea. *Tectonophysics* 289, 257–280.
- Williams G.E., 1994. Acraman: A major impact structure from the Neoproterozoic of Australia. In: (eds. B.O. Dressler, R.A.F. Grieve and V.L. Sharpton) Large Meteorite Impacts and Planetary Evolution: Boulder, Colorado, *Geological Society of America Special Paper* 293, 209–224.
- Wong A.M., Reid A.M. and Hall S.A., 1993. Characterization of the Marquez Dome buried impact crater using gravity and magnetic data. *Lunar and Planetary Science* 24, 1533–1534.
- Zhang P., Rasmussen T.M. and Pedersen L.B., 1988. Electric resistivity structure of the Siljan impact region. *Journal of Geophysical Research* 93, 6485–6501.

METEORIITSETE PLAHVATUSSTRUKTUURIDE GRAVI- JA MAGNETOMEETRIA

Kokkuvõte

Teie käes olev dissertatsioon käsitleb meteoriitsete plahvatusstruktuuride geofüüsikalisi tunnuseid ning neid põhjustavaid protsesse. Erilist tähelepanu on pööratud kraatrisiseste ja -väliste kivimite füüsikaliste omaduste rollile struktuursete mudelite loomisel (artikkel I ja II) ning erosiooni mõjule meteoriidikraatrite geofüüsikalistele anomaaliatele (artikkel III).

Suur osa meteoriitsetest plahvatusstruktuuridest põhjustab mõõdetava gravi- ja magnetanomaalia. Lihtkraatri (läbimõõduga alla 2 (4) km setteliste (kristalliinsete) märklauakivimite korral) iseloomulikuimaks geofüüsikaliseks tunnuseks on ümar negatiivne gravitatsiooniline anomaalia, mille on põhjustanud purustunud ja bretšastunud kivimite ning võimalike struktuuritäitvate setendite madal tihedus. Negatiivne anomaalia võib olla ümbritsetud kraatrivalli suhteliselt tihedamate kivimite loodud ringja positiivse anomaaliaga. Kompleksstruktuuride (läbimõõduga üle 2 (4) km setteliste (kristalliinsete) märklauakivimite korral) puhul võib gravitatsioonilise kollapsi käigus struktuuri keskele tekkinud tihedam kõrgendik põhjustada negatiivse anomaalia sees paikneva lokaalse positiivse anomaalia.

Plahvatusstruktuuride magnetanomaaliad on magnetiseerituse vektoriaalse iseloomu tõttu varieeruvamad kui gravianomaaliad ning sõltuvad ka struktuuri geograafilisest asukohast. Meteoriidiplahvatus ning sellele järgnevad protsessid on võimelised kivimite magnetiseeritust tekitama, muutma ja hävitama. Tavaliselt assotsieerub lihtkraatriga ümar, negatiivne lokaalne anomaalia, kuid kompleksstruktuurid loovad keerukamaid magnetväljasid.

Plahvatusjärgsed geoloogilised protsessid on võimelised aja vältel kraatrite geofüüsikalisi anomaaliaid muutma ja isegi hävitama. Osaliselt seetõttu ei käsitleta geofüüsikalisi anomaaliaid meteoriidikraatri olemasolu tõestava andmestikuna.

Gravi- ja magnetomeetrilise modelleerimise võimalused meteoriidstruktuuride sisemuse kirjeldamiseks on ilmestatud kahe näite, Bosumtwi (Gaana; artikkel I) ja Kärddla (Eesti; artikkel II) varal. Mõlemal juhul eelnesid struktuuri mudeli loomisele kivimiproovide füüsikaliste omaduste (tihedus, poorsus, magnetiline vastuvõtlikkus, jääkmagnetiseerituse intensiivsus) mõõtmised. Kärddla (läbimõõt 4 km, vanus 455 mln. aastat) struktuuri puhul koostati 2,5-dimensiooniline mudel, kasutades samal ajal nii kraatri gravitatsioonilist kui ka magnetvälja, kivimite füüsikalisi omadusi ning geoloogilist andmestikku. Modelleerimise tulemusel tõestati, et positiivsed ringjad gravi- ja magnetanomaaliad Kärddla kraatri ümber on põhjustatud kraatrivalli tihedamate ja magnetilisemate kristalliinsete kivimite poolt. Negatiivseid anomaaliaid see-

vastu loovad suhteliselt madala tiheduse ning nõrga magnetiseeritusega plahvatusbretšad ning plahvatusjärgsed settekivimid.

Bosumtwi (läbimõõt 11,5 km, vanus 1,07 mln. aastat) kraatri puhul analüüsi aeromagnetilist kaarti, uurimaks maetud magnetilise materjali jaotust kraatri sees. Koostati mudel, mida toetavad kraatri ümbert võetud kivimiproovide füüsikalised ning paleomagnetilised mõõtmistulemused. Modelleerimise tulemusena selgub, et kraatrisisene magnetiline materjal on normaalpolaarsusega ning on tekkinud ja säilinud peamiselt struktuuri põhjaosas. Magnetiline andmestik viitab ka keskkõrgendiku olemasolule.

Artikkel III käsitleb erosiooni mõju meteoriidikraatrite gravi- ja magnetanomaaliatele. Uuringuteks loodi ruumiline 30 km läbimõõduga kristalliinsetel kivimitel paiknev kraatrit iseloomustav mudel, mida modifitseerides arvutati järk-järgult tema poolt loodud gravi- ja magnetväli. Erosiooni peamine efekt seisneb negatiivse gravianomaalia amplituudi vähenemises, kuid peaaegu märkamatus läbimõõdu vähenemises. Keskkõrgendikele vastava positiivse gravianomaalia amplituud ei vähene nii intensiivselt kui pea-anomaalial. Kraatritele vastava magnetanomaalia amplituud väheneb oluliselt pärast struktuuritäitvate sulakivimiläätsede ning bretšade erodeerumist.

PUBLICATIONS

Plado J., Pesonen L. J., Koeberl C. and Elo S., 2000.
The Bosumtwi meteorite impact structure, Ghana: A magnetic model.
Meteoritics & Planetary Science 35, 723–732.

The Bosumtwi meteorite impact structure, Ghana: A magnetic model

J. PLADO¹*, L. J. PESONEN^{2,3}, C. KOEBERL⁴ AND S. ELO³

¹Institute of Geology, University of Tartu, Vanemuise 46, 51014 Tartu, Estonia

²Department of Geophysics, University of Helsinki, P.O. Box 4, FIN-00014 Helsinki, Finland

³Geological Survey of Finland, P.O. Box 96, FIN-02151 Espoo, Finland

⁴Institute of Geochemistry, University of Vienna, Althanstrasse 14, A-1090 Vienna, Austria

*Correspondence author's e-mail address: jplado@math.ut.ee

(Received 1999 August 18; accepted in revised form 2000 March 7)

Abstract—A magnetic model is proposed for the Bosumtwi meteorite impact structure in Ghana, Africa. This relatively young (~1.07 Ma) structure with a diameter of ~10.5 km is exposed within early Proterozoic Birimian–Tarkwaian rocks. The central part of the structure is buried under postimpact lake sediments, and because of lack of drill cores, geophysics is the only way to reveal its internal structure. To study the structure below and beyond the lake, a high-resolution, low altitude (~70 m) airborne geophysical survey across the structure was conducted, which included measurements of the total magnetic field, electromagnetic data, and gamma radiation. The magnetic data show a circumferential magnetic halo outside the lakeshore, ~12 km in diameter. The central-north part of the lake reveals a central negative magnetic anomaly with smaller positive side-anomalies north and south of it, which is typical for magnetized bodies at shallow latitudes. A few weaker negative magnetic anomalies exist in the eastern and western part of the lake. Together with the northern one, they seem to encircle a central uplift. Our model shows that the magnetic anomaly of the structure is presumably produced by one or several relatively strongly remanently magnetized impact-melt rock or melt-rich suevite bodies.

Petrophysical measurements show a clear difference between the physical properties of preimpact target rocks and impactites. Suevites have a higher magnetization and have low densities and high porosities compared to the target rocks. In suevites, the remanent magnetization dominates over induced magnetization (Koenigsberger ratio > 3). Preliminary palaeomagnetic results reveal that the normally magnetized remanence component in suevites was acquired during the Jaramillo normal polarity epoch. This interpretation is consistent with the modelling results that also require a normal polarity magnetization for the magnetic body beneath the lake. The reverse polarity remanence component, superimposed on the normal component, is probably acquired during subsequent reverse polarity events.

INTRODUCTION

An impact origin for the nearly circular Bosumtwi structure in Ghana, Africa (centered at 06°30' N and 01°25' W) was first suggested by Maclaren (1931). The structure has a rim-to-rim diameter (*D*) of ~10.5 km (Figs. 1 and 2) and is mostly filled by Lake Bosumtwi, which has a diameter of ~8 km and maximum depth of 80 m (Jones *et al.*, 1981). The structure has an age of ~1.07 Ma (Koeberl *et al.*, 1997), which is the same as for tektites found in the neighbourhood at Ivory Coast (Fig. 1c) and for microtektites found in deep-sea sediment cores off the West African coast. The common age, as well as chemical and isotopic data (Lippolt and Wasserburg, 1966; Schnetzler *et al.*, 1966), indicate that the Lake Bosumtwi impact event is most likely the source crater for these tektites. Chemical data indicate a minor meteoritic component in the Ivory Coast tektites (Palme *et al.*, 1981; Jones, 1985; Koeberl and Shirey, 1993).

Because the crater is buried under the water and lake sediments, and because of the lack of drillings, geophysics have to be used to investigate its subsurface structure. The first magnetic field studies of the structure were made in 1960 by Hunting Surveys Ltd. for the Ghana Geological Survey Department (Jones *et al.*, 1981). The occurrence of a central negative anomaly of ~40 nT, with a positive flank anomaly of ~20 nT on the northern side (which is intersecting regional magnetic anomalies) was detected in this early survey. The anomaly was attributed to a breccia lens below the lake sediments. In addition, gravity measurements were collected around the lake (Jones *et al.*, 1981); yet because of the sparseness of data (none over

the lake), the gravity data reflect regional trends only and cannot be used to constrain the magnetic models.

In 1997, a high-resolution airborne geophysical survey across the Bosumtwi structure was carried out by the Geological Survey of Finland (GSF) in cooperation with the University of Vienna and the Ghana Geological Survey Department (Ojamo *et al.*, 1997; Pesonen *et al.*, 1998, 1999). It included measurements of the total magnetic field, electromagnetic field, and gamma radiation. Here we present a magnetic model of the structure, which is based on the new high-resolution residual maps, and constrained by petrophysical data of nine unoriented and four oriented rock samples (for location, see Fig. 2) collected around the structure.

STRUCTURE OF THE TARGET AND CRATER

Ghana occupies a major part of the Precambrian Shield, a segment of the West African Craton. The early Proterozoic (~2100 Ma) basement in Ghana is subdivided into the Birimian and Tarkwaian Supergroups (Eisenlohr and Hirdes, 1992). The Bosumtwi crater (Fig. 2) was excavated mainly in Birimian metasediments: graywackes, phyllites, and quartzites. Birimian metamorphosed volcanic rocks (basalts with some intercalated sediments) reach into the southeast corner of the lake (Jones *et al.*, 1981). Bedding of Birimian formations strikes northeast and dips subvertically. The deformational event and deposition of the Tarkwaian Supergroup followed the Birimian sedimentation. Tarkwaian coarse clastic sedimentary rocks, which are regarded as the detritus of Birimian rocks (Leube *et al.*, 1990), occur to the

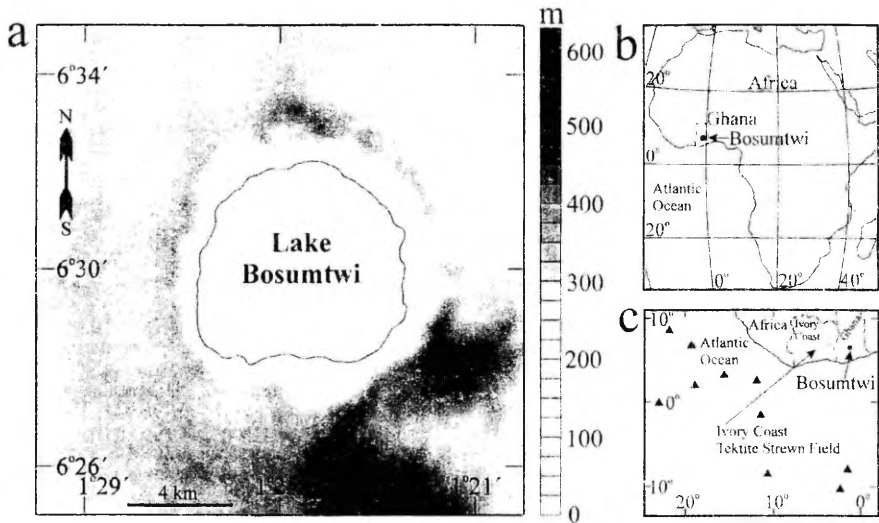


FIG. 1. (a) Topographical map of Lake Bosumtwi and surroundings, including lakeshore and bathymetry, after Jones *et al.* (1981) and McGregor (1937). (b and c) Location of the Bosumtwi region in western Africa with the Ivory Coast tektite strewn field. Deep-sea cores containing microtektites are marked by black triangles (after Glass *et al.*, 1991).

southeast of the crater. Some syndeformational granitic intrusions of "Cape Coast" type (Jones *et al.*, 1981) are cropping out around the north, west, and south sides of Lake Bosumtwi (Fig. 2).

The lake (with circular bathymetry (McGregor, 1937) and maximum water depth of ~80 m) and post-impact lake sediments hide the subsurface structure of the central part of the Bosumtwi crater but have preserved it against erosional processes. Based on the size criteria for terrestrial impact structures (e.g., Grieve and Pesonen, 1996), Bosumtwi should be a complex impact structure, but no evidence exists of a central uplift in lake bathymetric data (McGregor, 1937). It is possible that the central uplift has collapsed during the modification stage of the crater formation and is hidden underneath the lake sediments. The morphometric estimates of the structure, including the diameter of the central uplift, are given in Table 1.

METHODS AND DATA

Geophysical Field Surveys

In the 1997 survey, the total magnetic intensity was recorded with a Scintrex CS-2 magnetometer at a resolution of 0.001 nT. The nominal flight altitude was 70 m, flight directions north-south, and line spacing was 500 m. Magnetic recordings were obtained at every ~6.25 m along the flight lines. Positionings were done using differential global positioning system and flight elevations were measured with radar altimeters. Altogether, 30 profiles were recorded with an average length of 22 km. All original data (corrected for aircraft disturbances and for variations in elevation) were transformed into a grid of 100 × 100 m, from which various maps were prepared (see Pesonen *et al.*, 1998).

TABLE 1. Dimensions of the Bosumtwi structure.

Parameter	Equation/dimension	References
Rim-to-rim diameter	$D \approx 10.5 \text{ km}$	Jones <i>et al.</i> (1981)
Diameter of the collapsed disruption (i.e., transient) cavity	$D_{DC} \approx D_0^{0.15} D^{0.85} \approx 9 \text{ km}$	Croft (1985), for definition see Hildebrand <i>et al.</i> (1998)
Diameter of the central uplift	$D_{CU} \approx 0.22 D \approx 2.3 \text{ km}$	Pike (1985)
Apparent depth	$d_A \approx 0.15 D^{0.43} \approx 0.4 \text{ km}$	Grieve and Pesonen (1992)
True depth	$d_T \approx 0.52 D^{0.2} \approx 0.8 \text{ km}$	Grieve and Robertson (1979)
Maximum thickness of the allochthonous breccia lens	$h_B \approx d_T - d_A \approx 0.4 \text{ km}$	
Volume of impact melt	$V_M = 3.8 \times 10^{-4} D^{3.4} \approx 1.1 \text{ km}^3$	Lange and Ahrens (1979)
	$V_M = c D_{DC}^{3.38}$	Grieve and Cintala (1992)
	$2.9 < V_M < 3.4 \text{ km}^3$	

Abbreviations: D_0 = the transition diameter for simple-to-complex crater (~4 km for crystalline targets on Earth); apparent depth = depth from the rim to the upper surface of crater-filling allochthonous breccias; true depth = depth from the rim to the base of breccia lens, c = constant that depends on the impact velocity and type of the projectile. The volume of impact melt was calculated for iron and chondrite projectiles at impact velocities from 15 to 25 km s⁻¹.

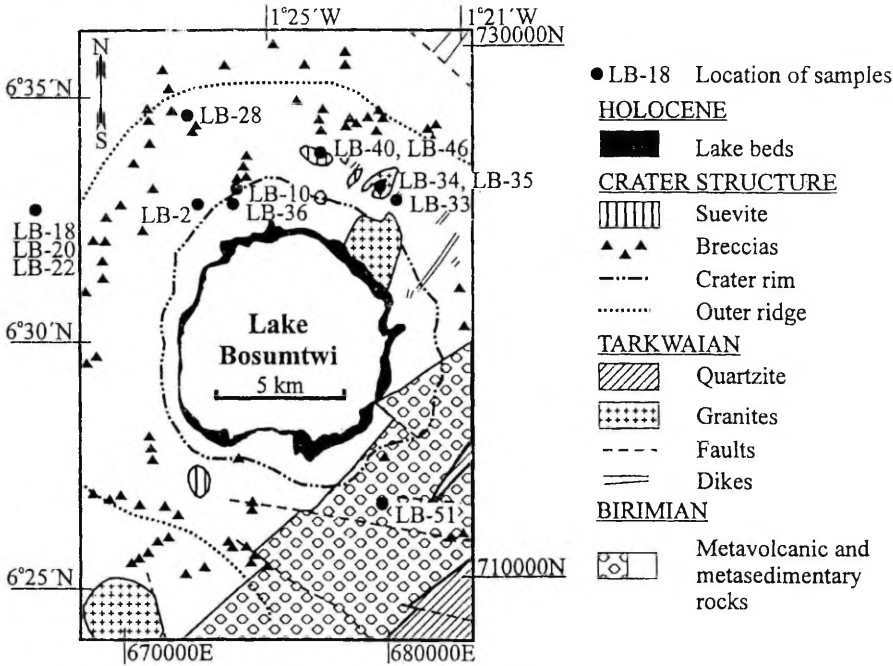


FIG. 2. Schematic geological map of the Bosumtwi area after Jones *et al.* (1981) and Reimold *et al.* (1998). The rectangular map area refers to area of aerogeophysical survey. Two coordinate systems, geographic and plain, are shown. Location of the investigated samples is shown with black dots.

Petrophysics

Our petrophysical data, which we use to constrain the geophysical modellings, are based on 13 samples collected in 1997. Sampling localities are shown in Fig. 2. Most of the samples were weathered. Eleven samples (6 granites, 4 graywackes, and 1 shale) were unshocked target rocks in the surrounding terrain of Lake Bosumtwi. The two impactites from an outcrop located ~2.8 km north of the crater rim are melt-rich suevites from the ejecta layer. These suevites, one graywacke and one granite sample, were collected in the field as oriented samples of which several specimens were prepared.

Density (δ), magnetic susceptibility (χ), and intensity of the natural remanent magnetization (NRM) were measured at the Palaeomagnetic Laboratory of the GSF-Espoo, using techniques described in Puranen and Sulkanen (1985). The porosities (ϕ) were measured using the water-saturation technique as described in Pesonen *et al.* (2000).

All oriented specimens were demagnetized with alternating magnetic fields (AF) to study their palaeomagnetic behaviour. Some specimens were also thermally demagnetized. The measurements were made using a superconducting quantum interference device (SQUID) magnetometer as described by Oja and Pesonen (1990). To determine the various remanence components

in the samples, joint analyses of stereographic plots, demagnetization decay curves, vector diagrams (Zijderveld, 1967), and principal-component analysis were used (Kirschvink, 1980; Leino, 1991).

RESULTS

Magnetic Maps

The regional magnetic field (Fig. 3) in the Bosumtwi crater area reveals several types of regional anomalies, the most striking ones being the northeast–southwest lineations by Birimian-Tarkwaian supracrustal strata (Eisenlohr and Hirdes, 1992). These anomalies have a range of wavelengths between 2 and 20 km, and amplitudes up to ~250 nT. Higher amplitudes and smaller wavelengths are measured to the southeast of the Bosumtwi Lake at the Birimian metavolcanic and, in particular, Tarkwaian quartzites. Similar short wavelength northeast–southwest trending regional anomalies appear to the northwest and southwest of the crater, which suggests that buried metavolcanic rocks are also present there. The regional features partially mask the more circular magnetic signatures of the Bosumtwi structure. As the impact-induced anomalies have wavelengths that are similar to the regional ones, it is difficult to separate them. For example, the negative anomaly, ~5 km in length, at the northern part of the lake (Fig. 3), interpreted as having an impact origin (Jones *et al.*, 1981), certainly includes some

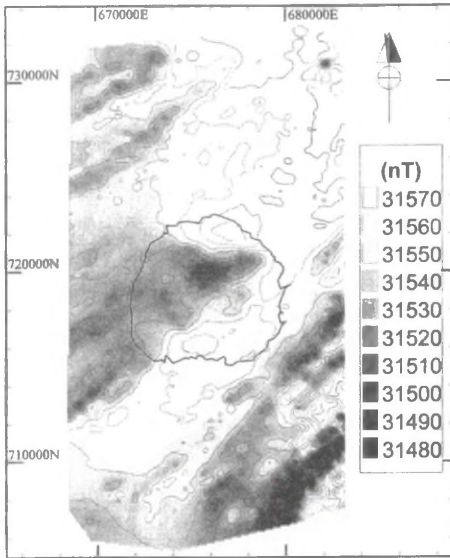


FIG. 3. Total field (nT) aeromagnetic map of the Bosumtwi impact structure. The data are from a high-resolution aerogeophysical survey conducted by the Geological Survey of Finland (Ojamo *et al.*, 1997; Pesonen *et al.*, 1998, 1999). Contour interval is 10 nT.

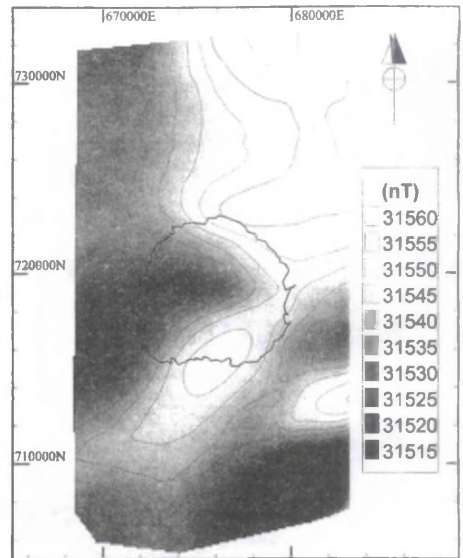


FIG. 4. Regional magnetic field (nT) map of the Bosumtwi area. To define the regional field, a two-dimensional-averaging with the area of 4×4 km filter for a grid of 100×100 m was applied to the total field aeromagnetic map (Fig. 3). Contour interval is 5 nT.

component from the negative linear regional anomaly from southwest of the crater. However, the structure shows clearly a group of differently shaped negative anomalies that are surrounded by two positive anomalies, one on the northern and one on the southern side. This type of anomaly pattern can, at low latitudes, be produced in two different ways.

First, a body with reversed magnetization at shallow latitudes can produce a positive anomaly with minor negative anomalies to the north and south. This case seems to be unlikely at Bosumtwi, as the northern positive feature lacks a negative side anomaly to the north, and the southern one lacks a side anomaly to the south. Moreover, the positive features are located too close to the rim of the structure to be produced by a large reversely magnetized body. Second, this type of anomaly pattern can be produced by a normally magnetized structure at shallow latitudes. Our preliminary modelling exercise showed that a highly magnetic anomalous source body with the remanent magnetization parallel to the ancient dipole field gives rise to a negative anomaly at low latitudes. At Bosumtwi latitude ($\sim 5^\circ$ N), the negative anomaly occurs slightly to the north of the body's centre and is accompanied with positive side anomalies on the northern and southern side of the major peak. This explanation is also supported by palaeomagnetic studies and further modelling experiments.

In order to remove the regional trends and to amplify the Bosumtwi related anomalies, we applied a two-dimensional-smoothing window with an areal operator of 4×4 km in a grid of 100×100 m. However, this technique removes mainly the large

wavelength regional effects as shown by the regional magnetic map (Fig. 4). Because of similar wavelengths of impact anomalies and elongated regional features, the usage of a smaller areal operator would affect impact anomalies. Because of the complicated magnetic field, other methods to describe the regional features (*e.g.*, polynomial regression) did not give reasonable results. The residual magnetic anomaly (Fig. 5) is obtained by subtracting the regional field from the original total field. It shows that both impact-induced and elongated regional anomalies are present, but the Bosumtwi structure is clearly truncating the regional magnetic trends. A circumferential magnetic halo with very low gradients (*h* in Fig. 5), correlating with the rim, ~ 0 nT in amplitude and ~ 12 km in diameter, appears around the lake. Because its diameter is larger than that of the collapsed disruption cavity, it likely represents fracturing and uplift of the rim that randomized the preexisting remanence magnetizations of the target rocks. The central part of the structure is characterised by relatively high gradients. At the center of the lake, there are four or six negative magnetic anomalies (*c*, dark spots) with two positive side anomalies (white spots), one on the northern side of the lake (*n*) and one on the southern side (*s*). The negative magnetic features surround the positive one, which points to a possible location of a central uplift (*cu*).

Physical Properties

Table 2 summarises the petrophysical data of the samples. A clear difference exists between the physical properties of target rocks and impact-derived suevites. The latter have low densities,

higher porosities, and higher magnetizations compared to the target rock values. The remanent magnetization of suevites prevails over induced magnetization (Koenigsberger ratio $Q > 3$). The target rocks have strikingly homogeneous physical properties with noticeable weak remanent magnetizations ($Q < 0.5$). Some minor differences in their magnetizations exist: the Papiakese granites have a relatively low susceptibility and the graphitic shale has a fairly high remanent magnetization.

The palaeomagnetic behavior of melt-rich suevites differs significantly from those of the target. Suevite LB-40 (Table 3) has two superimposed NRM components (normal (N) and reversed (R)) that are directed either parallel or nearly antiparallel to the present-day normal polarity magnetic field. In Fig. 6a, as an example, the palaeomagnetic behavior of the specimen LB-40-1a in the process of AF treatment is shown. It shows that the R component is much weaker and magnetically softer (can be removed at demagnetization fields of ≤ 15 mT) than the N polarity component, and we anticipate that the latter is a prevailing characteristic remanence component. Sample LB-46 also shows dual polarities (R and N) during AF treatment (Table 3), but the R component is much more scattered. In Fig. 6b, the behavior of LB-46-1b in the course of thermal demagnetization treatment is shown. In this sample, the R component is magnetically harder than the (N) component. The main magnetic mineral in the suevite is magnetite, because most of

the NRM is removed by thermal demagnetization up to 580 °C. However, a part of the NRM shows a Curie temperature of ~ 680 °C, indicating that hematite, carrying mainly the reversed component of NRM, is also present.

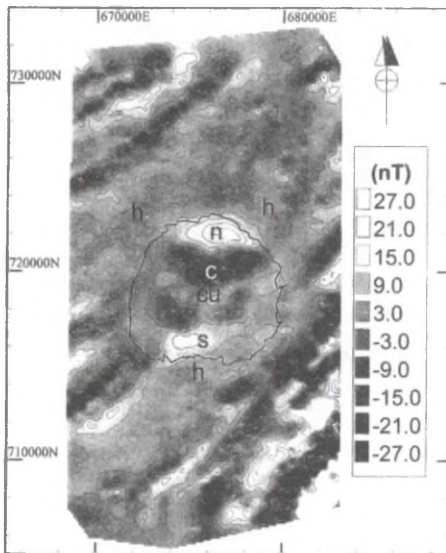


FIG. 5. Residual magnetic field (nT) map of the Bosumtwi impact structure. To obtain it, the regional effect (Fig. 4) was subtracted from the original total field aeromagnetic map (Fig. 3). The lakeshore is indicated. See text for description of different anomalies. Abbreviations: h = magnetic halo; c = central negative anomaly; n = northern positive anomaly; s = southern positive anomaly; cu = central positive anomaly, correlating with the possible location of the central uplift. Contour interval is 6 nT.

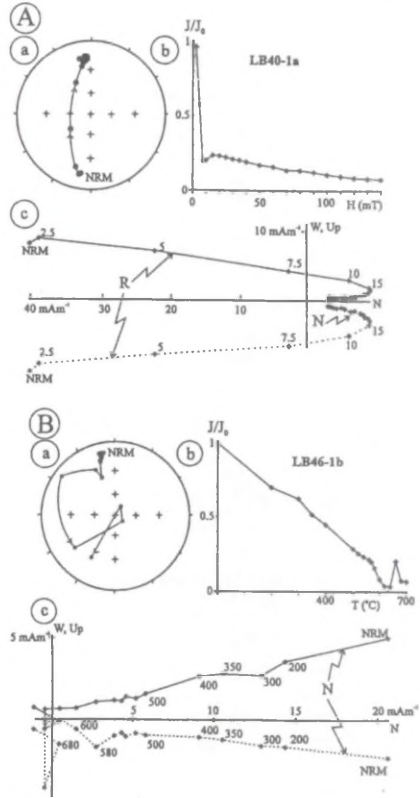


FIG. 6. (A) The AF demagnetization behavior of LB40-1a, and (B) thermal demagnetization behavior of LB46-1b, melt-rich suevite specimens. (a) Stereographic projection of directional data on demagnetization. NRM shows the natural remanent magnetization (without demagnetization); (b) intensity decay of the NRM during the treatment, where J_0 denotes the original intensity and J the intensity at the particular demagnetization step; (c) orthogonal demagnetization diagram. Solid (dotted) line denote vertical (horizontal) planes. Numbers by each demagnetization step denote peak alternating field (mT) or temperature (°C). N (R) denote the normal (reversed) component, respectively.

TABLE 2. Petrophysical properties of the rocks at Lake Bosumtwi structure.

Sample	n	δ_g	δ_w	ϕ	χ	NRM	Q
Target rocks							
Phyllite-graywacke							
LB-02	—	—	—	—	240	—	—
LB-10	2640	2470	10.4	230	0.15	0.03	
LB-22	2730	2640	4.9	250	0.14	0.02	
LB-33	—	—	—	160	0.18	0.04	
Granite dikes							
LB-18	2610	2410	9.7	240	0.33	0.05	
LB-20	2680	2550	6.7	180	0.09	0.02	
LB-36	2630	2480	8.0	180	0.55	0.12	
Pepiakese granite							
LB-34	—	—	—	30	0.10	0.07	
LB-35	2610	2510	6.0	30	0.20	0.16	
Shale							
LB-51	2730	2510	12.4	230	3.86	0.67	
Mean of target	10	2680	2510	8.3	150	0.6	0.13
Impactites							
Melt-rich suevite (ejecta)							
LB-40	2200	1770	36.2	430	34.90	3.22	
LB-46	2540	2310	15.0	230	38.73	6.68	
Mean of suevites	2	2370	2040	25.6	330	36.8	4.43

For sample locations, see Fig. 2a.

Abbreviations: n = number of samples; δ_g = grain density (kg m^{-3}); δ_w = wet density (kg m^{-3}); ϕ = porosity (%); χ = weak field susceptibility (10^{-6} SI); NRM = intensity of natural remanent magnetization (mAm^{-1}); Q = Koeningberger ratio (-).

The existence of both N and R components in the same specimens of suevites (Table 3) is puzzling. Because the samples are taken from small fall-out suevite outcrops, they have probably cooled rapidly. Therefore, it is unlikely that they represent two stable polarities acquired during the polarity change from Matuyama (R) to Jaramillo (N), ~1.072 Ma ago (Langereis *et al.*, 1997). More likely, only the N component, acquired during the Jaramillo period, is primary and the R component, carried mainly by hematite, is secondary, perhaps locked in during the weathering processes at later R epoch. This opinion is supported by the work of Glass *et al.* (1991), who found that Ivory Coast microtektites were deposited ~8 000 years after the onset of the Jaramillo N polarity epoch. The magnetic model also requires a presence of a net N polarity magnetization.

Palaeomagnetic data on target granite and graywacke samples reveal a high stability of NRM in the course of AF demagnetization. Due to relatively weak magnetizations and uncertain directions, the component analyses did not yield clear results. However, at weak fields, target-rock samples showed some evidence of stable components (Table 3), which may represent the N and R components obtained during the Birimian and Tarkwaian igneous and metamorphic episodes (Piper and Lomax, 1973), or the viscous remanent magnetization.

TABLE 3. Palaeomagnetism of the early Proterozoic basement in Ghana, and rocks of the Lake Bosumtwi structure (latitude 6.53° N; longitude 359.58° E).

Sample	N/n	Pol.	D (°)	I (°)	k	α_{95} (°)	$Plat$ (°)	$Plon$ (°)	A_{95} (°)	dp (°)	dm (°)
Early Proterozoic rocks of Ghana (after Piper and Lomax, 1973)											
Greenstone (age ≤ 2.2 Ga; latitude 6.2° N; longitude 359.3° E)											
5/74	N	320	26	11	19	50	282	15	11	21	
Dolerite dyke (age ~2.1 Ga; latitude 6.2° N; longitude 359.3° E)											
1/14	N	328	-11	21	11	56	249	8	6	11	
Dolerite intrusions (age ~2.1 Ga; latitude 5.5° N; longitude 352.8° E)											
5/29	R	156	40	20	14	53	212	13	10	17	
Lake Bosumtwi target rocks											
Phyllite-graywacke											
LB-33	1	N	314	14	—	—	44	273	—	—	—
	2	R	171	-18	—	—	81	287	—	—	—
Pepiakese granite											
LB-34	3	N	16	-4	5	63	72	117	45	32	63
	1	R	180	12	—	—	77	178	—	—	—
Mean of target*	4/7	N+R	351	4	8	36	80	246	25	18	36
Lake Bosumtwi impactites											
Melt-rich suevite (ejecta)											
LB-40	3	N	5	5	9	43	81	145	31	22	43
	3	R	186	14	66	15	75	156	16	8	15
LB-46	3	N	359	7	32	22	81	186	16	11	22
	3	R	233 [†]	16	14	34	35	104	25	18	35
Mean of suevites*	3/9	N+R	3	-1	44	19	81	159	13	9	19

For sample locations, see Fig. 2a.

*For mean calculations, the reversed polarity data were inverted.

[†]Data not included for mean.

Abbreviations: N/n = number of sites / number of specimens used to calculate the mean direction; pol. = polarity; D = declination; I = inclination; k = Fisher's (1953) precision parameter; α_{95} = the radius of a cone of 95% confidence about the mean; $Plat$ and $Plon$ = the latitude and longitude of the virtual geomagnetic poles (VGPs); A_{95} = the radius of a cone of 95% confidence about the pole determined from sample means D and I ; dp , dm = semiaxes of an oval of 95% confidence of the pole.

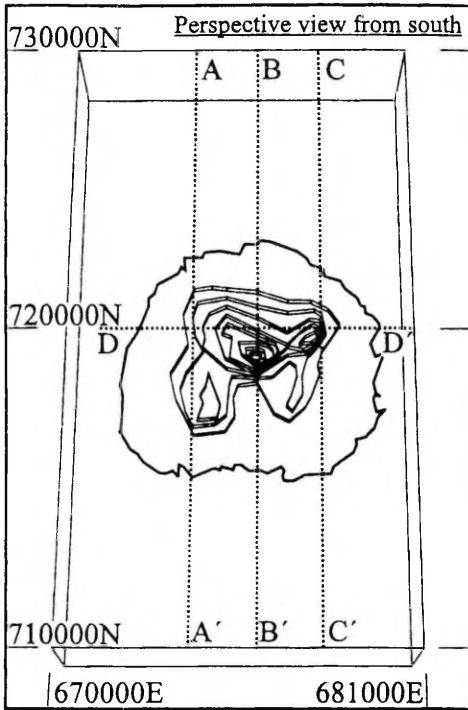


FIG. 7. Perspective view of the Lake Bosumtwi magnetic model from the south. The model consists of eight polygonal layers, each with a thickness of 50 m. The top of the largest uppermost layer is at the depth of 200 m below the sea level. All the layers have identical magnetic properties as described in text. Dotted lines denote the location of profiles A-A', B-B', C-C', and D-D'.

MODEL INTERPRETATIONS AND DISCUSSION

The magnetic model interpreted from the residual magnetic map is shown in Figs. 7 and 8. For the model, we used the following International Geomagnetic Reference Field (Pesonen *et al.*, 1994) parameters: field intensity $F = 31\,500$ nT; inclination $I = -12.5^\circ$; declination $D = 354.1^\circ$. Susceptibility of the background (χ_b) was set to 0. The model consists of eight polygonal 50 m thick layers with horizontal upper and lower surfaces and vertical sides. The top of the largest uppermost layer is at the depth of 200 m below sea level. All layers have identical magnetic properties: $\chi = 3300 \times 10^{-6}$ SI, NRM = 0.367 Am $^{-1}$, $Q = 4.43$, and remanence directions ($D = 3^\circ$; $I = -1^\circ$). The forward modelling technique was used, where we calculated a magnetic response curve along several north-south and west-east profiles. By changing the shapes of polygonal prisms, we tried to match the model curves to fit the observed data by trial-and-error techniques. The best matching was achieved when the depth range for the prisms varied between 200 and 600 m, which is consistent with theoretical impact models of this size and with the previous model of Jones *et al.* (1981). Because of the number of

several independent variables (susceptibility, remanent magnetization, thickness, dip, and depth of the polygons), the model is not unique.

The polygonal layers form a homogeneous structure with a relatively complicated shape in plan view (Fig. 7). In cross-sections (Fig. 8), the model can be described as a half-lens. It is surrounding the possible location of the central uplift on the northern side but also exists on the western and eastern side of this possible uplift. This magnetically homogeneous model has a maximum thickness of 400 m at the northern part of the structure.

We assume the modelled structure to be melt-rich-suevite breccia or an impact-melt lens. The relative "freshness" of the crater and the lack of postimpact deformation and erosion in the central depression suggests that the impact-produced rocks may be deposited around the central uplift, that is, the depression is filled more or less symmetrically. Thus, there should be also breccias in the southern part of the crater filling, but they did not acquire a high magnetization. The presence of biotite-rich granite intrusion, cut by the lake in its northeastern part (Fig. 2), may give some clues for the high magnetization at the northern part of the lake. It is possible that shock decomposed biotite partly into ferromagnetic iron oxides; therefore, the suevites have acquired their NRM directions by the postshock thermochemical processes.

Modelling required stronger magnetizations than those measured for suevite (Table 2) outside the crater, because they are too weak to produce the observed magnetic anomaly. The supposed melt-rich material inside the structure has to be several times more magnetic than the fall-out suevite. It is possible that ejected breccias have lost some of their magnetization because of weathering on the surface, or that they are less magnetic than possible melt rocks within the crater. The relatively high Koenigsberger ratio used in the model was the same as that observed for the ejected suevites. Therefore, we assume that most of the impact anomaly is due to a thermoremanent magnetization (TRM). The direction of remanent magnetization ($D = 3^\circ$; $I = -1^\circ$) is very similar to the direction of the magnetic field ($D = 354.1^\circ$; $I = -12.5^\circ$) at Bosumtwi.

Slowly cooling crystalline impact-melt rocks may acquire TRM in the direction of the magnetic field at the time of impact, for example, Manicouagan, Canada (Larochelle and Currie, 1967), and Lappajärvi (Pesonen *et al.*, 1992). At a given crater size, composition and properties of target rocks largely control the volume and magnetic contrast of melt rocks and, therefore, the magnetic anomaly. High magnetization is observable if high amounts of ferrimagnetic minerals are produced by the cooling melt, as in impactites of the Mien ($\chi \approx 2000 \times 10^{-6}$ SI) or Dellen ($\chi \approx 20\,000 \times 10^{-6}$ SI) structures (Henkel, 1992). Bosumtwi, with its Ferrich target (0.5–9.2 wt% of Fe_2O_3 ; Koeberl *et al.*, 1998), could yield melt rocks with this type of magnetization as well. However, Lappajärvi melts and breccias show relatively low susceptibilities ($200\text{--}700 \times 10^{-6}$ SI; Kukkonen *et al.*, 1992). In some cases, the observed magnetic anomalies are mainly due to remanent magnetization. High Koenigsberger ratios of breccias and impact-melt rocks are observed at, for example, Mien ($Q \approx 10$; Stanfors, 1973) and Haughton ($Q > 10$; Pohl *et al.*, 1988).

Additionally to the TRM, several other processes may change the magnetization during the impact. Our model does not exclude any of them, but, because of the limitations of the data, we can not confirm them either. Shock may induce a drop in the magnetic susceptibility and often (but not always) also in the NRM (Hargraves and Perkins, 1969; Cisowski and Fuller, 1978; Pesonen,

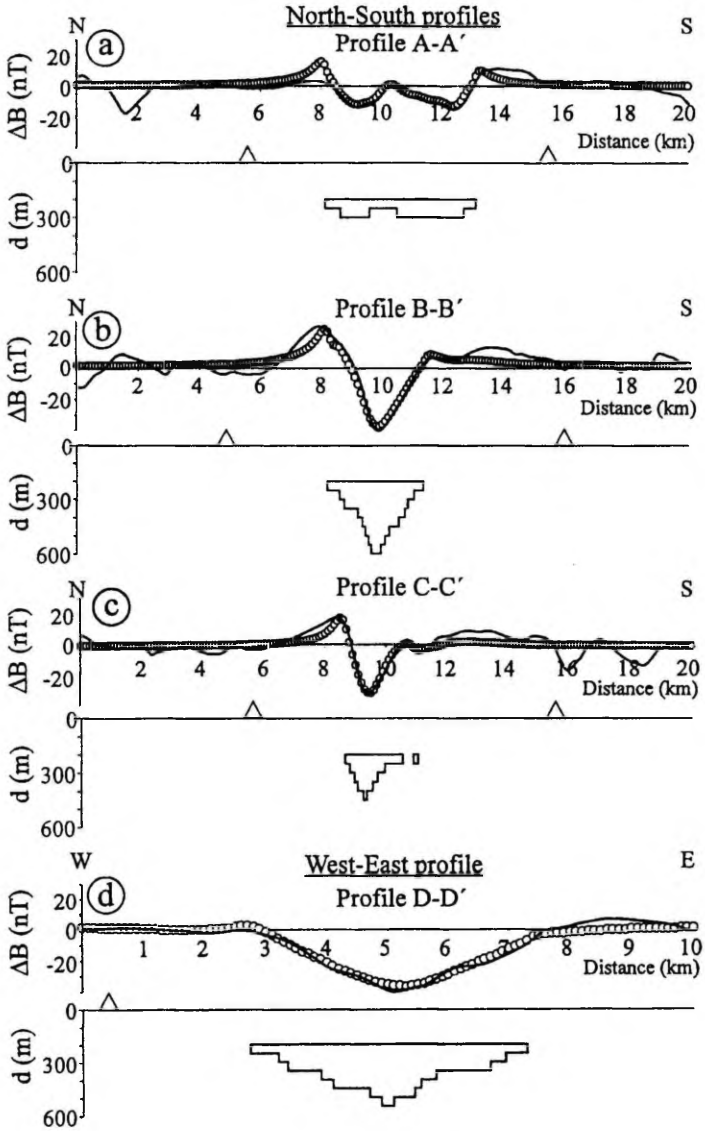


FIG. 8. Magnetic profiles. (a) Profile A-A'; (b) profile B-B'; (c) profile C-C'; (d) profile D-D', across Bosumtwi structure. Panels (a-c) are from north to south; (d) from west to east. Location of profiles is shown in Fig. 7. Solid lines denote residual magnetic field. Open circles denote calculated values. Below the profile curves the cross-section of the magnetic model of the magnetic body producing the calculated values is shown. See text for magnetic field, background, and polygon properties.

1996; Scott *et al.*, 1997). However, the shocked bedrock may also acquire a new remanence by transient stresses, the shock remanent magnetization (SRM), along the direction of the Earth's magnetic field at the time of impact (e.g., Halls, 1979). Postimpact processes, such as alteration, may produce a chemical remanent magnetization (CRM), as was noticed at Lake St. Martin structure (Coles and Clark, 1982).

One possibility to constrain the model is to compare the volume of magnetic material in our model with the theoretical volume of the melt due to the impact. The latter depends on the kinetic energy of the projectile, and properties of target (Melosh, 1989). There are two estimates of the amount of melt at nearly noneroded impact structures formed into crystalline rocks and with a size comparable to Bosumtwi. The Kaluga structure ($D = 15$ km) was estimated (Masaitis *et al.*, 1980) to contain 8 km^3 of melt rock. Gurov and Gurova (1985) have calculated the volume of impact-melt rock within the Boltysh structure ($D = 25$ km) to be 11 km^3 . Algorithms proposed by Lange and Ahrens (1979) and Grieve and Cintala (1992) give 1.1 and 2.9–3.4 km^3 of melt in Bosumtwi (Table 1), including the fraction of melt ejected outside the structure. Considering the fact that not all of the melt must be highly magnetic, and the model is not unique, the melt volume in our model ($\sim 2.2 \text{ km}^3$) corresponds quite well to the results of the calculations.

According to the estimates by Pilkington and Grieve (1992) and Plado *et al.* (2000), one can expect that the Bouguer anomaly would be ~ 10 mGal at the Bosumtwi Lake. However, according to the present magnetic model and some modelling experiments, we assume that the negative gravity anomaly is weaker in the northern part of the lake. This is due to the high content of melt rocks, which are usually denser than melt-less impact breccias (e.g., Lappajärvi; Kukkonen *et al.*, 1992). Some gravity features due to the central uplift may appear.

CONCLUSIONS

The following conclusions can be drawn from the present study.

(1) The negative magnetic anomaly, associated mainly with the central-northern part of the Bosumtwi structure, is produced by a ≤ 400 m thick magnetic lens of normally magnetized material. This body could consist of impact-melt breccias and impact-melt rocks. Palaeomagnetic data, supported by a magnetic model, show that the magnetic body has acquired its bulk remanent magnetization during the Lower Jaramillo normal polarity event, after the Matuyama–Jaramillo polarity change.

(2) Physical properties of suevites collected north of the crater rim differ significantly from those of the surrounding preimpact metamorphic rocks. High porosity, low density, and relatively high magnetization characterize the suevites.

(3) Highly magnetic material inside the structure seems to have formed—and been preserved—mostly in the northern part of the structure and probably outlines the possible location of a central uplift. It is possible that shock decomposed biotite from the granitic intrusion at the northeastern edge of the lake into ferromagnetic iron oxides, which give rise to the magnetic anomaly in the north-central part of the structure.

(4) The model proposed here could be better constrained by a more extensive sampling of impactites and target rocks around the lake. The model is testable by detailed gravity and seismic reflection methods. However, to really prove its validity deep drilling into the structure is required.

Acknowledgements—We are grateful to Mauri Terho, Heli Ojamo, Heikki Hautaniemi, Jukka Multala, Tarja Manninen (all GSF), and Herbert Henkel (Royal Institute of Technology, Stockholm) for help and discussions. Local support by the Ghana Geological Survey Department and its Director, C. E. Oduro, is appreciated. Help by W. U. Reimold and D. Brandt with collecting samples is acknowledged. We greatly appreciate the reviews of A. R. Hildebrand, J. Pohl, and H. Joesdicke. This work was supported in part by the Austrian Fonds zur Förderung der wissenschaftlichen Forschung, project Y58-GEO (to C. K.).

Editorial handling: A. Deutsch

REFERENCES

- CISOWSKI S. M. AND FULLER M. (1978) The effect of shock on the magnetism of terrestrial rocks. *J. Geophys. Res.* **83**, 3441–3458.
- COLES R. L. AND CLARK J. F. (1982) Lake St. Martin impact structure, Manitoba, Canada: Magnetic anomalies and magnetizations. *J. Geophys. Res.* **87**, 7087–7095.
- CROFT S. K. (1985) The scaling of complex craters. *J. Geophys. Res.* **90** (Suppl.), C828–C842.
- EISENLOHR B. N. AND HIRDES W. (1992) The structural development of the early Proterozoic Birimian and Tarkwaian rocks of southwest Ghana, West Africa. *J. Afr. Earth Sci.* **14**, 313–325.
- FISHER R. A. (1953) Dispersion on a sphere. *Proc. Royal Soc. London* **217**, 295–305.
- GLASS B. P., KENT D. V., SCHNEIDER D. A. AND TAXE L. (1991) Ivory Coast microtektite strom field: Description and relation to the Jaramillo geomagnetic event. *Earth Planet. Sci. Lett.* **107**, 182–196.
- GRIEVE R. A. F. AND CINTALA M. J. (1992) An analysis of differential impact melt-crater scaling and implications for the terrestrial impact record. *Meteoritics* **27**, 526–538.
- GRIEVE R. A. F. AND PESONEN L. J. (1992) The terrestrial impact cratering record. *Tectonophysics* **216**, 1–30.
- GRIEVE R. A. F. AND PESONEN L. J. (1996) Terrestrial impact craters: Their spatial and temporal distribution and impacting bodies. *Earth, Moon and Planets* **72**, 357–376.
- GRIEVE R. A. F. AND ROBERTSON P. B. (1979) The terrestrial cratering record, I. Current status of observations. *Icarus* **38**, 212–229.
- GUROV E. P. AND GUROVA E. P. (1985) Boltysh astrobleme: Impact crater pattern with a central uplift (abstract). *Lunar Planet. Sci.* **16**, 310–311.
- HALLS H. C. (1979) The Slate Islands meteorite impact site: A study of shock remanent magnetization. *Geophys. J. Royal Astron. Soc.* **59**, 553–591.
- HARGRAVES R. B. AND PERKINS W. E. (1969) Investigations of the effect of shock on natural remanent magnetism. *J. Geophys. Res.* **74**, 2576–2589.
- HENKEL H. (1992) Geophysical aspects of meteorite impact craters in eroded shield environment, with special emphasis on electric resistivity. *Tectonophysics* **216**, 63–89.
- HILDEBRAND A. R. *ET AL.* (1998) Mapping Chicxulub crater structure with gravity and seismic reflection data. In *Meteorites: Flux with Time and Impact Effects* (eds M. M. Grady, R. Hutchison, G. J. H. McCall and D. A. Rothery) pp. 155–176. Geological Society Special Publications **140**, London, U.K.
- JONES W. B. (1985) Chemical analyses of Bosumtwi crater target rocks compared with Ivory Coast tektites. *Geochim. Cosmochim. Acta* **49**, 2569–2576.
- JONES W. B., BACON M. AND HASTINGS D. A. (1981) The Lake Bosumtwi impact crater, Ghana. *Geol. Soc. Amer. Bull.* **92**, 342–349.
- KIRSCHVINK J. L. (1980) The least-squares line and plane and the analysis of palaeomagnetic data. *Geophys. J. Royal Astron. Soc.* **62**, 699–718.
- KOEBERL C. AND SHIREY S. B. (1993) Detection of a meteoritic component in Ivory Coast tektites with rhenium-osmium isotopes. *Science* **261**, 595–598.
- KOEBERL C., BOTTOMLEY R., GLASS B. P. AND STORZER D. (1997) Geochemistry and age of Ivory Coast tektites and microtektites. *Geochim. Cosmochim. Acta* **63**, 1745–1772.
- KOEBERL C., REIMOLD W. U., BLUM J. D. AND CHAMBERLAIN C. P. (1998) Petrology and geochemistry of target rocks from the Bosumtwi impact structure, Ghana, and comparison with Ivory Coast tektites. *Geochim. Cosmochim. Acta* **62**, 2179–2196.
- KUKKONEN I. T., KIVEKÄS L. AND PAANANEN M. (1992) Physical properties of kårnåite (impact melt), suevite and impact breccia in the Lappajärvi meteorite crater, Finland. *Tectonophysics* **216**, 111–122.
- LANGÉ M. A. AND AHRENS T. J. (1979) Impact melting early in lunar history. *Proc. Lunar Planet. Sci. Conf.* **10th**, 2707–2725.
- LANGEREIS C. G., DEKKERS M. J., DE LANGÉ G. J., PATERNE M. AND VAN SANTVOORT P. J. M. (1997) Magnetostratigraphy and astronomical

- calibration of the last 1.1 Myr from an eastern Mediterranean piston core and dating of short events in the Brunhes. *Geophys. J. Int.* 129, 75–94.
- LAROCHELLE A. AND CURRIE K. L. (1967) Palaeomagnetic study of igneous rocks from the Manicouagan structure, Quebec. *J. Geophys. Res.* 72, 4163–4169.
- LEINO M. A. H. (1991) *Paleomagneettisten Tulosten Monikomponenttiansalyysi Pienimman Neltösunnan Meretelmällä* (in Finnish). Report Q29.1/90/1, Laboratory for Palaeomagnetism, Department of Geophysics, Geological Survey of Finland, Espoo, Finland. 15 pp.
- LEUBE A., HIRDES W., MAUER R. AND KESSE G. O. (1990) The early Proterozoic Birimian Supergroup of Ghana and some aspects of its associated gold mineralization. *Precambrian Res.* 46, 139–165.
- LIPPOLT H. J. AND WASSERBURG G. J. (1966) Rubidium-Strontium-Messungen an Glimsirn vom Bosumtwi-Krater und an Elfenbeinküsten-Tektiten. *Z. Naturforschung* 21a, 226–231.
- MACLAREN M. (1931) Lake Bosumtwi, Ashanti. *Geographical J.* 78, 270–276.
- MASAITIS V. L., DANILIN A. I., MASHCHAK M. S., RAIKHLIN A. I., SELIVANOVSKAYA T. V. AND SHADENKOV E. M. (1980) *The Geology of Astroblemes* (in Russian). Nedra Press, Leningrad, Russia. 231 pp.
- MELOSH J. (1989) *Impact Cratering—A Geological Process*. Oxford Univ. Press, New York, New York, USA. 245 pp.
- MCGREGOR D. P. (1937) Results of a hydrographic survey of Lake Bosumtwi. *Gold Coast Geol. Surv.* 8, 39–46.
- OJA A. S. AND PESONEN L. J. (1990) *SQUID-Magnetometer in Palaeomagnetic Research* (in Finnish). Open file report Q29.1/90/1, Laboratory for Palaeomagnetism, Geophysics Department, Geological Survey of Finland, Espoo, Finland. 32 pp.
- OJAMO H., PESONEN L. J., ELO S., HAUTANIEMI H., KOEBERL C., REIMOLD W. U. AND PLADO J. (1997) The Bosumtwi Impact Structure, Ghana: International geophysical co-operation at the best (abstract). In *Sovellusten geofysikan XI neuvottelupäivät* (eds. P. Kaikkonen, K. Komminaho and H. Salmirinne), p. 10–11. Oulun yliopisto, Oulu, 22–23.10.1997.
- PALME H., GRIEVE R. A. F. AND WOLF R. (1981) Identification of the projectile at the Brent crater, and further considerations of projectile types at terrestrial craters. *Geochim. Cosmochim. Acta* 45, 313–323.
- PESONEN L. J. (1996) The Iso-Naakkima meteorite impact structure: Physical properties and paleomagnetism of a drill core (abstract). *Meteorit. Planet. Sci.* 31 (Suppl.), A105–A106.
- PESONEN L. J., MARCOS N. AND PIPPING F. (1992) Palaeomagnetism of the Lappajärvi impact structure, western Finland. *Tectonophysics* 216, 123–142.
- PESONEN L. J., NEVANLINNA H., LEINO M. A. H. AND RYNO J. (1994) The Earth's Magnetic Field Maps of 1990.0. *Geophysica* 30, 57–77.
- PESONEN L. J., KOEBERL C., OJAMO H., HAUTANIEMI H., ELO S. AND PLADO J. (1998) Aerogeophysical studies of the Bosumtwi impact structure, Ghana. *Geol. Soc. Amer. Abstracts with Programs* 30, A-190.
- PESONEN L. J., PLADO J., KOEBERL C. AND ELO S. (1999) The Lake Bosumtwi meteorite impact structure, Ghana: Magnetic modelling (abstract). *Meteorit. Planet. Sci.* 34 (Suppl.), A91–A92.
- PESONEN L. J., ELO S., LEHTINEN M., JOKINEN T., PURANEN R. AND KIVEKÄS L. (2000) The Lake Karikkoseikå impact structure, central Finland—New geophysical and petrographic results. *Geol. Soc. Amer. Special Paper* 339, 131–147.
- PIKE R. J. (1985) Some morphologic systematics of complex impact structures. *Meteoritics* 20, 49–68.
- PILKINGTON M. AND GRIEVE R. A. F. (1992) The geophysical signature of terrestrial impact craters. *Rev. Geophys.* 30, 161–181.
- PIPER J. D. A. AND LOMAX K. (1973) Palaeomagnetism of Precambrian Birimian and Tarkwaian rocks of West Africa. *Geophys. J. Royal Astron. Soc.* 34, 435–450.
- PLADO J., PESONEN L. J. AND PUURA V. (2000) The effect of erosion on gravity and magnetic signatures of complex impact structures: Geophysical modelings and applications. *Geol. Soc. Amer. Special Paper* 339, 229–239.
- POHL J., ECKSTÄLLER A. AND ROBERTSON P. B. (1988) Gravity and magnetic investigations in the Houghton impact structure, Devon Island, Canada. *Meteoritics* 23, 235–238.
- PURANEN R. AND SULKANEN K. (1985) Technical Description of Microcomputer-controlled Petrophysical Laboratory. Open File Report Q15/27/85/1, Dept. of Geophysics, Geological Survey of Finland, Espoo, Finland. 252 pp.
- REIMOLD W. U., BRANDT D. AND KOEBERL C. (1998) Detailed structural analysis of the rim of a large complex impact crater: Bosumtwi Crater, Ghana. *Geology* 26, 543–546.
- SCHNETZLER C. C., PINSON W. H. AND HURLEY P. M. (1966) Rubidium-Strontium age of the Bosumtwi crater area, Ghana, compared with the age of the Ivory Coast tektites. *Science* 151, 815–819.
- SCOTT R. G., PILKINGTON M. AND TANCZYK E. I. (1997) Magnetic investigations of the West Hawk, Deep Bay and Clearwater impact structures, Canada. *Meteorit. Planet. Sci.* 32, 293–308.
- STANFORS R. (1973) The Mien structure—A cryptoexplosion formation in the Fennoscandian basement. PhD. thesis, Lund University, Sweden. 144 pp.
- ZIJDVERELD J. D. (1967) A.C. demagnetization in rocks. In *Methods in Paleomagnetism* (eds. D. W. Collinson, K. M. Creer and S. K. Runcorn), pp. 254–286. Elsevier, New York, New York, USA.

Plado J., Pesonen L. J., Elo S., Puura V. and Suuroja K., 1996.
Geophysical research on the Kärđla impact structure, Hiiumaa Island, Estonia.
Meteoritics & Planetary Science 31, 289–298.

Geophysical research on the Kärđla impact structure, Hiiumaa Island, Estonia

JÖRI PLADO¹*, LAURI J. PESONEN², SEppo ELO², VÄINO PUURA^{1,3} AND KALLE SUUROJA⁴

¹Institute of Geology, Tartu University, EE-2400 Tartu, Estonia

²Department of Geophysics, Geological Survey of Finland, SF-02150 Espoo, Finland

³Institute of Geology, Estonian Acad. Sci., EE0101 Tallinn, Estonia

⁴Geological Survey of Estonia, EE0100 Tallinn, Estonia

*Correspondence author's e-mail address: jplado@math.ut.ee

(Received 1995 June 22; accepted in revised form 1995 December 13)

Abstract—The 4 km wide and 500 m deep circular Kärđla impact structure in Hiiumaa Island, Estonia, of middle Ordovician age (~455 Ma), is buried under Upper Ordovician and Quaternary sediments. To constrain the geophysical models of the structure, petrophysical properties such as magnetic susceptibility, natural remanent magnetization (NRM), density, electrical conductivity, porosity and P-wave velocity were measured on samples of crystalline and sedimentary rocks collected from drill cores in different parts of the structure and the surrounding area. The results were used to interpret the central gravity anomaly of ~3 mGal and the magnetic anomaly of ~100 nT and also the surrounding weak positive anomalies revealed by high precision survey data.

The unshocked granitic rocks outside the structure have a mean density of ~2630 kgm⁻³. Their shocked counterparts have densities of ~2400 kgm⁻³ at a depth of ~500 m, increasing up to 2550 kgm⁻³ at a depth of 850 m. Porosity and electrical conductivity decrease, but P-wave velocity increases as density increases away from the impact point. Thus, the gradual changes in the physical properties of the rocks as a function of radial distance from the crater centre are consistent with an impact origin for Kärđla. As in many other impact structures, the magnetization of the shocked rocks are also clearly lower than those of unshocked target rocks.

A new geophysical and geological model of the Kärđla structure is presented based on geophysical field measurements and data on gradual changes in petrophysical parameters of the shocked target and overlying rocks, together with structural data from numerous boreholes. An important feature of this model is the lack of an observable geophysical signature of the central uplift observed in drillcores.

INTRODUCTION

The number (~145) of proven impact structures on Earth is relatively small (Grieve and Pesonen, 1992; 1996) compared with the impact crater records of other terrestrial planets. The small number on Earth is due to: (1) the ability of terrestrial erosion and other geological processes to erase the signatures of many impact craters, particularly those of older ones. More than half of the impact structures identified are younger than 200 Ma (Grieve and Pesonen, 1996); (2) the insufficient search for marine impact craters; only four structures, of which two have been proven (Jansa *et al.*, 1989; Hildebrand *et al.*, 1991) and two are of possible (Flodén and Bjerkeus, 1994; Gudlaugsson, 1993) impact origin, are situated on marine areas; (3) the short history of research on this subject (Melosh, 1989). To date, 23 identified impact structures have been found in the Fennoscandia-Baltic area, which represents an eroded Precambrian Shield and its southern slope in northern Europe (Fig. 1; Pesonen, 1996; Martti Lehtinen, 1995, pers. comm.).

Rocks affected by impact are situated around and below impact structures over distances exceeding ~2× their diameter in the case of simple or complex structures (Melosh, 1989). However, in the case of large multi-ring impacts (*e.g.*, those at Sudbury and Vredefort) the impact cratering process had an influence on the composition and evolution of the lithosphere comparable to that of endogenic geological processes (Glikson, 1995).

One of the indicative criteria for identifying a possible impact structure is geophysical characteristics (*e.g.*, gravity and magnetic anomalies in the area of the structures, Henkel and Pesonen, 1992; Pesonen, 1994). Studies of geophysical data on impact structures have augmented our knowledge of impact-generated physical effects



FIG. 1. Map showing the 23 meteorite impact structures in Fennoscandia (after Pesonen, 1996).

on target rocks and their surroundings. Many geophysical effects are proportional to the contrasts in physical properties between the shock-affected rocks in the structures and those outside the structure, to their relative volumes and to structural attitudes (Henkel and Pesonen, 1992).

Many terrestrial impact structures were initially identified through related geophysical anomalies, and their impact origin was established later through geological studies. An example is the Kärđla crater in Hiiumaa Island, Estonia (Fig. 1). This structure is 4 km in diameter, 500 m deep and ~455 Ma old. The research history of this structure has been summarized by Puura and Suuroja (1992) and Plado (1993). In general, the evidence of different shock stages in Kärđla is as follows: fracturing of the target rocks penetrates to a depth exceeding 700 m from the contemporary Quaternary ground level; planar deformation features (PDFs) in quartz clasts (shock pressure 10–30 GPa; Grieve and Pesonen, 1992); conical fractures (probably shatter cones) in the sandstone, limestone and claystone blocks in down-slumped breccia; occurrences of typical impact-associated rocks, for example, low temperature breccias and fractured basement rocks showing an increase in K_2O content with respect to unshocked rocks (Puura and Suuroja, 1992; Puura *et al.*, 1994). Thus much evidence from different fields (geochemistry, geology, petrology, structural geology, geophysics) supports an impact origin for Kärđla. On the basis of cratering models and shock effects, Henkel and Pesonen (1992) and Pesonen (1993) have argued that there should be a systematic radial dependence between the physical properties of rocks and distance from the crater centre in much the same way as shown for the decay of shock pressure in the Charlevoix structure by Grieve *et al.* (1990). Such radial dependencies have been reported (*e.g.*, Dyrelius, 1988; Järvälä *et al.*, 1995), but due to the lack of continuous exposures or multiple drillings, they are not well documented.

The Kärđla impact structure provides an ideal target for testing the behaviour of physical properties as a function of radial distance since it has been penetrated by a very dense grid of drill holes, which provide test material in both vertical and horizontal directions from centre to rim.

The purpose of this study is (1) to show that the gradual changes observed in the physical properties of the crater and surrounding rocks in the Kärđla structure could be applied in the search for and studies of meteorite craters, (2) to describe the petrophysical properties of rocks inside the Kärđla crater and in its immediate vicinity, (3) to link the petrophysical properties of rocks with geophysical field data and (4) to constrain the gravity and magnetic models of the structure with petrophysical data.

KÄRDĽA IMPACT STRUCTURE

The circular Kärđla structure lies in the northeastern part of Hiiumaa Island, Estonia (Figs. 1 and 2). Figure 2a shows the location of the structure on the island and the sites of drill holes (F351, F352, F361, F364) outside the structure. Figure 2b shows the present topography of Kärđla and the sites of drill holes (K1, K18, 415, F173, F175, 383) inside the structure and in its rim wall. The Kärđla structure was formed in a platform area where the crystalline basement was covered with a thin sedimentary veneer. The basement consists of microcline granites, migmatized amphibolites and gneisses probably of Mesoproterozoic age, although no isotopic ages have yet been determined for crystalline rocks on Hiiumaa. Structurally the basement of Hiiumaa is part of the Svecofennian (~1.9 Ga; Puura and Huhma, 1993) granitic block

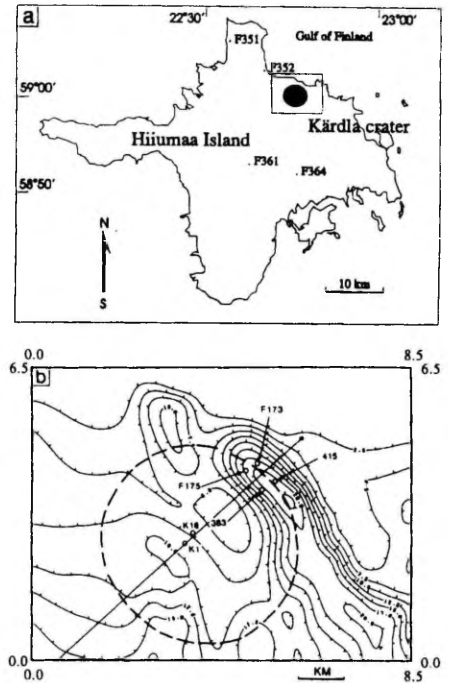


FIG. 2. (a) Location of Kärđla structure (No. 54) on Hiiumaa Island, Estonia, and of drill holes (F351, F352, F361, F364). The reference for geophysical maps and (b) topographic map (contour interval 2.5 m) of Kärđla are shown. The location of the gravity and magnetic profiles and drill holes (K1, K18, 415, F173, F175, 383) are also marked.

of southwestern Estonia. These granulites have undergone retrograde metamorphism of amphibolitic grade (Puura *et al.*, 1983). At the moment of impact, a shallow sea, ~20 m deep, covered the sea floor (Puura *et al.*, 1989). In the cratering process, the basement and the preimpact early Cambrian (~570–550 Ma old), early and middle Ordovician (~480–455 Ma old) ~140 m thick sedimentary cover, which is found slightly outside the crater rim wall, were elevated and tilted outwards. The crater rim wall and the allochthonous breccias, which comprise sedimentary and crystalline rocks, became a source of terrigenous debris that affected the composition of the postimpact marine sediments in the surroundings and in the crater. Connected to the sea through two gaps, the central depression acted as a sedimentary trap and so is occupied by the most complete and thickest postimpact Ordovician sequence. Quaternary marine and lacustrine deposits, with an average thickness of 15 m, fill depressions in the topography (Puura and Suuroja, 1992). The crater is barely visible in the landscape today (see Fig. 2b).

Recent studies of cores from holes K1 and K18 drilled into the centre of the structure revealed a ~110 m high central uplift within an annular depression. The middle hole, K18, had penetrated 35 m into this central uplift, which has a diameter of ~300 m. Hole K1,

drilled ~310 m southwest of K18, missed it. Kärđla is thus a relatively small but complex meteorite crater with a central uplift. It is notable that the diameter of Kärđla (4 km) is the very same as the transition diameter between single and complex craters in crystalline terranes (Grieve and Pesonen, 1992). We suppose here that the presence of seawater on top of target facilitated the formation of central uplift.

The impact age (middle Ordovician) was determined micropaleontologically (Bauert *et al.*, 1987; Grahn and Nölvak, 1993). Using global stratigraphic charts (Harland *et al.*, 1990; Cowie and Bassett, 1989), Bauert *et al.* (1987) dated the Kärđla event to the lowermost Caradoc (455 Ma). The chitinozoan zone of *Lagenochitina? dalbyensis* established (Grahn and Nölvak, 1993) in the oldest postimpact sediments in the drill core 383 (in Paluküla, northeastern margin of the Kärđla structure, Fig. 2b) corresponds to the lowermost *Diplograptus multidentis* graptolite zone and is of early Idavere age (~455 Ma).

According to Lindström *et al.* (1992), the Tvären (No. 12), Kärđla (No. 54) and Lockne (No. 48) structures (Fig. 1) may have originated from a triplet impact in a shallow marine area. Conodonts of the *Amorphognatus tvaerensis* Zone (Lindström *et al.*, 1992) have been recorded from the postimpact sediments of these craters. Grahn and Nölvak (1993) used chitinozoas to specify and correlate also Granby (No. 25) with the Lockne, Kärđla and Tvären impact events. According to their preliminary findings, the Lockne event is either contemporaneous with or slightly younger than the Kärđla event. The Tvären structure is clearly older (Kukruse Stage, ~460 Ma) than Lockne or Kärđla as shown by the occurrence of chitinozoan fauna in the oldest postimpact beds.

METHODS AND DATA

Geophysical Field Surveys

The gravity and magnetic data on Hiiumaa Island were from measurements made by the Geological Survey of Estonia in 1972–1973 (Suuroja *et al.*, 1974). Gravity measurements were made with two gravimeters (GRK-2, GAK-PG) in two stages. First, a base network of 2000 m × 1000 m was created with GRK-2 gravimeters. The gravimeter was read twice at each station and measurements were repeated at all survey stations. The stations were positioned by means of topographic maps and levelled. The standard error of measurements is 0.04 mGal. At the second stage, measurements at survey points were made with gravimeter GAK-PG. The distance between points along profiles oriented NE-SW was 200 m and the distance between profiles was 500 m. The gravimeter was read twice at each station on two occasions. The standard error in the gravity measurements made at survey points was 0.1 mGal. The survey points were positioned by pacing with a compass or by means of topographic maps and levelled. The standard error in this positioning was 25 m. The observed gravity data were corrected for tidal and instrumental variations, latitude and elevation. A standard Bouguer reduction was made, assuming a mean density of 2300 kgm⁻³, which is typical of sedimentary rocks in the East European platform.

The vertical component (*Z*) of magnetic field intensity was measured with two magnetometers (M-27) with an accuracy of ±3 nT in two stages. First, a grid of base stations that was practically the same as that in the gravity survey was established. One magnetometer was used to carry out the survey and the other to monitor diurnal and other more rapid magnetic field fluctuations at 10 min intervals at the fixed base station during the magnetic survey. The line spacing was 500 m and the station spacing along the profiles was 100 m. The magnetometer was read twice at each station. The standard error of the readings was 10 nT (Suuroja *et al.*, 1974).

In 1975, local gravity and magnetic anomaly maps were compiled at 1:25,000 scale. The results of these geophysical investigations were used in the present study. The original contour maps were first digitized, and then new maps, including horizontal gradient maps, were produced for this study.

Petrophysical Sampling

This study is based on rock samples from seven subvertical (±10°) drill holes, bored by the Geological Survey of Estonia. They have an average

weight of ~400 g and a volume of 200 cm³ and were taken with a hammer from cores of all available rock types, including postimpact sediments, impact rocks and preimpact target rocks.

Most of the samples (69) were obtained from the 815.2 m deep drill core K1 and from the 431.4 m deep drill core K18 at the centre of the Kärđla structure (Fig. 2b). To establish the petrophysical properties of rim wall rocks, 11 samples were taken from drill core 415, 11 from drill core F173 and 4 from core F175 at or near the rim. Fifteen samples (cores F361 and F364; Fig. 2a) were taken to determine the petrophysical properties of unshocked rocks in the surrounding terrain, which is mainly Proterozoic granite.

The samples represent different lithologies as follows: (1) 82 specimens of shocked rocks, of which 56 are impact breccias and fractured granitic rocks from the allochthonous and subautochthonous sequence of the crater, 15 are fractured granites and 11 are fractured amphibolites from the rim wall of the crater; (2) 15 specimens of unshocked autochthonous granites from the basement of Hiiumaa Island at distances exceeding twice the diameter of the crater; (3) 13 specimens of postimpact sediments, of which 10 are limestones, 2 marls and 1 siltstone, all of Ordovician age.

Petrophysical Measurements

The petrophysical data (magnetic susceptibility, natural remanent magnetization; density, electrical conductivity; porosity, obtained with water-saturation technique; and seismic P-wave velocity) of 110 samples were measured at the Petrophysical Laboratory of the Geological Survey of Finland. The instruments and techniques have been described by Puranen and Sulkanen (1985).

Palaeomagnetic Measurements

Fifteen specimens of impact breccias, fractured granites and autochthonous granites were demagnetized with alternating magnetic fields (a.f.) to study the palaeomagnetic behaviour of the Kärđla rocks and to find evidence of shock in the remanent magnetization. The measurements were made at the Palaeomagnetic Laboratory of the Geological Survey of Finland using a Molspin apparatus with steps of 2.5 mT–10 mT up to 100 mT. Since the drill cores were unoriented and often broken, no absolute palaeomagnetic directions were obtained, thus impairing the usefulness of palaeomagnetic information for dating (*e.g.*, Pesonen *et al.*, 1992).

Geophysical Modelling

The geophysical profile across the Kärđla crater was interpreted using the interactive GRAVMAG software program package (Pedley, 1991). An interactive forward modelling program for simultaneous interpretation of gravity and magnetic data, GRAVMAG uses 2.5D polygonal "blocks," whose dimensions and physical properties can be varied and the corresponding gravity and magnetic anomalies calculated.

Models are constrained using the results of petrophysical measurements, drill core data and the data from previous geophysical investigations in the crater area (Suuroja *et al.*, 1974). By the reason that GRAVMAG uses the total intensity of the magnetic field (*F*), it was calculated from observed vertical component *Z* (*T*) using the following equation:

$$F = Z / \sin i \quad (\text{nT}), \quad \text{Eq. (1)}$$

where *i* is the inclination (in degrees) of the magnetic field at the Kärđla site (~72°). Equation (1) is an approximation only since no account of horizontal component is taken into account. However, modelling experiments using another program showed that this approximation, in the area of high inclination, causes inaccuracies comparable with the standard error of the measurements (10 nT).

RESULTS

Geophysical Investigations

A slightly distorted, circular, negative gravity anomaly ~ -3 mGal in amplitude and 4 km in diameter, and a negative magnetic anomaly ~ -100 nT in amplitude are associated with the Kärđla impact structure (Figs. 3 and 4). Irregularities in the anomaly patterns are mainly due to variations in density and magnetic contrasts in the bedrock (Table 1).

Petrophysical Investigations

The meteorite impact that created the Kärđla crater produced a series of rocks differing significantly in lithology and petrophysics

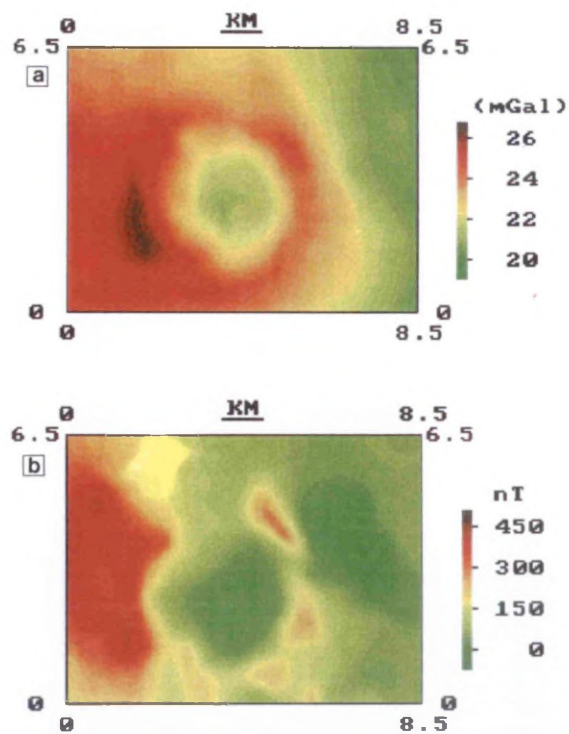


FIG. 3. (a) Bouguer gravity anomaly and (b) magnetic anomaly (vertical component) of Kärda structure. For location, see Fig. 2a. Maps produced at the Geological Survey of Finland from the original gravity data of Suuroja *et al.* (1974).

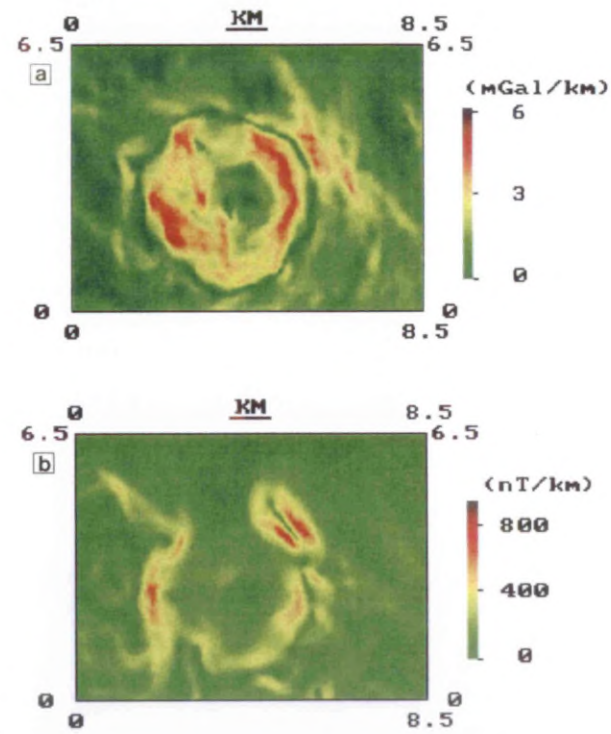


FIG. 4. (a) Horizontal gradient of Bouguer gravity anomaly of Fig. 3a. (b) Horizontal gradient of magnetic anomaly of Fig. 3b. See Fig. 3 for locations and data processing.

Plado J., Pesonen L. J. and Puura V., 1999.
The effect of erosion on gravity and magnetic signatures of complex
impact structures: geophysical modelings and applications.
In: (eds. B. O. Dressler and V. L. Sharpton)
Large Meteorite Impacts and Planetary Evolution II, Boulder, Colorado.
Geological Society of America Special Paper 339, 229–239.

from those of unshocked Precambrian bedrock in the surroundings. At the centre (drill hole K1), the rocks of the Käråla structure form distinct layers in the crater structure, as seen in Fig. 5, with postimpact sediments at the top, impact breccias in the middle and

subautochthonous granites (target) at the bottom. Note that the breccia lens consists of two layers intersected by a thin (~40 m) lens of fractured and probably allochthonous granitic layer. The lower breccia lens is only 20 m thick. At the rim wall (Fig. 6), the

TABLE 1. Mean values and standard deviations of petrophysical properties of Käråla rocks

Rock type	Location	N*	δ_w	δ_g	ϕ	v_p	χ	NRM	Q	ρ
Post-impact Sediments										
Limestone	Centre	10	2555 ±104	2782 ±61	8.5 ±5.5	4280 ±1040	40 ±20	40 ±30	51.4 ±49.2	760 ±1720
Marl	Centre	2	2513 ±97	2783 ±40	9.7 ±4.4	4120 ±700	40 ±0	50 ±0	21.3 ±7.7	110 ±30
Siltstone	Centre	1	2174 ±1244	2720 ±100	20.1		50	40	62.4	90
Impact Rocks (crater area)										
Impact breccia	Centre	28	2390 ±120	2624 ±92	9.3 ±4.3	4020 ±700	2860 ±2800	120 ±110	2.0 ±3.4	5430 ±2230
Fractured granitic rock	Centre	22	2464 ±83	2616 ±63	5.5 ±3.6	4560 ±980	4800 ±4760	380 ±460	2.3 ±1.6	2460 ±5450
Fractured granitic rock	Central uplift	6	2502 ±104	2601 ±18	3.8 ±3.6	5150 ±530	8290 ±7190	290 ±320	0.8 ±0.2	20980 ±23560
Fractured granitic rock	Rim wall	15	2600 ±40	2646 ±25	1.8 ±1.4	5300 ±490	650 ±750	150 ±140	15.3 ±24.4	15200 ±23700
Fractured amphibolite	Rim wall	11	2760 ±130	2787 ±123	0.9 ±1.0	5780 ±510	3740 ±5230	330 ±320	5.2 ±3.6	52400 ±39300
Unshocked Target Rocks (outside crater)										
Unfractured granitic rock	Surroundings	15	2630 ±70	2653 ±15	0.9 ±2.6	5880 ±680	15750 ±12990	770 ±640	2.9 ±4.7	98300 ±79900

Rock type: rocks above/below the dashed line are postimpact sedimentary/impact-generated or impact-influenced rocks. Unfractured granitic rocks from ~25 km from impact centre (see Fig. 2a). Location: centre, drill holes K1 and K18, central uplift, drill hole K18; rim wall, drill holes 415, F173 and F175; surroundings, drill holes F361 and F364 (see Fig. 2 and text). N* = number of specimens; δ_w = wet density (kgm^{-3}); δ_g = grain density (kgm^{-3}); ϕ = porosity (%); v_p = P-wave velocity (ms^{-1}); χ = magnetic volume susceptibility (10^{-4} SI); NRM = intensity of natural remanent magnetization (mAm^{-1}); Q = Koenigsberger ratio (-); ρ = specific resistivity (Ωm). Roughly 60% of unshocked granitic specimens had resistivities >100 $\text{K}\Omega\text{m}$ (above the detection limit). For calculations, a value of 100 $\text{K}\Omega\text{m}$ was used for these samples.

fractured granite basement is intersected by a layer (~2.9 m) of fractured amphibolite, which also occurs at the bottom of drill core F173. Table 1 summarizes the petrophysical data of each lithological unit of drill cores K1 (at the centre) and F173 (in rim wall). In Figs. 5 and 6, the petrophysical data are plotted along the drill cores, thus emphasizing the gradual change in petrophysical values as a function of decreasing shock (approximate radial distance away from crater centre).

Density—The density of the rocks of the Käråla structure is fairly variable between lithological units (Table 1; Figs. 5 and 6). The postimpact limestones have a mean density of 2555 kgm^{-3} , which is comparable to values for similar rocks from other parts of Estonia (2570 kgm^{-3} ; Maasik, 1959). However, densities decline towards the lowermost part of the Ordovician sequence owing to the increase in clay content. The post-impact siltstone in the lowermost part of the sediments filling the depression has the lowest density (2179 kgm^{-3}).

The density of impact breccias ($\sim 2390 \text{ kgm}^{-3}$) is clearly lower than that of unshocked granite ($\sim 2630 \text{ kgm}^{-3}$) from the basement of Hiiumaa Island and that of slightly shocked granite ($\sim 2460 \text{ kgm}^{-3}$) from the basement of the Käråla structure (cores K1 and K18). The same decreasing trend in density is seen in many other terrestrial impact craters (e.g., Lappajärvi, Finland, Elo *et al.*, 1992; Gosses Bluff, Australia, Barlow, 1979; Clearwater West, Canada, Plante *et al.*, 1990; *etc.*). This is because the breccias, which consist of various mixtures of clasts of crystalline rocks, disintegrated sandy material of Cambrian sandstone and siltstone and particles of Ordovician carbonate rocks, have high porosity and thus low density. The porosity-corrected density (grain density) appears to be slightly smaller in impact-affected granites than in unshocked target granites (Table 1). This could be due to microfracturing caused by the shock. The density contrast between fractured ($\sim 2460 \text{ kgm}^{-3}$) and unfractured target rocks ($\sim 2630 \text{ kgm}^{-3}$) is $\sim 170 \text{ kgm}^{-3}$, thus partly causing the negative gravity anomaly. The highest densities ($\sim 2760 \text{ kgm}^{-3}$) are found in amphibolites from drill-core 415 in the rim. Granitic rocks in the rim are also characterized by fairly high densities ($\sim 2600 \text{ kgm}^{-3}$), which are only slightly lower than those of unshocked granites ($\sim 2630 \text{ kgm}^{-3}$) and higher than those of the counterparts at the centre (2470 kgm^{-3}). The relatively high density of granites in the rim wall produces the gravity highs at the rim around the central minimum (Figs. 3a and 4a).

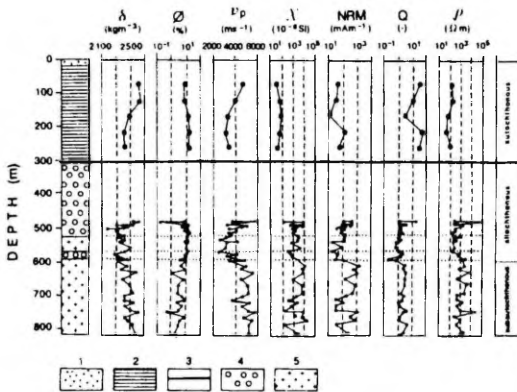


FIG. 5. Petrophysical properties of rocks from drill core K1 taken at centre of structure (see Fig. 2b). From left to right: wet density (δ_w), porosity (ϕ), P-wave velocity (v_p), magnetic susceptibility (χ), intensity of natural remanent magnetization (NRM), Koenigsberger ratio (Q) and specific resistivity at ρ at 500 Hz. Lithologies: 1 = Quaternary deposits, 2 = postimpact sediments, 3 = boundary between postimpact sediments and impact-influenced rocks, 4 = impact breccia, 5 = fractured subautochthonous granite.

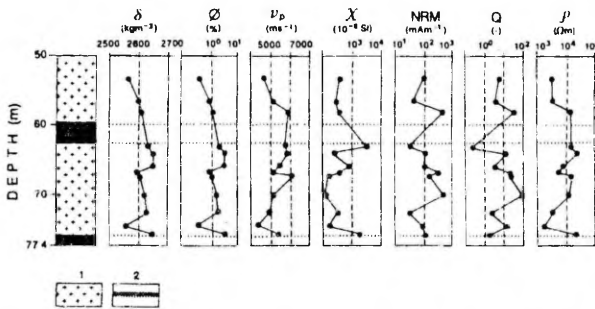


Fig. 6. Petrophysical properties of rocks from drill core F173 taken at rim wall (see Fig. 2b). See Fig. 5 for explanation. Lithologies: 1 = fractured granite, 2 = fractured amphibolite.

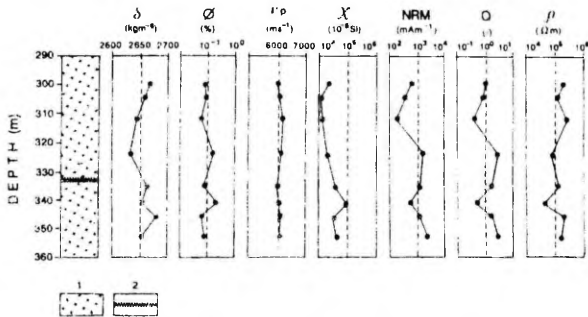


Fig. 7. Petrophysical properties of rocks from drill core F361 taken at basement of Hiiumaa Island (see Fig. 2a). See Fig. 5 for explanation. Lithologies: 1 = granite, 2 = amphibolite.

The density minima in all rock types (Figs. 5, 6, 7) clearly coincide with the high porosity, low P-wave velocity and low electrical resistivity values. The same tendency is shown by the similar rocks of the Lappajärvi impact structure (Kukkonen *et al.*, 1992).

However, the density of fractured granitic rocks at the centre of the crater floor increases with depth (Fig. 5). In the uppermost part of drillhole K1, the mean density of subautochthonous granitic rocks is $\sim 2400 \text{ kg m}^{-3}$, but in the lowermost part it is already 2550 kg m^{-3} (Fig. 7). If these data are compared with the mean density (2630 kg m^{-3}) of the unshocked granites collected several diameters away from crater centre, it can be estimated (using the linear regression) that the impact-caused changes in densities of rocks in the centre of the crater extend to the depth (h) of $\sim 950 \text{ m}$. It gives the h/D ratio $0.95/4.0 = 0.24$ at the present erosional level. Analysis of the P-wave velocity (v_p) data gives similar morphometric estimates. We know of only two impact structures where density measurements have been made at great depth, namely Ries (Ernstson and Pohl, 1974) and Siljan (Dyrelus, 1988). Both showed the same tendency of density to change as a function of depth. Part of density increase is probably due to compression, but we propose that another part could be related to gradual decrease in shock-induced stress and fracturing with depth.

Seismic P-wave Velocity—The v_p in the limestone is relatively low ($\sim 4280 \text{ ms}^{-1}$; Table 1), but there is a large variation in the

values ranging from 3000 to 6000 m/s. Values are lower in the lowermost part of limestones, where sediments are more clay-like.

The v_p in the impact breccias is characterized by large variations ranging from 2980 to 5880 ms^{-1} with a mean value of 4020 ms^{-1} , which is much lower than that in unfractured granitic rocks ($\sim 5880 \text{ ms}^{-1}$; Table 1). In general, the low values of v_p can be attributed to higher porosity due to increased fracturing caused by the impact. The P-wave velocities in unfractured granite samples do not show large variations. Averages for the fractured granitic rocks from the crater bottom at the centre ($\sim 4560 \text{ ms}^{-1}$) and from the rim ($\sim 5300 \text{ ms}^{-1}$) are clearly lower than those for unshocked granites. The overall trend in v_p of fractured granites from the subautochthonous sequence (drill-core K-1; Fig. 5) shows an increase in v_p with depth. The v_p in amphibolitic rocks from the rim wall is clearly higher than in other rocks of the crater, as would be expected from their higher densities. However, the influence of fracturing due to shock on v_p in rim amphibolites ($\sim 5780 \text{ ms}^{-1}$) is evident when the values are compared with those of typical unfractured amphibolites (6800 m/s; Dortman, 1992).

Porosity—The average porosities of the overlying postimpact sediments range from 8.5% (limestones) to 20.1% (siltstones) (Table 1). These high porosities are primary features typical of Ordovician sedimentary rocks caused by structures and fabrics in these sediments and not by impact.

In the shock-affected rock sequence, the porosity varies from 0.6% (fractured granite) to 18.5% (impact breccia); while in the unshocked target rocks, it is typically $< 1\%$ (Table 1). We propose that the increased porosity is mainly due to fracturing and brecciation caused by shock and crater-forming processes. In fractured granitic rocks, at the centre of the crater, the average porosity is 5.5% (Table 1) and decreases with depth (Fig. 5) in harmony with the decrease in the level of shock-induced stress, thus fracturing with depth (Pilkington and Grieve, 1992). Porosity values are very low and uniform (0.1–1.1% in amphibolites and 0.4–4.4% in granites) in the fractured rim rocks.

Electrical Conductivity—Resistivity of postimpact sediments is low ($< 1000 \text{ } \Omega\text{m}$); it was highest for limestone ($\sim 900 \text{ } \Omega\text{m}$) and lowest for marl and siltstone ($\sim 100 \text{ } \Omega\text{m}$) (Table 1). The unshocked granitic rocks in the surroundings have high electrical resistivities ($> 100 \text{ k}\Omega\text{m}$). Roughly 60% of unshocked granitic specimens had resistivities $> 100 \text{ k}\Omega\text{m}$ (above the detection limit). Resistivities are lower in the subautochthonous granitic rocks ($\sim 2460 \text{ } \Omega\text{m}$) and in impact breccias ($\sim 5430 \text{ } \Omega\text{m}$) at the centre of the crater due to a shock-induced increase in the porosity (brecciation, microfracturing) and thus in the H_2O content of shocked rocks. Resistivity, however is a very variable petrophysical parameter, and standard deviations of resistivity data on fractured granitic rocks at the centre of the crater are at least twice as high as their means (Table 1). The correlation between resistivity and density (Fig. 8) of impact breccias and subautochthonous granites is not clear: specimens with similar density may have resistivities differing by a

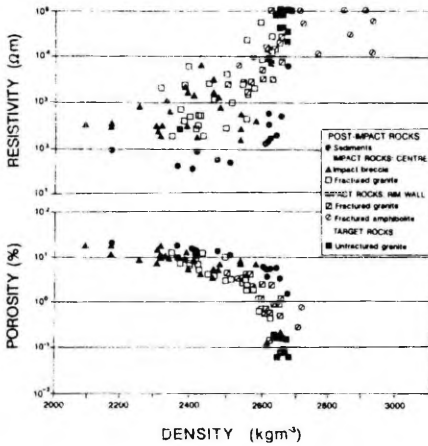


Fig. 8. Resistivity (upper) and porosity (lower) vs. density for drill cores K1, K18, 415, F173, F175, F361 and F364. Locations of drill holes are shown in Fig. 2.

factor of 30. There is a high correlation between resistivity and porosity. The process of impact cratering also affects the resistivity values of rim wall rocks, which yield relatively low resistivity (~ 52 k Ω m in amphibolites and ~ 15 k Ω m in granites) compared with the typical resistivities (10^5 Ω m– 10^7 Ω m) of unshocked target rocks (Dortman, 1992). The sharp decrease in resistivity of shocked rocks in the Käråla impact structure calls for detailed resistivity sounding in the Käråla area (e.g., Grieve and Pesonen, 1992; Eio *et al.*, 1992).

Magnetic Properties.—The magnetic susceptibility ($\sim 40 \times 10^{-6}$ SI) and NRM intensity (~ 40 mAm $^{-1}$) of postimpact sediments are typical of limestones and silts (Table 1). The Q-values (Koenigsberger ratio) of the sediments are fairly high (5–100), but since the susceptibilities and NRMs are very weak, the high values could be due to instrumental noise and dia- and paramagnetic contributions to susceptibility, they cannot be regarded as reliable.

The magnetic properties of the shock-influenced rock sequence are very different from those of the unshocked target rocks (Figs. 5 and 7; Table 1). Both impact breccias and subautochthonous granites have weak susceptibilities (~ 3000 – 3500×10^{-6} SI) and NRM intensities (~ 120 – 380 mAm $^{-1}$). Slightly higher susceptibilities ($\sim 8290 \times 10^{-6}$ SI) and NRM intensities (~ 290 mAm $^{-1}$) are observed in granites from the central uplift (Table 1). The average Q-values of these rocks (~ 2) are more variable in breccias (0.2–20) than in subautochthonous granites (0.4–4.6). The Q-values of the Käråla rocks are clearly lower than those of impact-influenced rocks in other impact craters (e.g., Lappajärvi, Pesonen *et al.*, 1992). Nevertheless, all magnetic properties decrease slightly in the subautochthonous sequence of the crater with depth (Fig. 5).

The Q-values are higher for the rim wall rocks (up to 5 in amphibolites and 15 in granites): the magnetic susceptibility and NRM intensity averages are $\sim 3740 \times 10^{-6}$ SI and ~ 330 mAm $^{-1}$ in amphibolites and $\sim 650 \times 10^{-6}$ SI and ~ 150 mAm $^{-1}$ in granites, respectively (Table 1). Thus, the enhanced Q-values in rim wall rocks are mainly due to decreased induced magnetization in comparison with surroundings.

The unshocked granites have susceptibilities ($\sim 15750 \times 10^{-6}$ SI) and NRM intensities (~ 770 mAm $^{-1}$; Fig. 6) resulting in moderately high Q-values (~ 3 ; Table 1), which are higher than those of Precambrian granites of Fennoscandia (Puranen, 1989).

Palaeomagnetism

Palaeomagnetic data on seven unshocked target granites reveal a very high stability of NRM in the course of a.f. demagnetization, possibly due to the presence of hematite or very fine-grained magnetite. The NRM intensities range from 250 to 1000 mAm $^{-1}$ (with Q-values ranging from 1.0 to 2.2), and the inclinations of NRM are systematically shallow. Since there is no significant viscous remanent magnetization (VRM) due to the present Earth's magnetic field (PEF), the remanent vectors could not be reoriented with VRM technique (Järvelä *et al.*, 1995); thus we were unable to obtain a palaeomagnetic apparent polar wander path (APWP) age for this shallow "target" NRM component. We point out however, that the component differs from the NRM directions recorded in impact generated rocks. Impact breccias (three specimens) carry a relatively weak and semistable NRM, with intensity ~ 10 – 100 mAm $^{-1}$ and Q-values ≤ 1 . The inclination of the characteristic NRM of the breccias is negative in all three cases. This weak NRM in breccias is probably due to randomizing of NRM vectors caused by brecciation process.

The subautochthonous granites from the central uplift (borehole K18) have weak (20–100 mAm $^{-1}$) and moderately hard NRM. The NRM is clearly composed of two to three components, of which the hardest one has a shallow inclination similar to those of the unshocked target rocks. The nature of other components is unclear, but one of them could be a VRM or shock remanent magnetization (SRM). Owing to lack of orientation, no ages can be assigned for these components.

Seven samples from the central subautochthonous granites below the crater bottom reveal systematic changes in their palaeomagnetic behaviour as a function of depth. The NRM intensity decreases while hardness increases downwards. The deepest samples from 240 m below the crater bottom behave in a similar fashion to the samples of unshocked target rocks, which supports the concept that the shock effects on magnetic properties are only seen in rocks of the crater floor (impact breccias) or just below the crater proper (slightly fractured granites), not in those at deeper depths.

In summary, palaeomagnetic measurements reveal systematic differences in magnetic behaviour of the rocks as a function of depth or lateral distance from the centre. These are most likely caused by shock but due to lack of orientation of the drill-cores; attesting to SRM in the rocks, or dating these components, is not possible.

Gravity and Magnetic Models

The NE-SW gravity and magnetic profiles interpolated from the local gravity and regional magnetic data are shown in Fig. 9 together with the interpretation model obtained with GRAVMAG. The location of the profile in the Käråla structure is marked in Fig. 2b.

The interpretations were based on lithostratigraphic drilling data on different structural units of the crater and on the density and magnetic susceptibility means of different rock types. The profile (Fig. 9) runs across the gravity and magnetic maximum, which is congruent with a slightly eroded rim wall in the northeastern part of the structure.

The 2.5 dimensional model consists of 10 blocks with a polygonal cross section. Their density and susceptibility values as

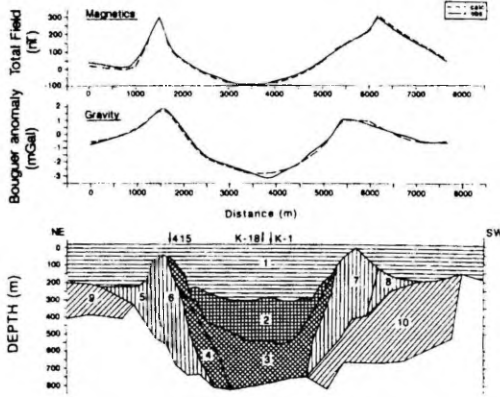


FIG. 9. (a) Magnetic (total component) and (b) gravity profiles across Kärda structure. Profiles are shown in Fig. 2b. Solid (dashed) lines denote observed (calculated) values, respectively. (c) The geophysical model of Kärda structure producing the calculated profiles in (a) and (b). Model consists of 10 lithostratigraphical units of which (1) is for postimpact sediments and (2)–(10) are for various impact-generated or affected target rocks as explained in text. The vertical scale is exaggerated $\times 2.6$.

deducted from petrophysical measurements differ (Table 1), as do their half strike values. The topmost layer (unit 1) consists of postimpact sediments (limestone, clay-like limestone, marl, silt and siltstone). The average density of this block is 2555 kgm^{-3} , the average susceptibility is $40 \times 10^{-6} \text{ SI}$ and the half strike 1000 m. Unit 2, with a susceptibility of $500 \times 10^{-6} \text{ SI}$ and a half strike of 1000 m, represents impact breccias with a low density of 2350 kgm^{-3} . The negative gravity and magnetic anomalies of Figs. 3 and 4 are mainly due to these two units. Units 3 and 4 correspond to shocked subautochthonous granitic rocks with nearly identical densities ($\sim 2600 \text{ kgm}^{-3}$) but differing magnetic susceptibilities, $30,000 \times 10^{-6} \text{ SI}$ for unit 4 and $6000 \times 10^{-6} \text{ SI}$ for unit 3, respectively. The half strike of these polygons is 500 m. The positive gravity and magnetic anomalies are caused by rocks uplifted to near surface in the rim wall: units 5, 6, 7 and 8 represent impact-influenced rocks in the rim with a half strike of 500 m and high densities (2800 kgm^{-3}) but variable susceptibilities (unit 5: $17,000 \times 10^{-6} \text{ SI}$, unit 6: $20,000 \times 10^{-6} \text{ SI}$, unit 7: $6000 \times 10^{-6} \text{ SI}$ and unit 8: $25,000 \times 10^{-6} \text{ SI}$). These relatively high susceptibility values are due not to the impact but to the mafic amphibolite lithology of target rocks. Units 9 and 10 indicate strongly magnetized bodies with susceptibilities of $20,000$ and $40,000 \times 10^{-6} \text{ SI}$, respectively. The density of these units is 2630 kgm^{-3} and the half strike is 5000 m. The density and susceptibility of the unshocked target rock (background) are 2630 kgm^{-3} and $16,000 \times 10^{-6} \text{ SI}$, respectively.

An interesting feature is that the central uplift, as shown by drill core data, has no observable geophysical signal, due to the small size of the central uplift and its considerable depth. Modelling experiments (Plado, 1993) of the central uplift with observed density contrasts reveal no observable anomalies caused by the central uplift consistent with observations. The main reason for this is the depth of the central uplift with respect to ground surface. As

the differences between the means of impact-influenced granites of the central uplift and impact-generated breccias are $\sim 110 \text{ kgm}^{-3}$ in density, $\sim 5400 \times 10^{-6} \text{ SI}$ in magnetic susceptibility and $\sim 170 \text{ mA}^{-1}$ in NRM intensity (Table 1), the absence of anomalies is not due to the lack of sufficient petrophysical contrast between central uplift and surroundings. The lack of a gravity signal of the central uplift has been noticed over other buried and relatively well-preserved impact structures with even larger diameters than that of Kärda (e.g., Kaluga, Russia, $D = 15 \text{ km}$; Dabizha and Fedynsky, 1977).

The present model explains well the gravity and magnetic anomalies and, without the central uplift, is consistent with the geology and petrophysics of the Kärda structure. A similar modelling procedure has been applied at several impact craters (e.g., Lappajärvi, Elo *et al.*, 1992; Mien, Henkel, 1982; *etc.*), but at Kärda the validity of the model could be checked with lithostratigraphical data from several drill cores. The model represents the present erosional and burial level; the original geophysical anomalies were of course different. Instantly after the impact, the positive gravity and magnetic anomalies, corresponding to the rim of the structure, were probably more intensive. Intensities of the positive gravity and magnetic anomalies decreased due to smoothing of the wall during backsurge and postimpact erosion. Intensities of the negative anomalies increased gradually due to the deposition of sediments into the depression after the impact.

DISCUSSION

The Kärda meteorite impact event generated various types of rocks in the centre of the structure, the physical properties of which differ clearly from those of the unshocked target rocks.

The impact had a much smaller effect on the properties of the rim wall rocks. In comparison with unshocked granites outside the rim, the density contrast of rim wall granites is only 30 kgm^{-3} . Similarly, porosity is higher and P-wave velocity and electrical resistivity are lower in the rim wall rocks than in unshocked target rocks (Table 1). Therefore, the impact did not only move blocks upwards to form the rim wall; it also slightly fractured the wall rocks, changing the physical properties of the rim rocks. Unfortunately, we have no reference data from similar investigations of other terrestrial impact structures.

The magnetic properties of the structure are more complicated than the gravity properties. The high susceptibilities and NRM intensities of the unshocked target rocks have not been preserved in the impact structure (Table 1, Figs. 5 and 7). Various impact-related processes may cause changes in the magnetism of impact rocks, such as growth of SRM, shock demagnetization and reduction of susceptibility by shock (e.g., Pohl, 1971; Hargraves and Perkins, 1969; Pesonen, 1993, 1994). Here we conclude that the impact process resulted in a reduction in the magnetization intensity of the target rocks and produced a random orientation of NRM vectors. Of importance is that the Q-values of impact-produced low-temperature breccias ($Q \sim 2.0$) and impact-influenced granites ($Q \sim 1.9$) at the bottom of the Kärda structure are very low due to high values of susceptibilities ($\sim 2860 \times 10^{-6} \text{ SI}$ for breccias and $\sim 5490 \times 10^{-6} \text{ SI}$ for subautochthonous granites) in comparison with NRM intensity data ($\sim 120 \text{ mA}^{-1}$ for breccias and $\sim 380 \text{ mA}^{-1}$ for subautochthonous granites; Table 1). This is in contrast to the fairly

high, or enhanced, Q-values of high-temperature impact rocks in many other terrestrial impact structures (e.g. Lappajärvi, Pesonen *et al.*, 1992; Rochechouart, Pohl and Soffel, 1971). The NRM intensities of breccias and subautochthonous granites are relatively weak but become stronger with depth (Fig. 5).

CONCLUSIONS

The following conclusions can be drawn from this study. The physical properties of the Kärđla meteorite impact-generated rocks differ markedly from those of the unshocked target rocks. The impact lens is characterized by increased porosity in comparison with the surroundings. High porosity is responsible for high electrical conductivity and low density. Also the low P-wave velocity is partially influenced by the high porosity.

The density contrast between the unshocked target granites and fractured subautochthonous granites is $\sim 170 \text{ kg m}^{-3}$, which is similar to the observed contrast (177.5 kg m^{-3}) in seven other terrestrial impact craters (Pilkington and Grieve, 1992). The density contrast between impact-produced breccias and unshocked target is, however, clearly higher (240 kg m^{-3}). The density contrast between target and rim wall granites is less distinct ($\sim 30 \text{ kg m}^{-3}$).

The magnetic susceptibility and remanence of shocked rocks vary but are generally weaker than those of the target. There is no marked enhancement in Q-values of impact breccias, due to relatively low temperatures during the impact. The impact probably randomized NRM vectors by brecciation process.

The deepest impact-caused changes in densities of subautochthonous granites in the centre of the crater extend to $\sim 950 \text{ m}$. It gives the depth/diameter ratio $0.95/4.0 = 0.24$ at the present erosional level.

The central uplift does not produce an observable geophysical signal owing to its small size and considerable depth.

Acknowledgements—We thank J. Kirs and T. Meidla (University of Tartu) for their assistance in preparing the manuscript, L. Kivekäs (Geological Survey of Finland) for her help with the petrophysical measurements, T. Ruotoistenmäki (Geological Survey of Finland) for his assistance in modelling and G. Häkli for revising the English, Dr. M. Pilkington and Dr. J. Pohl for constructive comments. The figures were drawn by S. Nässling. Financial support for the research was given by ESF and ISF.

Editorial handling: R. A. F. Grieve

REFERENCES

- BARLOW B. C. (1979) Gravity investigations of the Cosses Bluff impact structure, central Australia. *Bur. Min. Res. J. Aust. Geol. Geophys.* 4, 323–339.
- BAUERT H. A., MÄNNIL R. M. AND SUUROJA K. A. (1987) O vremeni obrazovaniya Kärđlaskogo kratera (in Russian). In *Tezisy dokl. XX Vsesoyuznoy meteoritnoy konf. I* (Moscow), 48.
- COWIE J. W. AND BASSETT M. G. (1989) 1989 global stratigraphic chart with geochronometric and magnetostratigraphic calibration. *Episodes* 12 (2), 1.
- DABIZHA A. I. AND FEDYNSKY V. V. (1977) Features of the gravitational field of astrolems (in Russian). *Meteoritika* 36, 113–120.
- DORTMAN N. B. (1992) *Petrofizika. Spravochnik V tryoh knigah. Kniga pervaya. Gornyye porody i poleznye iskopyayemye* (in Russian). Nedra, Moscow, 391 pp.
- DYKELIUS D. (1988) The gravity field of the Siljan ring structure. In *Deep Drilling in Crystalline Bedrock* (eds. A. Bodén and K. G. Eriksson), pp. 85–94. Springer, New York.
- ELO S., JOKINEN T. AND SOININEN H. (1992) Geophysical investigations of the Lake Lappajärvi impact structure, western Finland. *Tectonophysics* 216, 99–109.
- ERNSTSON K. AND POHL J. (1974) Some comments on the geophysical logging measurements in the Nordlingen 1973 research borehole (in German). *Geol. Bavarica* 72, 81–90.
- FLODÉN T. AND BJERKEUS M. (1994) The proposed Ivar impact structure in the southern Baltic. *ESF Network "Impact Cratering and Evolution of Planet Earth," Second International Workshop: The Identification and Characterization of Impacts. Abstract Vol.* (eds. M. Lindström and R. Törnberg), p. 11.
- GLIKSON A. Y. (1995) Asteroid/comet mega-impacts may have triggered major episodes of crustal evolution. *EOS, Transactions, American Geophysical Union* 76(6), 49–55.
- GRAHN Y. AND NOLVAK J. (1993) Chitinozoan dating of Ordovician impact events in Sweden and Estonia. A preliminary note. *Geologiska Föreningens i Stockholm Förhandlingar* 115, 263–264.
- GRIEVE R. A. F. AND PESONEN L. J. (1992) The terrestrial impact cratering record. *Tectonophysics* 216, 1–30.
- GRIEVE R. A. F. AND PESONEN L. J. (1996) Terrestrial Impact Craters: Their spatial and temporal distribution and impacting bodies. In *The Earth, Planets and Moons. Special Issue* (ed. H. Rickman), in press.
- GRIEVE R. A. F., CODERRE J. M., ROBERTSON P. B. AND ALEXOPOULOS J. (1990) Microscopic planar deformation features in quartz of the Vredefort structure: Anomalous but still suggestive of an impact origin. *Tectonophysics* 171, 185–200.
- GUDDAUGSSON S. T. (1993) Large impact crater in the Barceta Sea. *Geology* 21, 291–294.
- HARGRAVES R. B. AND PERKINS W. E. (1969) Investigations of the effect of shock on natural remanent magnetism. *J. Geophys. Res.* 74, 2576–2589.
- HARLAND W. B., AMSTRONG R. L., GRAIG L. E., COX A. V., SMITH A. G. AND SMITH D. G. (1990) *A Geological Time Scale*. Cambridge University Press, Cambridge. 263 pp.
- HENKEL H. (1982) The lake Mien structure. *Geol. Surv. Sweden Geophys. Dep. Rep.* 8221.
- HENKEL H. AND PESONEN L. J. (1992) Impact craters and crateriform structures in Fennoscandia. *Tectonophysics* 216, 31–40.
- HILDEBRAND A. R., PENFIELD G. T., KRING D. A., PILKINGTON M., CAMARGO Z. A., JACOBSEN S. AND BOYNTON W. V. (1991) Chicxulub crater: A possible Cretaceous-Tertiary boundary impact crater on the Yucatan Peninsula, Mexico. *Geology* 19, 867–871.
- JANSA L. F., PE-PIPER G., ROBERTSON P. B. AND FRIEDENREICH O. (1989) Montagnais: A submarine impact structure on the Scotian Shelf, eastern Canada. *Geol. Soc. Am. Bull.* 101, 450–463.
- JÄRVELÄ J., PESONEN L. J. AND PIETÄINEN H. (1995) *On palaeomagnetism and petrophysics of the Iso-Naakkima impact structure, southeastern Finland*. Open File Report Q19/29.1/3232/95/1, Laboratory for Palaeomagnetism, Dept. of Geophysics, Geological Survey of Finland, Espoo. 43 pp.
- KUKKONEN I. T., KIVEKÄS L. AND PAAANANEN M. (1992) Physical properties of kärkeite (impact melt), suevite and impact breccia in the Lappajärvi meteorite crater, Finland. *Tectonophysics* 216, 31–40.
- LINDSTRÖM M., FLODÉN T., PUURA V. AND SUUROJA K. (1992) The Kärđla, Tvären, and Lockne craters—possible evidences of an Ordovician asteroid warm. *Proc. Estonian Acad. Sci. Geol.* 41, 2, 45–53.
- MAASIK V. (1959) *Gravitatsionnoye pole na territorii Estonskoj SSR i ego primineniye* (in Russian). Report of Investigation, Geological Survey of Estonia, Tallinn, 110 pp.
- MELOSH H. J. (1989) *Impact Cratering: A Geologic Process*. Oxford Univ. Press, New York. 245 pp.
- PEDLEY R. C. (1991) GRAVMAG—User Manual. Interactive 2.5 D Gravity and Magnetic Modelling Program. British Geological Survey, Keyworth, Nottingham (unpubl.).
- PESONEN L. J. (1993) Terrestrial craters: Geophysics. Report on topic 4. *ESF Network "Impact Cratering and Evolution of Planet Earth," Post-Nordlingen Newsletter* (eds. A. Montanari and J. Smith), pp. 8–13.
- PESONEN L. J. (1994) Palaeomagnetic dating of impact craters. *ESF Network "Impact Cratering and Evolution of Planet Earth," Second International Workshop: The Identification and Characterization of Impacts Abstract Vol.* (eds. M. Lindström and R. Törnberg), p. 29.
- PESONEN L. J. (1996) The Impact Cratering Record of Fennoscandia. In *Earth, Moon and Planets. Special Issue* (ed. H. Rickman), in press.
- PESONEN L. J., MARCOS N. AND PIPPING F. (1992) Palaeomagnetism of the Lappajärvi impact structure, western Finland. *Tectonophysics* 216, 123–142.
- PILKINGTON M. AND GRIEVE R. A. F. (1992) The geophysical signature of terrestrial impact craters. *Rev. Geophysics* 30, 161–181.
- PLADO J. (1993) *Petrophysical research into the Kärđla meteorite crater, Hiiumaa, Estonia*. Graduation thesis, Tartu University. 42 pp.
- PLANTE L., SEGUN M.-K. AND RONDOT J. (1990) Etude gravimétrique des astrolems du Lac à l'Eau Claire, Nouveau-Québec. *Geoexploration* 26, 303–323.

- POHL J. (1971) On the origin of the magnetization of impact breccias on Earth. *J. Geophys.* 37, 549–555.
- POHL J. AND SOFFEL H. (1971) Palaeomagnetic age determination of the Rochechouart impact structure, France. *J. Geophys.* 37, 857–866.
- PURANEN R. (1989) *Susceptibilities, iron and magnetite content of Precambrian rocks in Finland*. Report of Investigation 90, Geological Survey of Finland, Espoo. 45 pp.
- PURANEN R. AND SULKANEN K. (1985) *Technical description of microcomputer-controlled petrophysical laboratory*. Open File Report Q15/27/85/1, Dept. of Geophysics, Geological Survey of Finland, Espoo. 252 pp.
- PUURA V. AND HÜHMA H. (1993) Palaeoproterozoic age of the East Baltic granulitic crust. *Precambrian Research* 64, 289–294.
- PUURA V. AND SUUROJA K. (1992) Ordovician impact crater at Kärda, Hiiumaa Island, Estonia. *Tectonophysics* 216, 143–156.
- PUURA V., VAHER R., KLEIN V., KOPPELMAA H., NIIN M., VANAMB V. AND KIRS J. (1983) *Kristallineskii fundament Estonii* (in Russian with English summary). Nauka, Moscow. 208 pp.
- PUURA V. A., KALA E. A. AND SUUROJA K. A. (1989) Stroyeniye astroblemy Kärda (in Russian with English summary). *Meteoritika* 48, 150–161.
- PUURA V., KIRS J., PLADO J., SUUROJA K. AND SUUROJA S. (1994) Shocked rocks of the Kärda crater: Divergency in chemistry, mineralogy, fluid inclusions and petrophysical properties. *ESF Network "Impact Cratering and Evolution of Planet Earth," Third International Workshop: Shock wave behaviour of solids in nature and experiments. Abstract vol.* (eds. U. Schärer, J.-C. Doukhan and P. Agrinier), p. 54.
- SUUROJA K. A., GROMOV O. B., KALA E. A. AND GROMOVA G. A. (1974) Otshot o poiskah podnjatii kristallitsheskogo fundamenta v vostotshnoi tshasti ostrova Hiiumaa i otsenke ih na granitnyi shtseben (in Russian). *Report of Investigation, Geological Survey of Estonia, Tallinn*. 254 pp.
-

Effect of erosion on gravity and magnetic signatures of complex impact structures: Geophysical modeling and applications

J. Plado

Institute of Geology, University of Tartu, 51014 Tartu, Estonia

L. J. Pesonen

Laboratory for Palaeomagnetism, Geological Survey of Finland, FIN-02151 Espoo, Finland

V. Puura

Institute of Geology, University of Tartu, 51014 Tartu, Estonia

ABSTRACT

The changes in the gravity and magnetic anomalies of meteorite impact structures as a function of erosion have been investigated. The model structure represents a typical midsize, complex impact crater in Precambrian target rocks, with a diameter of 30 km and a height of the central uplift of 1.5 km. We used a three-dimensional forward modeling technique. Six erosional levels from 1 to 6 km which successively followed the crater formation time, were modeled from the time of primary erosional leveling of the surface to the time when the structure was completely eroded. In the gravity field, the major effect of erosion is a pronounced decrease in the amplitude of the negative anomaly, with only minor change in its diameter (or half-width), making the gravity anomaly appear progressively more flat. The amplitude of the central positive anomaly due to the structural uplift also decreases with erosion but not as rapidly as the main anomaly. The diameter of the central gravity anomaly is unaffected by erosion. The model agrees with observations of gravity amplitudes and erosion levels of 13 impact structures with diameter ranges of 20–40 km. The magnetic anomalies also change during erosion but in a more complex way than the gravity anomalies. Moreover, the shape and amplitudes of magnetic anomalies and their changes due to erosion are latitude-dependent. Therefore, the magnetic data and modeling results presented in this chapter are valid only for Fennoscandia.

INTRODUCTION

In comparison with other terrestrial planets, the relatively small number (~170) of meteorite impact structures on Earth is due to the active geologic processes reshaping the Earth's surface. A great number of impact structures have been completely destroyed during the convergent plate tectonic processes of subduction and crustal collision. In addition, geologic processes such as volcanism, sedimentation, deformation, and erosion either deform, hide or remove the

morphologic features of terrestrial impact structures (Grieve and Pesonen, 1992, 1996). Therefore, indirect methods, particularly high-resolution geophysical techniques, have become important in tracing new impact structures beneath cover sediments and in identifying the remnants of those impact structures that have been severely eroded or deformed by tectonism (Pilkington and Grieve, 1992; Elo et al., 1992; Ormö and Blomqvist, 1996; Scott et al., 1997; Plado et al., 1997; Pesonen et al., this volume). Moreover, the geophysical data are useful in calculating the morphometric parameters

Plado, J., Pesonen, L. J., and Puura, V., 1999, Effect of erosion on gravity and magnetic signatures of complex impact structures: Geophysical modeling and applications, in Dressler, B. O., and Sharpton, V. L., eds., *Large Meteorite Impacts and Planetary Evolution II*: Boulder, Colorado, Geological Society of America Special Paper 339.

(e.g., the melt volumes) of buried impact craters (Pilkington and Grieve, 1992). These applications of geophysics in impact cratering research are, however, hampered by the fact that the geophysical anomalies of impact structures depend strongly on the state of erosion and on the degree of deformation of the structures.

Very little has been done to estimate the changes in the geophysical anomalies of impact structures as a function of erosion and deformation (e.g., Pesonen et al., 1993). Pilkington and Grieve (1992) were the first to point out a trend (a decrease) in the amplitudes of the negative gravity anomalies of impact structures caused by progressive erosion. Plado et al. (1997) attempted to model the changes in gravity and magnetic anomalies of impact structures due to erosion and deformation. However, they used a 2.5-dimensional modeling technique, which turned out to be insufficient to accurately describe the anomalies of the truly three-dimensional structures.

In this chapter we present novel geophysical modeling results whereby the effect of erosion on gravity and magnetic anomalies was investigated using a three-dimensional approach as applied to a hypothetical, midsize complex impact structure in a Precambrian shield area. We restricted the modeling to consider only the effect of erosion on gravity and magnetic anomalies of impact structures; the effect of deformation is presented elsewhere (Plado et al., 1997). The main emphasis was on analysis of the gravity data, as the magnetic anomalies are more complex and depend on several parameters including the geographic site (latitude) of the structure.

In the first portion of this study we show that the erosion produces distinct changes in the amplitudes of gravity and magnetic anomalies and less pronounced changes in their widths. Based primarily on the gravity modeling, we demonstrate that some parameters derived from the gravity anomalies are practical useful measures of the erosion level of an impact structure. In the second portion we test our model on 13 real impact structures for which gravity and erosion level data are available (Pilkington and Grieve, 1992).

THE MODEL

Figure 1 shows the cross section of a hypothetical impact structure and its morphometric parameters following Croft (1985) and Melosh (1989). The original diameter (D) (rim to rim) is 30 km, characterizing the model structure as a typical midsize, complex crater in the global data base of impact structures (Grieve and Pesonen, 1996). The height (h_{CU}) and the diameter (D_{CU}) of the central structural uplift are calculated from D using equations (1) and (2) (see Melosh, 1989):

$$h_{CU} = 0.06D^{1.1} \approx 2.5 \text{ km} \quad (1)$$

and

$$D_{CU} = 0.22D = 6.6 \text{ km}. \quad (2)$$

Croft (1985) has given an expression for the diameter of the transient cavity (D_{TC}) for complex terrestrial impact structures (Eq. 3),

$$D_{TC} \equiv D_Q^{0.15 \pm 0.4} D^{0.85 \pm 0.04} = 22 \text{ km}, \quad (3)$$

where D_Q is the transition diameter for simple-to-complex crater (≈ 4 km for crystalline targets on Earth). The depth (h_{TC}) of the transient cavity has been estimated to be roughly one-third or one-fourth of its diameter D_{TC} (Melosh, 1989). The maximum rim height of the final crater (with $D = 30$ km) lies between 0.5 and 1 km (Fig. 1).

To simplify the computations, we conventionally leveled the surface (dotted line in Fig. 1A). Thus, we assume that the structural rim and the uppermost 1 km of the central uplift have been eroded away. The depression is filled by 0.2-km-thick impact

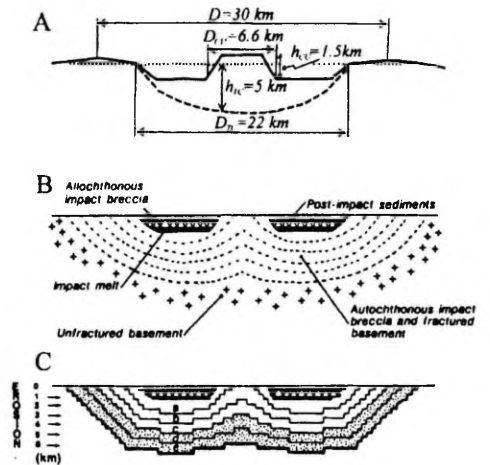


Figure 1. A, Schematic cross section of a complex impact structure with its dimensions. Dashed line indicates the shape of the transient cavity (TC); dotted line indicates the pre-impact target rock level. Symbols are explained in text. B, An idealized distribution of various impact produced/influenced lithologies as it could be in the complex structure of A. Dashed lines describe the artificial layers to count for the gradual changes of density and magnetic properties within the structure in the autochthonous breccias and fractured bedrock. C, A simplified geophysical model for a plan view, consisting of several vertical prisms that have 16 corner points on a plan view (see Fig. 2). The thickness of each prism is 500 m, except the two prisms describing the allochthonous impact breccia with thicknesses of 500 and 300 m, and the prism of the impact melt, which has a thickness of 200 m. The model is directly derived from Figure 1B. Letters (a through e) indicate five subparallel layers to describe the autochthonous breccias (a-c) and fractured basement (d-e) within which radial changes in density and magnetic properties take place progressively (see Table 1). Arrows mark erosional levels at 1, 2, 3, 4, 5, and 6 km. No vertical exaggeration.

melt layer (volume, $V = 48 \text{ km}^3$) and a 0.8-km-thick allochthonous impact breccia ($V = 221 \text{ km}^3$) that is covered by 0.5-km-thick postimpact sediments ($V = 180 \text{ km}^3$). Below the impact melt layer, filling the bottom of the transient cavity, there is a ~6-km-thick bowl-shaped unit consisting of autochthonous breccias and fractured basement (Fig. 1B). The shape of these layers follows that of the primarily flattened final crater of Figure 1A with the structural uplift at the center. However, since the modeling does not allow a continuous parameterized change in the breccias and fractured target rocks to take place, we have split them artificially into five successive layers with equal thicknesses of 1 km (Fig. 1C, Table 1) where layers *a* through *c* correspond to the autochthonous breccias and layers *d* through *e* to fractured basement, respectively. Below layer *e* the basement is virtually unaffected by the shock.

Geometry of the model

The final model is shown in Figure 1C and consists of several vertical prism-like bodies with 16 corner points on a plan view (Fig. 2) and with a diameter decreasing stepwise downward. The thickness of the prisms in both the autochthonous breccia layer and the fractured bedrock layer is 500 m. The two prisms in the allochthonous impact breccia have thicknesses of 500 and 300 m, respectively, whereas the impact melt prism is 200 m thick.

Modeling density variations

In the model, the density is increasing radially away from the point of impact (Figs. 1 and 2; Table 1), as is the case in many

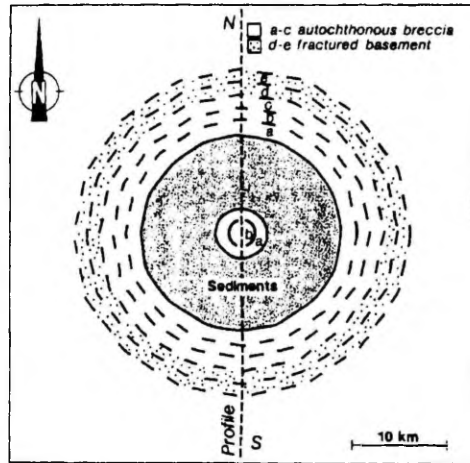


Figure 2. Plan view of the modeled area ($50 \times 50 \text{ km}$), including distribution of the uppermost layers of the vertical prisms. The impact is supposed to take place at the center of the area. Location of the central profile (north-south), described in Figures 6 and 7, is shown. Letters *a* through *e* as in Figure 1.

TABLE 1. PHYSICAL PROPERTIES OF ROCK LAYERS

Rock Type	ρ (kgm^{-3})	χ (10^{-6} S)	NRM (Am^{-1})	Q	D ($^{\circ}$)	I ($^{\circ}$)	Age (Ma)
Surrounding (mica schist)	2689	300			304	73	2680
Autochthonous breccia and fractured basement							
Layer 1	2480	200	0.04	4.9	328	41	1930
Layer 2	2530	220	0.043	4.8	328	41	1930
Layer 3	2580	240	0.046	4.7	328	41	1930
Layer 4	2620	260	0.049	4.6	321	57	2680 + 1930
Layer 5	2660	280	0.052	4.5	321	57	2680 + 1930
Impact melt	2500	2000	0.82	10	328	41	1930
Allochthonous (impact) breccia	2380	50	0.01	5	328	41	1930
Post-impact sediments	2350	100	0.01	2.44	328	41	1930

ρ = density.

χ = magnetic susceptibility.

NRM = intensity of natural remanent magnetization.

Q = Koernigsberger ratio.

D and I = declination and inclination of NRM, respectively.

known complex impact structures. This increase of density with depth is caused by the decrease of porosity and fracturing in impact rocks and also in the upper part of the fractured target, as observed, for example, in Clearwater West, Canada (Plante et al., 1990), in Siljan ring in Sweden (Dyrelus, 1988), in Lappajärvi and Iso Naakkima in Finland (Kukkonen et al., 1992; Pesonen, 1996), and in Kärdla, Estonia (Plado et al., 1996). The model density values for the various layers are taken from the data of impact structures of Lappajärvi (Kukkonen et al., 1992) and Kärdla (Plado et al., 1996) and are listed in Table 1. The density is increasing downward from the postimpact sediments ($2,350 \text{ kg m}^{-3}$) to allochthonous impact breccia ($2,380 \text{ kg m}^{-3}$) to the five layers of autochthonous breccia and fractured basement ($2,480$ – $2,660 \text{ kg m}^{-3}$). The impact melt has a density of $2,500 \text{ kg m}^{-3}$ while the surrounding target rock (mica gneiss) has a density of $2,689 \text{ kg m}^{-3}$.

Modeling magnetic variations

Considering investigations of terrestrial impact structures and laboratory experiments, the effects of the transient shock on magnetic properties of different rock types of the impact structures are more variable than those in density. Generally, shock produces a drop in the magnetic susceptibility and often (but not always) also in the natural remanent magnetization (NRM), thus causing the weak magnetic relief associated with many impact structures (Hargraves and Perkins, 1969; Pohl et al., 1975; Cisowski and Fuller, 1978; Pilkington and Grieve, 1992; Pesonen, 1996; Scott et al., 1997). However, in some cases the impact influenced rocks may acquire a new remanence by transient stresses, the shock remanent magnetization (SRM), along the direction of the Earth's magnetic field at the time of impact (e.g., Halls, 1979).

Slowly cooled crystalline impact melt rocks may acquire a thermoremanent magnetization (TRM) in the direction of the magnetic field at the time of impact, e.g. Manicouagan, Canada (Larochelle and Currie, 1967) and Lappajärvi, Finland (Pesonen et al., 1992). The volume and magnetic contrast of melt, and therefore the magnetic anomaly, is largely controlled by the composition and properties of target rocks.

To describe the direction of the NRM in the model, we used the remanent magnetization directions of the Fennoscandian paleomagnetic data base (Pesonen et al., 1989, 1991). The use of this data base requires the knowledge of the ages of the impactites and target rocks. In our model, the age of the surroundings (=unshocked target rocks) was $\sim 2,680 \text{ Ma}$ (i.e., Archean) and the impact occurred at $1,930 \text{ Ma}$. The age of the postimpact sediments was also assumed to be $1,930 \text{ Ma}$. The polarity of the magnetic field was normal. The remanent magnetization directions in Table 1 were taken from the NRM data of rocks having ages of $2,680$ and $1,930 \text{ Ma}$ in the paleomagnetic data base of Fennoscandia. For the uppermost three layers of the autochthonous breccia and fractured basement (layers *a*–*c* in Fig. 1C), we used the same NRM direction as for the impact melt, assuming that these layers have an SRM. For the two low-

ermost layers (layers *d* and *e* in Fig. 1C), we used the vectorial sum of the pre-impact and impact NRM directions, respectively.

The shape and amplitudes of magnetic anomalies depend on latitude, in addition to the previously discussed geometrical and petrophysical properties of the rock units constituting the structure. Since the magnetic data and modeling results are not reduced to the pole, the results presented in this chapter are valid only for Fennoscandian latitudes ($\sim 60^\circ$ – 70°).

The values for the magnetic properties in the model used for different layers of the structure were assigned according to literature values of known Precambrian and impact rocks described by Puranen (1989), Pesonen et al. (1989), Pilkington and Grieve (1992), and Järvelä et al. (1995), and are listed in Table 1. The density and magnetic properties for the various layers of our model structure were stated to be conforming. However, physical and chemical processes taking place during the impact and later on may alter the petrophysical properties of these rocks. Post-impact thermal and chemical processes (Pilkington and Grieve, 1992) may cause considerable changes in the impact-generated rocks independent of geologic boundaries. In our simple model, we did not consider all these effects. The direction, amplitude, and range of NRM produced by postimpact thermochemical processes are different for every particular impact case. Therefore, the magnetic properties of each structure should be studied individually and separately from the gravity model.

To confirm density and magnetic layers, we assumed the following conditions: (1) that the cooling of the structure took place rapidly, (2) that the crater rim was eroded away and the crater depression was rapidly filled by postimpact sediments, and (3) that postimpact physical-chemical processes affecting physical properties of the rocks in the structure were not taking place.

The magnetic properties of the present Earth's magnetic field (intensity, 41 Am^{-1} ; declination, 6° ; inclination, 73.5°) used in calculations correspond to the values for the central part of the Fennoscandian Shield (latitude, $\sim 62^\circ$) and were same for all models.

Modeling Methods

The main objective of the modeling was to study the progressive changes in the gravity and magnetic anomalies of the structure through six successive erosional levels (h_E) at 1-km intervals. The first level ($=0 \text{ km}$, Fig. 1C) corresponds to the early postimpact phase when the surface became flattened at the target level. The lowermost erosional level ($=6 \text{ km}$) corresponds to the level where the main units of the structure (i.e., the postimpact sediments; the allochthonous breccia; the impact melt; the autochthonous breccia, layers *a*–*c*; and the upper part of fractured basement layer *d*) have been eroded, and only the lowermost part of the fractured basement, layer *e*, has been preserved. The other erosional levels (corresponding to h_E values of 1, 2, 3, 4, and 5 km in Fig. 1C) lie between levels 0 and 6 km.

The gravity and magnetic anomaly values were calculated over a $50 \times 50 \text{ km}$ area (Figs. 3 and 4) centered on the impact point

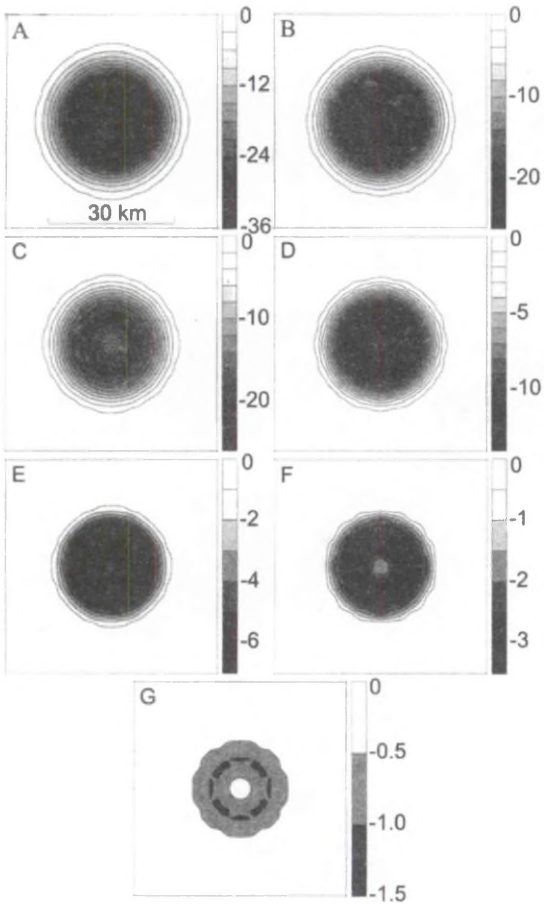


Figure 3. Plan views (50×50 km) of the gravity anomalies (mGal) of: A, early postimpact, at various erosion levels: B, 1 km; C, 2 km; D, 3 km; E, 4 km; F, 5 km; G, 6 km. The impact is taking place at the center of the area. Note that the amplitude scale varies.

using the ModelVision Software Package by Encom Technology Pty, Ltd., Australia (1995). Using this three-dimensional program, the Bouguer gravity and the total magnetic field intensities for observation points with a grid of 2×2 km were calculated. The models are simplified from the real geologic situation with no background variations in gravity and magnetism and with no regional trends. The final maps of the gravity (Fig. 3) and total field magnetic anomalies (Fig. 4) are produced with kriging for the same grid size as the calculations were done above, and shown at seven successive erosional levels. The north-south profile data of the

gravity and magnetic anomalies and the effects of erosion on these profiles and their derivatives (horizontal and vertical gradients) are shown in Figures 6 and 7 at the various erosional levels.

To numerically study the progressive effect of erosion on the gravity anomaly, we used the following parameters to describe the shape of the gravity anomaly (see Parasnis, 1979): diameter (D_G), the half-width ($W^{1/2}$), maximum amplitude (A) of the main negative gravity anomaly, and corresponding values (d_{CU} , a_{CU} , and $w^{1/2}_{CU}$) for the central positive anomaly (due to structural uplift) (Fig. 5).

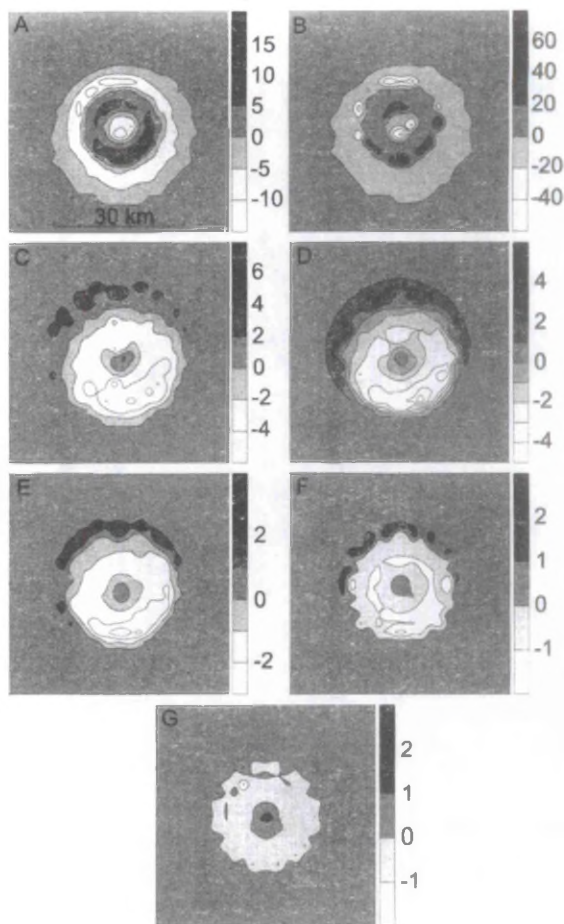


Figure 4. Plan view of the magnetic anomalies (total intensity, nT) of: A, early postimpact, at various erosion levels: B, 1 km; C, 2 km; D, 3 km; E, 4 km; F, 5 km; and G, 6 km. The impact is taking place at the center of the area. Note that the amplitude scale varies.

RESULTS

Anomaly maps

The gravity anomaly of the model (Fig. 3A) is perfectly circular and has a diameter of ~ 36 km, thus slightly exceeding the original diameter of the structure. It is due to the radial distribution of the density layers, extending farther than the original rim. The half-width of the anomaly is 25.2 km. The minimum value of the gravity anomaly is -36 mGal, which is consistent with a complex impact

structure of this size unaffected by erosion (Pilkington and Grieve, 1992) (Fig. 6). The central uplift produces a positive gravity high of 6.2 mGal at the center of the main negative gravity anomaly (Figs. 3A and 6A) as is often observed in many complex impact structures, e.g., Vredefort, South Africa (Henkel and Reimold, 1997) and Lappajärvi, Finland (Elo et al., 1992). The horizontal gradient of the gravity anomaly (Fig. 6B) shows two peaks, one minima and one maxima symmetrically on the sides of the center of the impact structure. The vertical gradient (Fig. 6C) shows two maxima and two minima and a central maximum due to structural uplift.

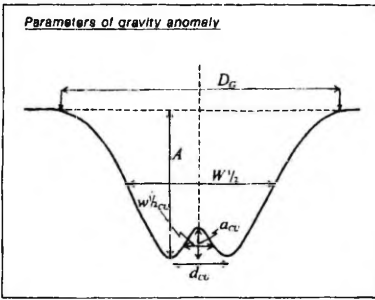


Figure 5. Schematic cross section of a gravity anomaly of a complex impact structure. The numerical parameters to describe the geometry of the anomaly are indicated. D_G , A , and $W'/2$ denotes the diameter, amplitude, and half-width, respectively, of the major negative anomaly; a_{CU} , a_{CU} and $w'/2_{CU}$ are corresponding values for the central positive anomaly, respectively.

The initial magnetic anomaly map (Fig. 4A) reflects two features. First, the strongly magnetic melt body produces a circular positive anomaly with maximum amplitude of 13.1 nT. It is surrounded by the negative anomaly, which is most intensive at the northwestern edge of the structure. Second, in the central part, the positive anomaly is distorted by the negative anomaly (-14.1 nT). This kind of magnetic anomaly is expected for a body in the Northern Hemisphere (Parasnis, 1979). Correspondingly, two magnetic highs and three lows are visible on the profile (Fig. 7A).

Effects of erosion on gravity anomalies

Erosion progressively removes the impact-produced gravity signatures. During the erosion of the structure, both the amplitude of impact gravity anomaly and its diameter decrease (Table 2; Figs. 3, 6A and 8A). Since the decrease is much stronger in amplitude, erosion progressively flattens the gravity

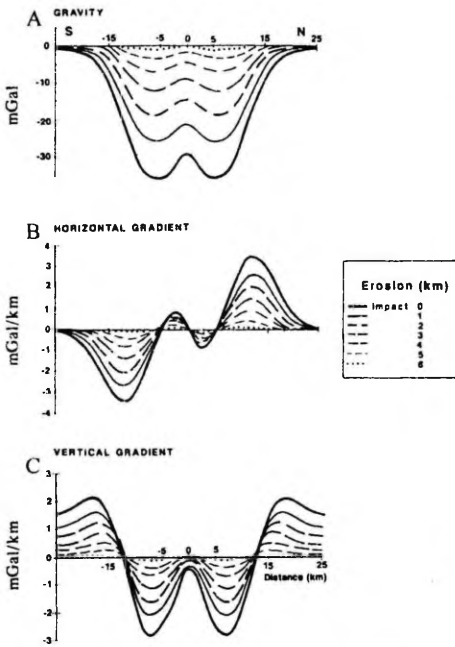


Figure 6. North-south profiles of the Bouguer gravity across the model as a function of erosion. A, Bouguer gravity; B, its horizontal gradient; and C, its vertical gradient. See Figure 2 for location. Curves are calculated for the impact time and at six erosional levels, as indicated in the index figure and shown in Figure 1C.

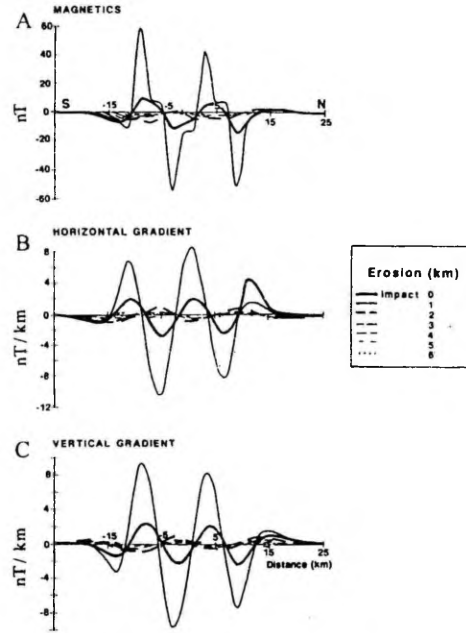


Figure 7. North-south profiles of the total magnetic field intensity across the model as a function of erosion. A, Magnetic (total component, nT); B, its horizontal gradient; and C, vertical gradient profiles across the hypothetical impact structure. See Figure 2 for location. Curves are calculated for the impact time and at six erosional levels, as indicated in the index figure and shown in Figure 1C.

TABLE 2. PROPERTIES OF IMPACT GRAVITY ANOMALIES IN DIFFERENT SITUATIONS

	—Impact Gravity Anomaly—			—Anomaly of— Central Uplift			
	h_E/D	A (mGal)	$W_{1/2}$ (km)	$ A/W_{1/2} $ (mGal/km)	a_{CU} (mGal)	$w_{1/2CU}$ (km)	$ A/a_{CU} $
Impact		-35.7	25.2	1.4	6.2	4.6	5.8
Erosion (km)							
1	0.03	-25.7	24.8	1.0	4.3	5.2	6.0
2	0.07	-18.4	24.2	0.8	3.7	5.8	5.0
3	0.10	-11.9	23.8	0.5	2.8	5.2	4.3
4	0.13	-6.8	23.2	0.3	1.9	5.4	3.6
5	0.17	-3.2	22.8	0.1	1.5	5.2	2.1
6	0.20	-0.9	22.4	0.0	0.7	5.0	1.3

h_E = depth of erosion.

D = the original impact rim diameter.

A = the maximum amplitude of impact gravity anomaly.

$W_{1/2}$ = half-width of the impact gravity anomaly.

a_{CU} = the maximum amplitude of gravity anomaly corresponding to the central uplift.

$w_{1/2CU}$ = half-width of the gravity anomaly corresponding to the central uplift.

anomalies of the impact structure. The flattening is clearly seen in the profile data (Fig. 6A) and can be numerically expressed by a parameter F , which is obtained by dividing the maximum gravity amplitude with its half-width ($A/W_{1/2}$) at each erosional level (Table 2; Fig. 8C). At all erosional levels the presence of the central uplift is seen as the positive peak within the central negative anomaly, although it decreases progressively with erosion (Fig. 8A). In spite of the significant decrease of the positive gravity anomaly of the central uplift during erosion, it remains relatively more pronounced, as compared with the corresponding negative impact anomaly.

The amplitudes of the horizontal and vertical derivatives also diminish with erosion (Figs. 6B, C). The locations of the maximum horizontal gradients do not shift considerably with erosion. Their position on the profiles approximately corresponds to the diameter of 24 km, which is $0.8 \times D$. This is the diameter where the vertical derivative curves intersect at 0 mGal/km. However, the central uplift produces significant shifts in the horizontal and vertical derivative curves during progressive erosion.

Effects of erosion on magnetic anomalies

Due to the highly magnetic (Table 1) impact melt layer, the first erosional model ($h_E/D = 0.03$) produces intensive magnetic anomalies up to 60 and -60 nT (Figs. 4B and 7A). The position of two positive and three negative anomalies conforms with those of the starting model. After the removal of impact melt layer, at the erosional level of 2 km and also in further erosional levels, the amplitude of the magnetic anomalies decreases and the configuration alters so that the position of negative and positive anomalies changes (Figs. 4 and 7). These five circular anomalies at different erosional levels are mainly negative, followed by positive anomalies at the northwest. These are due to weaker

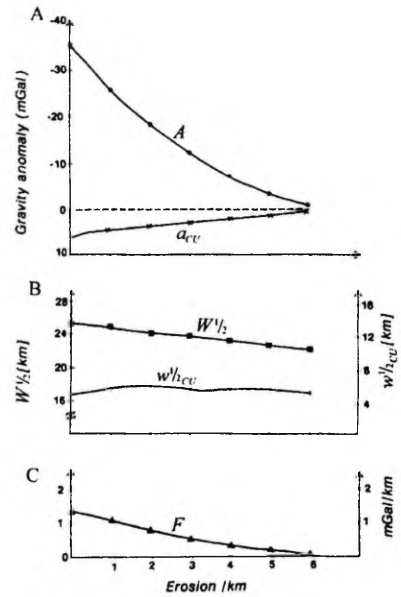


Figure 8. A, The effect of erosion on the amplitudes of gravity anomalies. Black circles indicate amplitude, A , of the main anomaly; crosses indicate amplitude (a_{CU}), respectively, of the central positive anomaly. B, Effect of erosion on the half-widths of the main anomaly ($W_{1/2}$, black squares) and of the central uplift anomaly ($w_{1/2CU}$, vertical bars). C, Effect of erosion on the parameter $F = A/W_{1/2}$ (amplitude of the main anomaly divided by its half-width).

magnetization of autochthonous impact breccia and fractured basement as compared with surroundings and main field direction. The central uplift produces a distinct magnetic high. The horizontal and vertical derivatives (Fig. 7B, C) also diminish after the removal of the melt layer. The amplitudes of the erosional magnetic anomalies are so weak, that, in real geologic situations (presence of regional field), they will go unnoticed.

Testing the model

Our erosional model shows clearly that the erosion decreases the amplitudes of the gravity and magnetic anomalies more effectively than their widths. The magnetic amplitudes depend not only on the shape of the structure and rock types and their petro-physical properties but also on the latitude of the structure. Therefore the magnetic data of various structures are not directly comparable unless transformed into the magnetic pole that is not done here. This is the prime reason why we restrict our model testing to the gravity data.

In Figure 9 we have tested our model by plotting the gravity amplitude and its change due to erosion (solid curve), together with the gravity data of 13 terrestrial impact structures for which gravity amplitudes and erosional levels have been measured or estimated. The data are listed in Pilkington and Grieve (1992) and include only structures with diameters ranging from 20 to 40 km. The gravity anomalies of these 13 test structures have been corrected to correspond with that of a nominal 30-km diameter, which was done by applying a linear fit (Eq. 4) to the gravity anomaly vs. D :

$$A = -0.068 D - 11.34 \quad (4)$$

This correction increases slightly the negative gravity amplitude of structures with $D < 30$ km, and decreases the amplitude of structures with $D > 30$ km. The effect of the above correction is 0.68 mGal (maximum).

Note that the erosion level index of Pilkington and Grieve (1992) runs from 1 (uneroded) to 7 (almost totally eroded) and does not correspond to the erosion values of 0–6 km of our model structure. The terrestrial impact data (Fig. 9) show clear trends in decrease of negative gravity anomalies due to progressive erosion in rough agreement with our model (solid curve). Figures 8 and 9 show that it could be possible to use the amplitude and half-width of the impact gravity anomalies as diagnostic criteria for estimating of the regional erosional level and the original diameter of the structure. The trend in Figure 9, described with the linear regression, allows us to calculate the erosional level (h_E) from the negative gravity anomaly (A) for a structure of ~30 km in original diameter:

$$h_E = (A + 31.8)/5.8 \text{ (km)}. \quad (5)$$

Including the original impact diameter, D , gives:

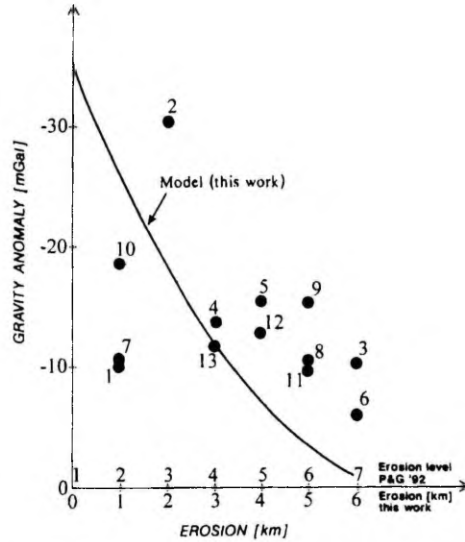


Figure 9. Testing the erosion model with gravity data of known impact structures. Vertical axis shows the negative gravity anomaly. Horizontal axis shows the erosion in kilometers for the model (solid curve) as redrawn from Figure 8A. The data points (black circles) denote data of 13 such complex impact structures for which the gravity data and also an estimate of the erosion level are available from Table 2 of Pilkington and Grieve (1992) after minor correction due to their departure from the nominal diameter of 30 km (see text). Note that the erosion level index of Pilkington and Grieve (1992) runs from 1 (uneroded) to 7 (almost totally eroded) and does not directly correspond to the erosion values of 0–6 km of this modeling structure. 1, Azuara, Spain; 2, Boltysh, Ukraine; 3, Carswell, Canada; 4, Clearwater East, Canada; 5, Clearwater West, Canada; 6, Gosses Bluff, Australia; 7, Houghton, Canada; 8, Lappajärvi, Finland; 9, Mistastin, Canada; 10, Ries, Germany; 11, Rouchouart, France; 12, Saint Martin, Canada; 13, Steen River, Canada.

$$h_E = D(A + 31.8)/171.0 \text{ (km)} \quad (6)$$

These theoretical equations results in overestimating h_E (~3.5 km for Gosses Bluff, Australia; ~2.9 km for Lappajärvi, Finland; ~0.3 km for Boltysh, Ukraine), especially for structures with low A . This is probably due to the heterogeneity of the target and subsequent geologic processes, postimpact thermal and geochemical processes and tectonic modification, which are able to reduce the negative gravity amplitude. These effects, however, are not considered in our model. Nevertheless, in general gravity data allow us to estimate the erosion level of impact structures, and, as a consequence, also the regional erosional level.

CONCLUSIONS

Impact events generate various types of rocks, differing in their physical properties from rocks unaffected by impact. Allochthonous impact breccias and fractured target rocks usually have lower density than their source rocks, and produce most of the negative gravity anomaly associated with impact. The amplitude of the gravity anomaly is dependent on the volume, shape, density contrast, and thickness of the rocks affected by the impact beneath the crater. In the case of a young impact crater, all these properties are largely controlled by the crater's diameter, i.e., by the energy of impact, and by the properties and state of the target rocks. However, erosion is able to change the volume of the structure as well as the distance to the source. Therefore, this allows us to use gravity anomalies to estimate the erosion level of impact structures. With the present modeling we found that the amplitude and diameter of the negative impact gravity anomaly significantly decrease due to erosion. Since the decrease is much stronger in amplitude, the erosion progressively flattens the gravity anomalies of impact structures.

Erosion may magnify the gravity response of the central uplift in comparison with the total anomaly. This conclusion is consistent with real situations: some deeply eroded complex impact structures, e.g., Vredefort, South Africa (Henkel and Reimold, 1997), and Lappajärvi, Finland (Elo et al., 1992), show positive gravity anomalies in their central parts. This is in good agreement with the fundamental conclusion, that central parts of craters represent blocks of less crushed rocks uplifted during the modification stage of crater formation (Melosh, 1989).

We have shown the model with the prevailing effect of a strongly remanent magnetized impact melt body, e.g., Dellen in Sweden (Henkel, 1992), and with a concentric region with decreased magnetization of target (e.g., Slate Islands, Canada) (Halls, 1979), located in Fennoscandia. The calculated magnetic anomaly reflects a circular positive anomaly surrounded by a negative, produced mainly by the melt layer. In the central part, the positive anomaly is distorted by the negative anomaly, corresponding to the central uplift. The removal of impact melt by erosion significantly decreases the amplitudes of the anomalies.

ACKNOWLEDGMENTS

We thank Seppo Elo, Geological Survey of Finland, and Markku Peltoniemi, Helsinki University of Technology, for helpful comments. The figures were drawn by Salme Nässling, Geological Survey of Finland. We also appreciate the thoughtful comments of Gary L. Kinsland, and W. A. Morris, and an anonymous reviewer. The earlier stage of this research was supported by the Center for International Mobility of Finland and by Grant 2063 from the Estonian Science Foundation.

REFERENCES CITED

- Cisowski, S. M., and Fuller, M., 1978. The effect of shock on the magnetism of terrestrial rocks. *Journal of Geophysical Research*, v. 83, p. 3441–3458.
- Croft, S. K., 1985. The scaling of complex craters: Proceedings, 15th Lunar and Planetary Science Conference: Houston, Texas, Lunar and Planetary Institute, p. 828–842.
- Dyrelius, D., 1988. The gravity field of the Siljan ring structure: Deep Drilling in Crystalline Bedrock, v. 1, p. 85–94.
- Elo, S., Jokinen, T., and Soininen, H., 1992. Geophysical investigations of the Lake Lappajärvi impact structure, western Finland: *Tectonophysics*, v. 216, p. 99–109.
- Encom Technology Pty Ltd., 1995. ModelVision, Geophysical data display, analysis and modeling, Version 1.20: Milson's Point, Australia, p. 1–212.
- Grieve, R. A. F., and Pesonen, L. J., 1992. The terrestrial impact cratering record: *Tectonophysics*, v. 171, p. 1–30.
- Grieve, R. A. F., and Pesonen, L. J., 1996. Terrestrial impact craters: their spatial and temporal distribution and impacting bodies: *Earth, Moon and Planets*, v. 72, p. 357–376.
- Halls, H. C., 1979. The Slate Islands meteorite impact site: a study of shock remanent magnetization: *Geophysical Journal of the Royal Astronomical Society*, v. 59, p. 553–591.
- Hargraves, R. B., and Perkins, W. E., 1969. Investigations of the effect of shock on natural remanent magnetism: *Journal of Geophysical Research*, v. 74, p. 2576–2589.
- Henkel, H., 1992. Geophysical aspects of meteorite impact craters in eroded shield environment, with special emphasis on electric resistivity: *Tectonophysics*, v. 216, p. 93–90.
- Henkel, H., and Reimold, W. U., 1997. Integrated gravity and magnetic modeling of the Vredefort impact structure—re-interpretation of the Witwatersrand basin as the erosional remnant of an impact basin: Stockholm, Royal Institute of Technology, Department of Geodesy and Photogrammetry, 90 p.
- Järvelä, J., Pesonen, L. J., and Pietariuen, H., 1995. On palaeomagnetism and petrophysics of the Iso-Naakkima impact structure, southeastern Finland: Espoo, Geological Survey of Finland, Internal Report Q19/29.1/3232/95/1, 53 p.
- Kukkonen, J. T., Kivekäs, L., and Paananen, M., 1992. Physical properties of karnäite (impact melt), suevite and impact breccia in the Lappajärvi meteorite crater, Finland: *Tectonophysics*, v. 216 (1/2), p. 111–122.
- Larochele, A., and Currie, K. L., 1967. Paleomagnetic study of igneous rocks from the Manicouagan structure, Quebec: *Journal of Geophysical Research*, v. 72, p. 4163–4169.
- Melosh, H. J., 1989. *Impact cratering: a geologic process*: New York, Oxford University Press, 245 p.
- Ormö, J., and Blomqvist, G., 1996. Magnetic modelling as a tool in the evaluation of impact structures, with special reference to the Tvären Bay impact crater, SE Sweden: *Tectonophysics*, v. 262, p. 291–300.
- Parasnis, D., 1979. *Principles of applied geophysics*: London, Chapman & Hall, 275 p.
- Pesonen, L. J., 1996. The Iso-Naakkima meteorite impact structure: physical properties and paleomagnetism of a drill core: *Meteoritics and Planetary Science*, v. 31 (suppl.), p. A105–A106.
- Pesonen, L. J., Torsvik, T. H., Elming, S.-Å., and Bylund, G., 1989. Crustal evolution of Fennoscandia—paleomagnetic constraints: *Tectonophysics*, v. 162, p. 27–49.
- Pesonen, L. J., Bylund, G., Torsvik, T. H., Elming, S.-Å., and Mertenan S., 1991. Catalogue of paleomagnetic directions and poles from Fennoscandia—Archean to Tertiary: *Tectonophysics*, v. 195, p. 151–207.
- Pesonen, L. J., Marcos, N., and Pipping, F., 1992. Paleomagnetism of the Lappajärvi impact structure, western Finland: *Tectonophysics*, v. 216 (1/2), p. 123–142.
- Pesonen, L. J., Masaitis, V., and Lindström, M., 1993. Report on topic 4: Terrestrial craters, geophysics, economics and formations, in Montanari, A., and Smit, J., eds., Post-Nördlingen Newsletter, Scientific Network of the European Science Foundation: Strasbourg, France, p. 8–11.
- Pilkington, M., and Grieve, R. A. F., 1992. The geophysical signature of terrestrial impact craters: *Reviews of Geophysics*, v. 30, p. 161–181.
- Plado, J., Pesonen, L. J., Elo, S., Puura, V., and Suuroja, K., 1996. Geophysical

- research on the Kärda impact structure, Hiiumaa Island, Estonia: *Meteoritics and Planetary Science*, v. 31, p. 289-298.
- Plado, J., Pesonen, L. J., and Puura, V., 1997. Gravity and magnetic modeling of a complex impact structure: effect of deformation and erosion, *in Proceedings, 27th Lunar and Planetary Science Conference, Abstracts: Houston, Texas, Lunar and Planetary Institute*, p. 42.
- Plante, L., Seguin, M.-K., and Rondot, J., 1990. Etude gravimétrique des astrolèmes du Lac à l'Eau Claire, Nouveau-Québec: *Geocxploration*, v. 26, p. 303-323.
- Pilkington, M., and Grieve, R. A. F., 1992. The geophysical signature of terrestrial impact craters: *Reviews of Geophysics*, v. 30, p. 161-181.
- Pohl, J., Bleil, U., and Hornemann, U., 1975. Shock magnetization and demagnetization of basalt by transient stress up to 10 kbar: *Journal of Geophysics*, v. 41, p. 23-41.
- Puranen, R., 1989. Susceptibilities, iron and magnetite content of Precambrian rocks in Finland: *Geological Survey of Finland Report of Investigation*, v. 90, p. 45.
- Scott, R. G., Pilkington, M., and Tanczyk, E. I., 1997. Magnetic investigations of the West Hawk, Deep Bay and Clearwater impact structures, Canada: *Meteoritics and Planetary Science*, v. 32, p. 293-308.

MANUSCRIPT ACCEPTED BY THE SOCIETY DECEMBER 16, 1998

CURRICULUM VITAE

JÜRI PLADO

Personal Information

Age: Born June 08, 1969
Citizenship: Estonian nationality and citizen
Current Addresses: Institute of Geology
University of Tartu
Vanemuise 46, 51014 Tartu, Estonia
Phone +372 7 375 815
Fax +372 7 375 836
E-mail jplado@math.ut.ee
Geological Survey of Finland
P.O. Box 96, FIN-02151 Espoo, Finland
Phone +358 205 50 2269
Fax +358 205 50 12
E-mail juri.plado@gsf.fi

Educational Background

Undergraduate: Institute of Geology, University of Tartu, Estonia, 1987–1993.
Diploma in Geology, 1993. Title of thesis: “Petrophysical research into the Kärđla meteorite crater, Hiiumaa, Estonia”
Post-graduate: Institute of Geology, University of Tartu, Estonia, 1993–1995.
Magister scientiarum in Applied Geology, 1995. Title of thesis: “Geophysical signatures of the Kärđla impact crater, Hiiumaa Island, Estonia”

Professional Experience

1993–1994: Assistant, Institute of Geology, University of Tartu
1995–1999: Lecturer, Institute of Geology, University of Tartu
1997: Assistant, Geological Survey of Finland
Since 1999: Scientist, Institute of Geology, University of Tartu
Since 2000: Geophysicist, Geological Survey of Finland

CURRICULUM VITAE

JÜRI PLADO

Isikuandmed

Sünniaeg: 8. juuni 1969
Rahvus: eestlane
Address: Tartu Ülikooli geoloogia instituut
Vanemuise 46, 51014 Tartu, Eesti
Telefon +372 7 375 815
Faks +372 7 375 836
E-post jplado@math.ut.ee
Soome Geoloogiakeskus
PL 96, FIN-02151 Espoo, Suomi
Telefon +358 205 50 2269
Faks +358 205 50 12
E-post juri.plado@gsf.fi

Haridus

Tartu Ülikool, diplom geoloogia erialal 1993. Diplomitöö teema: “Petrophysical research into the Kärđla meteorite crater, Hiiumaa, Estonia”
Tartu Ülikool, *magister scientiarum* rakendusgeoloogia erialal. Magistritöö teema: “Geophysical signatures of the Kärđla impact crater, Hiiumaa Island, Estonia”

Teenistuskäik

1993–1994: assistent, Tartu Ülikooli geoloogia instituut
1995–1999: lektor, Tartu Ülikooli geoloogia instituut
1997: assistent, Soome Geoloogiakeskus
alates 1999: teadur, Tartu Ülikooli geoloogia instituut
alates 2000: geofüüsik, Soome Geoloogiakeskus

DISSERTATIONES GEOLOGICAE UNIVERSITATIS TARTUENSIS

1. Пээп Мянник. Конодонты в верхнеордовикских и нижнесилурийских отложениях Эстонии. Тарту, 1992. 355 с.
2. Elvi Tavast. Fennoskandia kilbi lõunanõlva ja sellega piirnevate alade aluspõhja reljeef. Tartu, 1992. 357 lk.
3. Kaarel Orviku. Characterisation and evolution of Estonian seashores. Tartu, 1992. 19 p.
4. Анатолий Молодьков. ЭПР-анализ скелетного вещества моллюсков в хроностратиграфических исследованиях позднего кайнозоя. Тарту, 1992. 33 с.
5. Jaan Lutt. Late- and postglacial deposits on the Estonian shelf. Tartu, 1993. 31 p.
6. Reet Karukäpp. Gotiglatsiaalne morfogenees Skandinaavia mandriliustiku kagusektoris. Tartu, 1997. 181 p.
7. Argo Jõeht. Geothermal studies of the Precambrian basement and Phanerozoic sedimentary cover in Estonia and Finland. Tartu, 1998. 125 p.
8. Jüri Nemliher. Mineralogy of Phanerozoic skeletal and sedimentary apatites: an XRD study. Tartu, 1999. 134 p.
9. Kalle Kirsimäe. Clay mineral diagenesis on the Lower Cambrian "Blue Clay" in the northern part of the Baltic Paleobasin. Tartu, 1999. 113 p.



ISSN 1024-2658
ISBN 9985-56-